Universidade do Minho
Escola de Engenharia

Tomás Francisco Freitas Correia

Development of a medical device compatible with MRI/CT to measure ankle joint laxity

October 2022

Development of a medical device compatible with MRI/CT to measure ankle joint laxity

Tomás Francisco Freitas Correia

UMinho | 2022

Universidade do Minho
Escola de Engenharia

Tomás Francisco Freitas Correia

Development of a medical device compatible with MRI/CT to measure ankle joint laxity

Msc thesis in

Mechanical Engineering

Work done on the orientation of

Óscar Samuel Novais de Carvalho

Ana Isabel Neto Cardoso Leal

AGRADECIMENTOS

Esta dissertação apenas foi possível pelo apoio de várias pessoas e entidades que gostaria de dar uma palavra de apreço.

Em primeiro lugar, gostaria de agradecer ao Professor Filipe Samuel pela oportunidade de desenvolver a minha dissertação de mestrado no Center for Microelectromechanical Systems (CMEMs), na Universidade do Minho em parceria com a Clínica do Dragão.

Ao Professor Doutor Óscar Carvalho, pelo apoio, motivação e confiança que depositou em mim para a realização deste projeto.

À Professora Doutora Ana Leal, pela dedicação e pela partilha de conhecimento. Sem isso este trabalho não poderia ter sido levado a cabo.

Ao Doutor Renato Andrade, pela disponibilidade e pelo acolhimento e apoio que me facultou sempre que foi necessário ir à Cliníca do Dragão.

Aos meus amigos, por todos os momentos de ajuda, partilha e convívio, foi um prazer.

Por fim à minha família, pelo apoio e pelo amor que sempre me deram.

¡Sí se puede!

DECLARAÇÃO DE INTEGRIDADE

Declaro ter atuado com integridade na elaboração do presente trabalho académico e confirmo que não recorri à prática de plágio nem a qualquer forma de utilização indevida ou falsificação de informações ou resultados em nenhuma das etapas conducente à sua elaboração.
Mais declaro que conheço e que respeitei o Código de Conduta Ética da Universidade do Minho.

STATEMENT OF INTEGRITY

I declare that I have acted with integrity in the elaboration of this academic work and confirm that I have not resorted to the practice of plagiarism or any form of misuse or falsification of information or results in any of the stages leading to its preparation.
I further declare that I know and have respected the Code of Ethical Conduct of the University of Minho.

Universidade do Minho, 24 de outubro de 2022

ABSTRACT

The ankle joint in the human body experiences the most significant number of injuries across the whole musculoskeletal system, both in daily life and sports. The actual effect of the ankle's ongoing functional demand, particularly while engaging in sports that need the body to be raised off the ground regularly, is that this structure is exposed to challenging circumstances contrary to the optimal settings for balance and stability.

The analysis and diagnosis stages of these injuries are carried out during two distinct phases: a manual examination by an orthopaedist to assess the functional capacity using simulated movement and palpation of the area of peripheral pain and an imaging examination. Since the two tests are run at different times, it is challenging to combine the data. Furthermore, it is impossible to obtain the precision and repeatability needed for a procedure of this sort when using such diagnostic approaches.

That being said, Clínica do Dragão wanted to overcome these problems and needed a medical device to do the manual examination in an MRI environment. The manual exam needs to be made by a machine, and the creation of such a device is the goal of this work.

Firstly, the objectives that this device should complain with were created to define the final attributes of the equipment. Several meetings with the work group were conducted to determine the requirements that the product should respect and that would constitute the technical specifications in order to fulfil and define the project's primary aims.

The device was improved step by step for the conceptual design until a final concept could comply with all the demands of the design requirements. After developing a viable concept, the preliminary parts started to be designed until the initial design was finally fulfilled. After, the device was validated, beginning with the mechanical simulation of the different components and sub-systems until the cinematic validation of the final device.

The result is a medical device capable of linking a physical exam to a precise imaging test, such as an MRI. So, the laxity of the ankle joint may be quantified, which is beneficial for both patients and medical experts.

Keywords

Ankle Joint, Diagnosis, Medical Device, MRI, Laxity

RESUMO

A articulação do tornozelo é a articulação do corpo humano que sofre o maior número de lesões em todo o sistema musculoesquelético. A constante solicitação funcional do tornozelo, particularmente durante a prática de desporto, é que esta estrutura é exposta a circunstâncias perigosas que podem comprometer o equilíbrio e estabilidade desta articulação.

As etapas de análise e diagnóstico destas lesões são realizadas em duas fases distintas: um exame físico feito por um ortopedista para avaliar a capacidade funcional por meio de movimentos simulados e palpação da área de dor periférica, e um exame de imagem, onde a condição anatômica desta articulação é avaliada pela análise da posição relativa das diversas partes. Como os dois testes são executados em momentos diferentes, é difícil correlacionar os dados. Além disso, é impossível obter a precisão e a repetibilidade necessárias para um procedimento desse tipo ao usar tais abordagens diagnósticas.

Posto isto, a Clínica do Dragão pretendia ultrapassar estes problemas e por isso precisava de um dispositivo médico que permitisse fazer o exame manual dentro de RM. Este exame manual necessita de ser executado por um dispositivo, e a criação de tal dispositivo é o objetivo deste trabalho.

Primeiramente, foram criados os objetivos que este dispositivo deve possuir, com o intuito de definir os atributos finais do equipamento. Foram realizadas várias reuniões com o grupo de trabalho para determinar os requisitos que o dispositivo deveria respeitar e que constituiriam as especificações técnicas do projeto.

Em termos de projeto conceitual, o dispositivo foi aprimorado passo a passo até que um conceito final fosse capaz de preencher todas as especificações do projeto. Depois de desenvolver um conceito viável, as peças preliminares começaram a ser modeladas até que, finalmente, se desenvolveu o dispositivo preliminar. Após isso, foi feita a validação do mesmo, iniciando com a simulação mecânica dos diferentes componentes e subsistemas até a validação cinemática do dispositivo final.

O resultado é um dispositivo médico capaz de conciliar o exame físico a um exame de imagem preciso, como a RM. Assim, a laxidez da articulação do tornozelo pode ser quantificada, o que é benéfico tanto para pacientes quanto para especialistas médicos.

Palavras-chave

ARTICULAÇÃO DO TORNOZELO, DIAGNÓSTICO, DISPOSITIVO MÉDICO, RM, LAXIDEZ

TABLE OF CONTENTS

LIST OF FIGURES

LIST OF TABLES

List of Symbols

Initials, abbreviations and acronyms

CAD	Computer-Assisted Design
CAE	Computer-Aided Engineering
FEA	Finite Element Analysis
MRI	Magnetic Resonance Imaging
CT	Computer Tomography
PATD	Porto Ankle Testing Device
PKTD	Porto Knee Testing Device

Units

N	Newton
Nm	Newton meter
Nmm	Newton millimetre
m	Meter
mm	Millimetre
MPa	Mega Pascal

1. INTRODUCTION

1.1. MOTIVATION

Testing for ankle ligament laxity has always been a somewhat archaic and subjective process where each health professional could have a different opinion from another professional colleague when both examined the same patient. This is one of the reasons for patients with injuries in very complex areas, such as the ankle [1], often consult different experts in order to obtain a more objective assessment.

Despite all the advances that medicine has been making over the years due to the introduction of cutting-edge technologies, such as magnetic resonance, and improving treatment as a whole, there are still no deterministic methods that allow rigorously ascertaining the need for medical intervention, [1], [2].

Therefore, the objective of this dissertation is the creation/development of a device [3], [4] that tests the laxity ligaments during an MRI (Magnetic Resonance Imaging). This allows the medical team to assess laxity and determine the need for treatment and the type (operation, physiotherapy, etc.).

1.2. OBJECTIVES

This dissertation aims to develop solutions to create/ develop a medical device to measure ankle joint laxity quantitively. It is intended to carry out the device's design, modelling and virtual validation. The objectives can be defined as follows:

- Objective 1- A literature review aimed at apprehending the morphology of the ankle and knowing the types of injuries, as well as the way of testing the ligaments of this joint and understanding how to determine whether the patient needs treatment.
- Objective 2- Modelling the improvements to be implemented and changing existing geometries.
- Objective 3- Mechanical simulation of the various movements of the device in order to verify the feasibility of the conjunction of the multiple degrees of freedom and the strength of the components.

1.3. Structure of the Dissertation

This thesis aims to develop/ improve a new medical device to support the diagnosis of ankle ligament instability. This work is a very complex process because it is required to know the basics of ankle anatomy, kinematics and pathologies as diagnosis methods and all the design processes. For these reasons, this work was divided into six chapters:

Chapter 1 covers an overview of the thesis and presents the objectives, structure and contributions of this work.

Chapter 2 explains the concept of laxity, along with a brief description of this joint's ankle anatomy and kinematics. Finally, the pathologies and diagnosis methods are presented before showing the existing devices that are now being used.

Chapter 3 covers the design phase, from the definition of the objectives to the various concepts developed and, finally, the preliminary design.

In Chapter 4, the device is verified from the mechanical and kinematic points of view. Also, some geometries are changed to provide more mechanical resistance to some critical areas.

Chapter 5 briefly describes what the actuating system needs to be as well as the valve and flow regulator design. The layout of the pneumatic system is also presented.

In Chapter 6, the final device is shown with some systems that allow measuring the displacements of the foot.

Chapter 7 summarizes the conclusions of this dissertation while also giving future work perspectives.

Finally, the Gear Design is explained in the Appendix, and the technical sheet of the various materials possible to use is shown.

1.4. Contributions to this work

The first two chapters of the current thesis offer a survey of the literature and gather crucial background information. Introduction to the anatomy and function of the ankle, the laxity concept and the movements of the ankle articulation are described. The clinical methods used to diagnose ankle instability are reviewed, and the medical devices for diagnosis are explored.

The project's techniques are described and applied to all phases, from the generation of ideas to the choice of the final concept, to help design and develop the new medical equipment. This work contributes to creating a medical device capable of measuring ankle joint laxity quantitively.

2. STATE OF THE ART

This chapter will present a brief description of the anatomy of the ankle joint and expose the concept of laxity as well as the various movements that this joint allows.

Then, the different injuries that can arise will be shown, as well as the various methods of evaluating the pathologies. The differences between deterministic and non-deterministic methods will also be highlighted.

First, it is necessary to define what laxity is because this work aims to measure the laxity of the ligaments of the ankle joint. Now laxity is the relaxation of the ligaments that become loose during an accident that causes an injury. However, if the articulation is very lax, it will be necessary to undergo treatment. If this parameter is within acceptable limits, the patient will not need any intervention[1].

It is, therefore, necessary to define this factor in measurable quantities (SI units). However, measuring displacements and rotations of ligaments and/or bones with the naked eye is challenging. This is why this device has to act in the context of MRI or CT (Computerized Tomography). Thus, it is possible to carry out all the measurements required by the medical panel in order to ensure that the decision to intervene or not to intervene is correct [2].

Currently, this type of deterministic evaluation does not exist, and the assessment that is performed may have a different conclusion from doctor to doctor, which makes the definition of the severity of the injury highly subjective. The objective of this work is to help in this decision-making through the use of deterministic methods [3].

2.1. ANATOMY OF THE ANKLE JOINT

Anatomy is a science that studies the body's structures and how they work and interact with each other. In this section, it will be analysed the area in question in this work, the ankle.

First, it is essential to define the ankle and its location in the human body. The ankle corresponds to the joint existing in the connection between the foot and the leg, formed by three bones: talus, fibula and tibia [4] as shown in Figure 1.

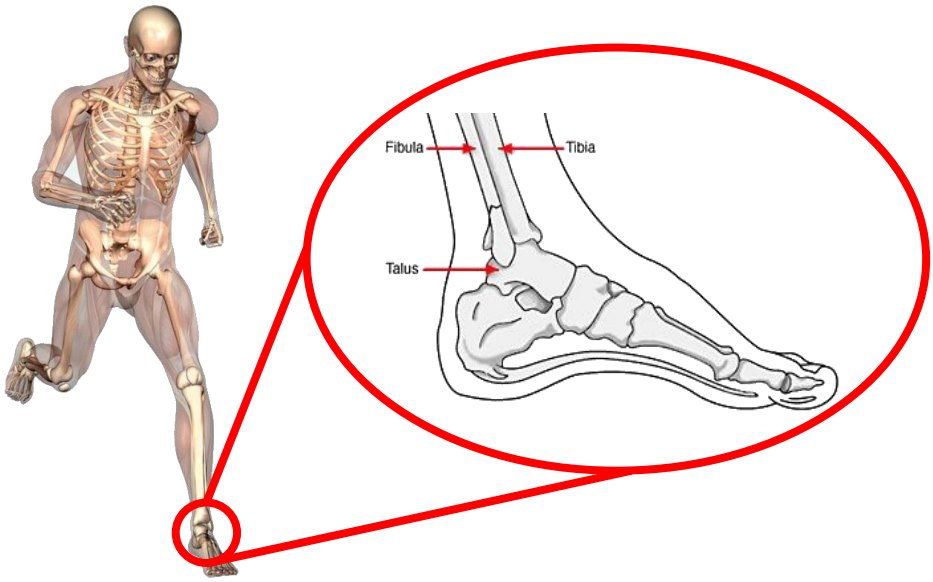

Figure 1- Ankle location.
(Adapted from [5], [6])

The talus has a cubic shape and is supported by the calcaneus, the heel bone that bears much of the impact during human locomotion [4], [7]. In contrast, the cuneiform, navicular and cuboid provide more flexibility to the foot. The tibia is a bone with a considerable length that supports much of the body's weight. It consists of a body and two ends. In the extremities, it connects to two joints, the knee and the ankle [4], [7]. Finally, the fibula is similar to the tibia, a body with two ends, whose main function is muscle fixation [4], [5] as seen in Figure 2.

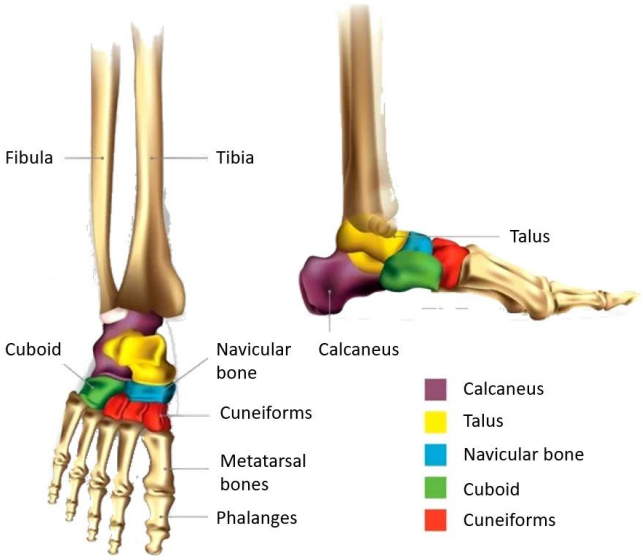

Figure 2- Nomenclature of the ankle bones.
(Adapted from [8])

Ligaments connect these bones and the rest of the foot and leg. In turn, these are activated through the muscles, thus allowing the movement of the other body parts [4], [7].

Ligaments are fibrous structures of collagen and elastic fibres. These elastic fibres allow some degree of deformation. However, they can be damaged if it is excessive. Thus, the ligaments unite the joints, stabilizing the bone sets and only allowing specific movements.

The ankle joint is made up of 4 ligaments [7], as shown in Figure 3:

- The deltoid ligament is located in the medial zone of the ankle joint.
- The anterior and posterior talofibular ligaments connect the talus to the fibula.
- The calcaneus-fibular ligament, which connects the calcaneus to the fibula.

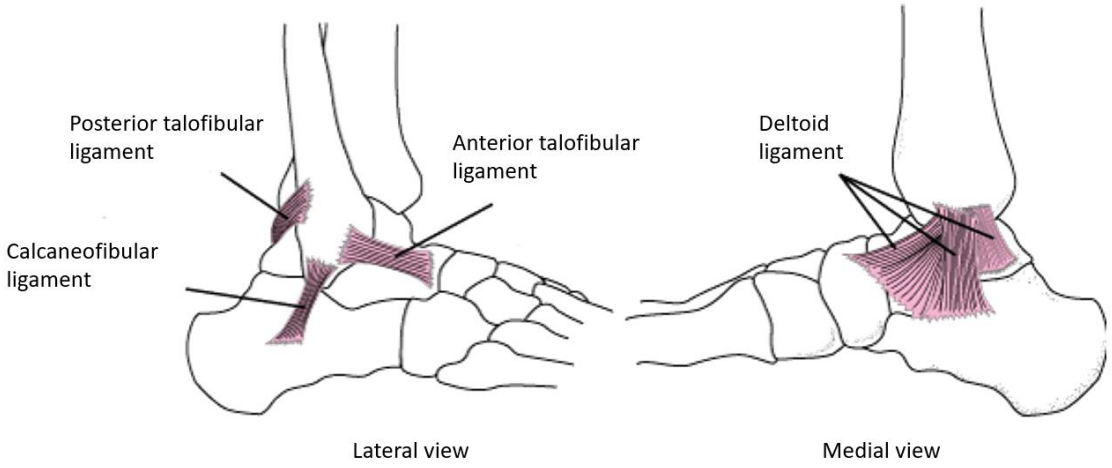

Figure 3- Location of the different ankle ligaments.
(Adapted from [9])

2.2. ANKLE KINEMATICS

So far, the anatomy of the ankle has been briefly discussed. The following section will show what types of degrees of freedom the ankle structure allows. These will be the movements that the device will have to perform in order to test the ligaments of the foot without causing or worsening the patient's injury.

First of all, it is necessary to address the convention of the principal planes of ankle movement [10]–[12].

The sagittal plane is located vertically from the front of the foot to the back, dividing the ankle into left and right zones. The frontal plane is located vertically from left to right, dividing the ankle into front and back. Finally, the transverse plane is positioned horizontally, dividing the ankle into an upper and lower zone, as schematically shown in Figure 4.

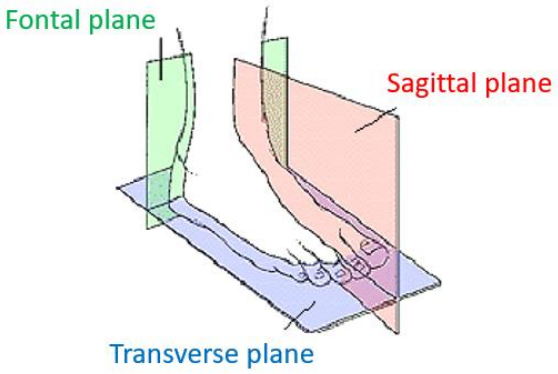

Figure 4- Ankle movement planes.
(Adapted from [13])

In terms of axes, see Figure 5.

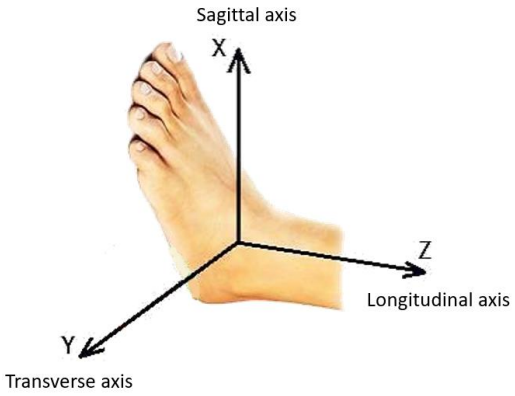

Figure 5- Ankle joint axis.
(Adapted from [14])

Now that the different agreed planes and axes have been addressed, the various degrees of freedom of the ankle will be shown [15], [16]. The ankle allows six movements that are performed in a single plane along an axis. Thus, the intersection of the various axes, the origin, is located in the centre of the ankle. This centre of rotation must be respected so that the movements performed are passive. The allowed motions are:

- Abduction and Adduction.
- Inversion and Eversion.
- Dorsal and Plantar Flexion.

The abduction and adduction movements are carried out along the longitudinal axis, thus located in the transverse plane [17]. In abduction, the foot rotates laterally in the negative direction, while in adduction, the foot rotates in the positive direction of the axis [17], Figure 6.

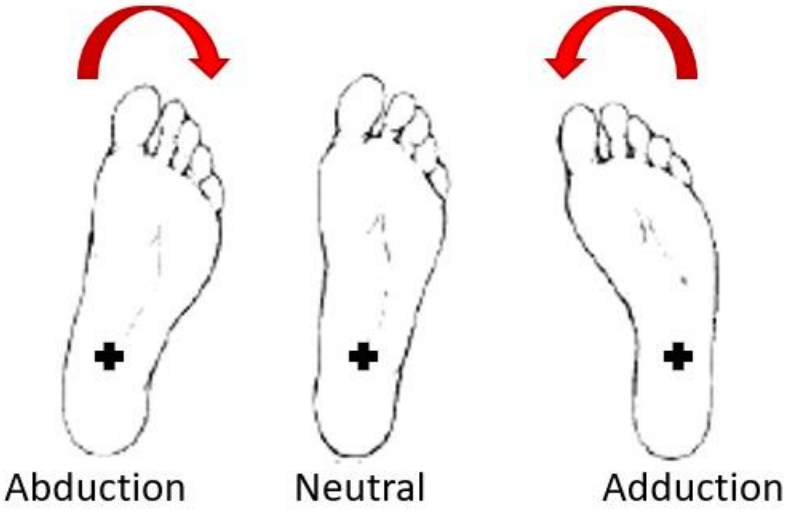

Figure 6- Representation of abduction and adduction movements (top view of the right foot).
(Adapted from [13])

In contrast, inversion and eversion movements are carried out along the sagittal axis, located in the frontal plane. In eversion, the foot rotates in the positive direction of the transverse and longitudinal axes (inwards and upwards). In an inversion, the foot rotates in the negative direction of the transverse axis and the positive direction of the longitudinal axis [11], [16] (outwards and upwards), Figure 7.

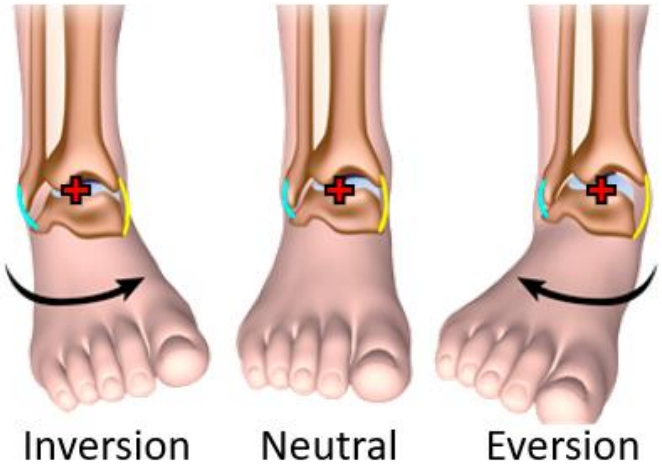

Figure 7- Representation of inversion and eversion movements.
(Adapted from [18])

Finally, the ankle allows dorsiflexion and plantar flexion to be carried out along the transverse axis located in the sagittal plane. In dorsiflexion, the foot rotates and moves in the positive direction of the sagittal axis (up), while in plantar flexion, it moves in the opposite direction (down) [10], [15], Figure 8.

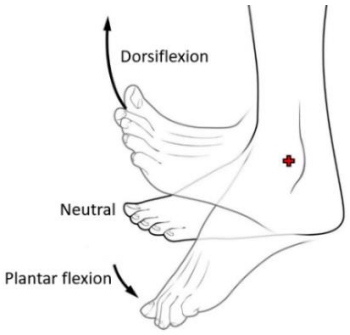

Figure 8- Representation of dorsiflexion and plantar flexion movements.
(Adapted from [19])

2.3. PATHOLOGIES AND METHODS OF INJURY EVALUATION

Knowing the different types of movement that the ankle joint can develop, the main associated pathologies will be presented, as well as the existing methods to detect them and obtain the need for intervention.

The three most common types of ankle injuries are [20]–[25]:

- Lateral sprain.
- Medial sprain.
- Lateral rotation.

The first is the most common [26]–[30]. The lateral sprain happens when the foot rotates inwards (rotation along the sagittal axis in the positive direction), Figure 9. The injured ligaments are the external ones, namely the posterior and anterior talofibular ligaments and the calcaneofibular ligament.

A medial sprain, like a lateral sprain, corresponds to a rotation of the foot along the sagittal axis but in the opposite direction (negative) [25], [31]. Therefore, it can be said that this lesion is identified by the excessive movement of the foot inwards, Figure 10. The most damaged ligament is the deltoid ligament.

Finally, there is lateral rotation, which is a rotation of the leg about the foot [32], [33](longitudinal axis in the negative direction) in which the most injured ligament is the anterior tibiofibular ligament, Figure 11. The occurrence of one of these injuries causes pain and requires a rigorous evaluation in order to determine the need for treatment or not. So far, the anatomy, kinematics and main pathologies of this joint have been presented, and the different methods for evaluating these injuries will be discussed.

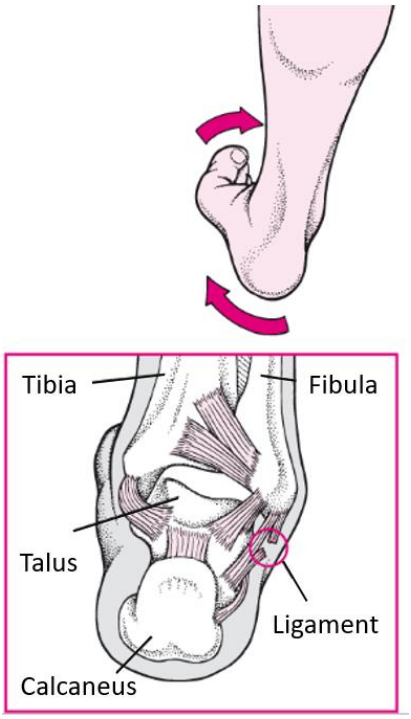

Figure 9- Schematic representation of a lateral sprain.
(Adapted from [34])

Figure 10- Schematic representation of medial sprain.
(Adapted from [35])

Figure 11- Schematic representation of lateral rotation.
(Adapted from [35])

Although injuries to the ankle joint are frequent and make it impossible to perform physical activity, there is still not a single path accepted by all institutions regarding the approach to be followed. The most serious problem lies in defining the best way forward for effective treatment. This difficulty is amplified by unclear and objective diagnostic methods, as in terms of intervention, existing treatments are quite capable [30].

The most used method is also the most traditional, the physical examination. In this exam, the doctor performs a series of movements to the foot based on the type of injury suffered [36]–[38]. Since displacements or rotations are not measured in this exam, the entire assessment is subject to the criterion of a natural person. However, this type of assessment can be dubious as it is qualitative.

During the exam, two types of tests are performed:

- Anterior drawer test.
- Varus stress test.

In the first, the examiner fixes the lower end of the tibia with one hand, and the other grasps the heel. It performs an anterior displacement of the astragalus about the tibia [39]–[50], Figure 12. With this test, the integrity of the tibiofibular ligaments is assessed. If the displacement is 10 mm above the average value, then it is considered that there is mechanical instability (laxity). The anterior drawer test evaluates the condition of the talofibular ligament and is therefore not used as much as these ligaments are only damaged in severe injuries [51].

Figure 12- Schematic representation of the anterior drawer test.
(Adapted from [52])

In the second test, the examiner performs the inversion movement evaluating the condition of the lateral ligaments. In this, the examiner immobilizes the lower leg with one hand and, with the other, acts while holding the calcaneus [47], [51], Figure 13.

Figure 13- Schematic representation of the varus stress test.
(Adapted from [52])

As a reference, it is considered that if the rotation is 10° higher than the average value, then there is joint instability and medical intervention is necessary [40]–[46], [48]–[51].

It is common in the physical examination to perform one last test, known as medial or lateral rotation, where the external ligaments responsible for stabilizing the foot when performing these movements are evaluated.

In addition to the physical examination, there are imaging tests such as magnetic resonance imaging (MRI), computed axial tomography (CAT) or radiography.

Radiography, commonly known as X-ray, is the most used exam as it allows the detection of bone fractures and is also the least expensive.

When visualizing soft tissues such as ligaments, tendons or cartilage, the ideal exam is MRI, which also allows the visualization of different planes, that is, various sections of the foot section. This tool is handy in the diagnostic phase [53]–[55].

Finally, there are still devices that simulate the physical examination performed by the examiner. These devices aim to improve diagnostic accuracy and make the conclusions of each examiner similar for the same patient. The most well-known device is the Telos Stress Device [56] during an X-ray. The significant disadvantage is that this device that intends to evaluate soft tissues is not compatible with MRI, the most suitable imaging exam for such tissues, Figure 14.

Figure 14- Telos Stress Device.
(Adapted from [57])

In terms of devices, this is the only one in the industry. However, due to the presented limitations, no device aims to compete with the one that will be designed in this thesis.

2.4. SUMMARY AND DISCUSSION

Now that all significant aspects have been covered, it can be said that the essential thing to carry out for the design phase is the kinematics of this joint. This information is crucial as the device needs to recreate these specific movements smoothly.

Also, understanding how the physical examination is made is relevant because the device needs to make the physical exam that a doctor makes while respecting the kinematics of the joint and while being suited for a very different range of foot sizes which is particularly challenging.

The devices available on the market don't compare to this one as what this medical equipment wants to accomplish is much more complex and helpful in the diagnostic phase than everything that exists.

Suppose the device can respect the kinematics of the joint. In that case, the evaluation of the injuries will be made correctly, the main goal of the thesis will be accomplished, and for the first time, there will be a way to assess the condition of the ankle deterministically.

3. PORTO ANKLE TESTING DEVICE DESIGN

3.1. PROBLEM DESCRIPTION

A medical device is any instrument, device or equipment destined to be used in the human body. Depending on the device's objective, these devices can be used in any phase of the diagnosis or treatment. In this case, the main goal is to help in the diagnosis phase to measure ankle joint laxity [58], [59]. This process is not very accurate. A doctor may believe that a patient needs some intervention, which means that an operation or other treatments will be necessary, and another thinks it is unnecessary [60]. The *Porto Ankle Testing Device (PATD)* wants to come in the diagnosis phase to help doctors determine the best treatment. To allow this to happen, *Clínica do Dragão* wants this device to replicate the exam that the doctor does on the patients in the MRI environment. This means that the medical team can then visualise the various tissues, ligaments and bones and evaluate if the displacements that have occurred are acceptable or not.

There is already a device, but this does not allow all the tests needed, and for this reason, there is a necessity to improve it or change it entirely to reach the goal of this thesis [58]

3.2. OBJECTIVES DEFINITION

To define the objectives of the device, a concept called an objectives tree which is composed of several levels where the higher ranks indicate a goal of more considerable relevance, and the lower levels indicate an objective of minor significance.

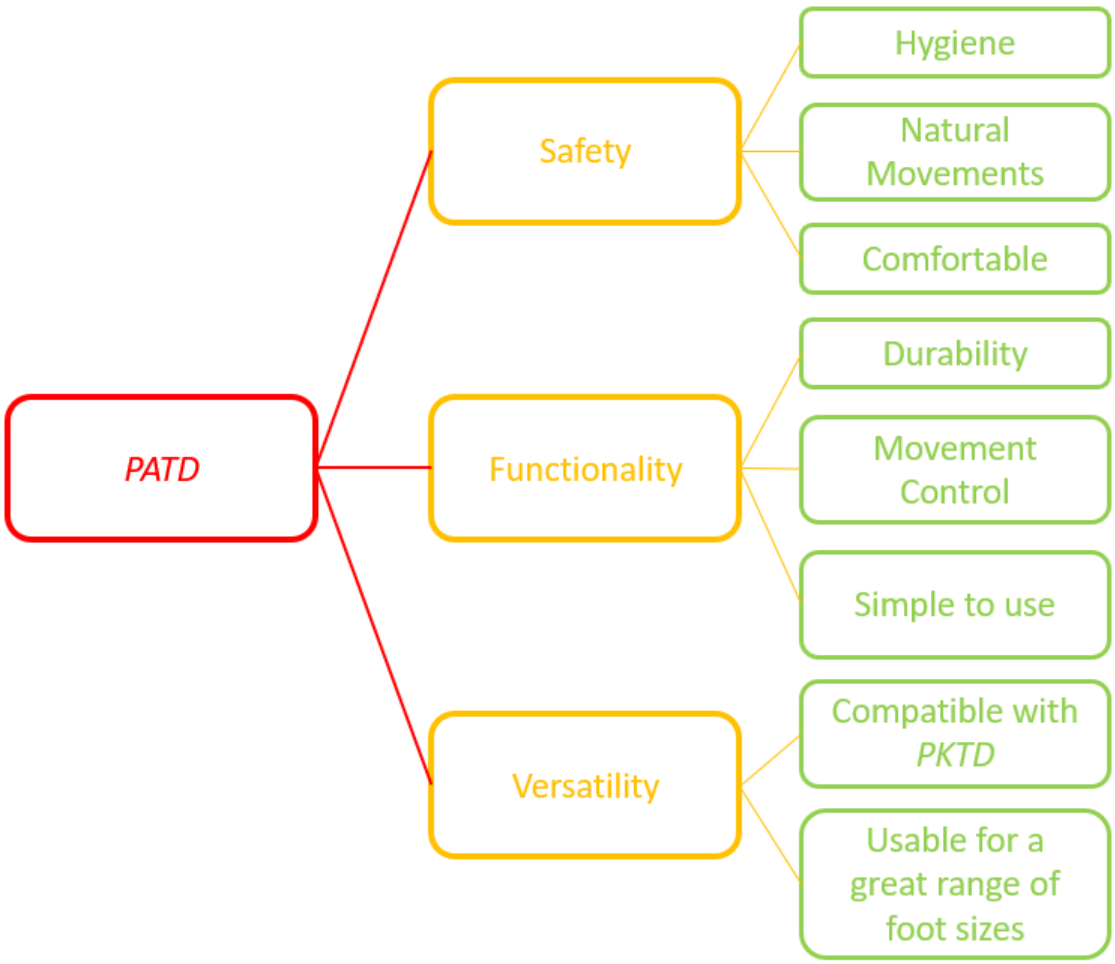

Figure 15- Objective tree of the *PATD*

In synthesis, it can be said that the main objectives are the main features related to the device's safety, functionality and versatility.

The first, safety, is more on the scope of not hurting the foot (comfort and natural movements), allowing the patient to make the exam without pain. The natural movement side is related to the fact that the movement of the device needs to be as close to the natural movement of the foot as possible. This will make sure that the injury does not worsen. The hygiene part of this objective is to ensure there isn't any contamination because the medical environment needs to be extremely clean.

The second objective, functionality, is perhaps the most important. This objective indicates that the device needs to be durable (not break with any minor misuse) and allow control of the various movements that will be made to the foot because the device aims to test the ligaments, not deteriorate the injury. It also needs to be easy to use because the MRI is extraordinarily costly, so the device has to be easy to operate.

Finally, the *PATD* has to be versatile. This means it must be compatible with the PKTD and usable for very different people with very different feet, making the device very appealing for customers that can purchase a product that can test both knee and ankle.

3.3. DESIGN REQUIREMENTS

The objectives definition is beneficial to understand what is required from the final solution, which also helps to define the project requirements more clearly. This is because these objectives are still unclear from an engineering point of view, and they need to be more specific.

In this regard, there were various conversations with professionals from *Clínica do Dragão* and some visits to the facilities to understand how the exam was realized and the exam environment. This was super important because it allowed us to judge better the conditions in which this device needs to operate.

That being said, the design requirements were defined from the objectives tree and the requirements discussed and demanded by *Clínica do Dragão.* They can be seen in Table 1.

Table 1- Design requirements.

1	It must be used during a clinical exam
2	It can evaluate the functional condition of the ankle ligament structure
3	It can evaluate the existence of joint instability
4	It must perform movements passively on the foot
5	The movements are controlled by a health technician
6	The device doesn't affect the characteristic hygiene of the medical environment
7	It can be used in the MRI/CT environment
8	The presence of the *PATD* doesn't affect the exam
9	It is compatible with the *PKTD*
10	It has an intuitive usage process
11	It can be used in the majority of the patients
12	It is quickly prepared for the exam

Next, a brief description of each requirement will be presented

1. It must be used during a clinical exam

This device must be used during the examination process of a patient with an injury in the ankle joint. It can be used in the diagnosis phase and in the post-operation step to assess the result of the

intervention. It also needs to be capable of testing both the left and right foot, as it is common to compare to injured ankle with the healthy one.

2. It can evaluate the functional condition of the ankle ligament structure

To be able to attend to this requirement, the device must be capable of doing all the movements pretended by the customer.

3. It can evaluate the existence of joint instability

This requirement is linked to the previous one; however, this one pretends to emphasize the fact that the device needs to assess, or in other words, measure. This way, the device will need to have graduated rules that allow measuring the displacements.

4. It must perform movements passively on the foot

This requirement intends to highlight that foot movement needs to be as natural as it can be because if not, the device can hurt and injure the patient.

5. The movements are controlled by a health technician

This means that the technician can choose the sequence of movements the patient will be subjected to and can easily control the device.

6. The device doesn't affect the characteristic hygiene of the medical environment

The device should not be made from materials compatible with the medical environment, such as polymers, metals that don't oxidate, etc.

7. It can be used in the MRI/CT environment

The MRI/CT are the best exams available to evaluate the ligaments' condition, and one of the main objectives of this thesis is to combine the physical exam with the imaging exam. This implies that the device must fit MRI and CT devices.

8. The presence of the *PATD* doesn't affect the exam.

In the MRI environment, materials that interfere with the electromagnetic field created during the exam cannot be used, such as iron, cobalt and nickel. The presence of elements that interfere with the electromagnetic field creates an attraction or repulsion phenomenon that can injury the patient.

9. It is compatible with the *PKTD.*

This device must be compatible with the PKTD. This means that they must link with each other, and this way, they can be sold together.

10. It has an intuitive usage process

As the PATD will be used by the technician responsible for the exam and they have education in the field of health, it can be thought that they don t know how to operate mechanical systems. That being said, the device operation must be accessible and intuitive, generating no confusion at the exam moment.

11. It can be used in the majority of the patients

This medical device is intended to be commercialized all over the world. For this reason, it must be capable of evaluating very different feet from people of different origins. Also, it needs to be able to test patients with disparate anthropometric measurements.

12. It is quickly prepared for the exam

The procedure for performing an MRI examination is already a relatively lengthy process. The technician must interrupt the exam to position the ankle in the desired stance and then capture the image. If the process of preparing the device is too lengthy and complex, the device could lose customers' interest.

3.4. TECHNICAL SPECIFICATIONS DEFINITION

The initially defined objectives are sometimes called design specifications, which is not correct because they only manifest affirmations of what the project should accomplish and do not impose either limitation on the mechanical project.

After that, the technical specifications were defined based on the design requirements list. These technical specifications translate from the engineering point of view boundary conditions and the functionalities that the device must have. These boundaries should be accurate because if they are too tight, there will be very few solutions, and if they are too wide, the choice of solutions will be challenging.

Table 2- Technical specifications

1	Perform the exam for both the left and right foot
2	Abduction movement from 0 to 60 degrees
3	Adduction movement from 0 to 60 degrees
4	Eversion movement from 0 to 60 degrees
5	Inversion movement from 0 to 60 degrees
6	Anterior translation of the astragalus up to 28 mm
7	It must be able to develop the above movements independently
8	It must be able to realize the abduction and adduction movements together with the anterior translation of the astragalus
9	Ankle dorsiflexion/plantar flexion angle adjustment (-15°, 0° and 15°) for foot positioning
10	The leg and foot fixation zone cannot affect motion transmission and cannot cause patient discomfort or pain
11	The fixation mechanism mustn't affect the foot movement
12	The mechanical system of manual drive
13	Need to fit in the MRI machine
14	Cannot be made of electromagnetic materials
15	Adjustment to the anthropometric needs of each patient
16	Does not cause any discomfort to the patient during the examination
17	PKTD is compatible with lower limb support and positioning

These technical specifications are referent to the device as a whole. Still, each component should also obey some geometric and dimensional character requirements so that these components can be integrated with the final device.

After this process, where all the needed specifications are defined, the concept design can be started.

3.5. Evolution of Concepts

Given the clinical and technical specifications this device needs, the work started by inspecting which ones the initial device already had, Figure 16.

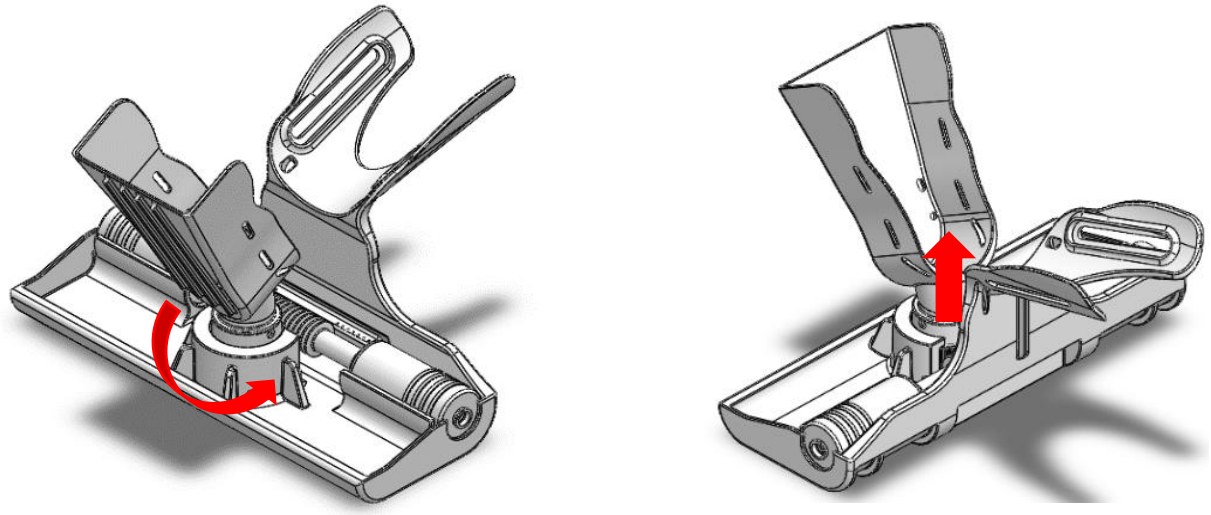

Figure 16- PATD version 1.0.

The initial device complies with the design requirements. Still, regarding the technical specifications, it falls short of expectations since it does not allow any rotation or adjustment of the dorsiflexion/plantarflexion angle of the foot. It only complies with the movement eversion/inversion and anterior translation of the astragalus.

It was also found a problem of fixation of the tibia that is uncomfortable for the patient since, in previous tests with the previous prototype, the patient sometimes does not support the anterior translation test in its entirety (i.e., in the total excursion) due to discomfort at the tibial attachment site. It should also be noted that the eversion and inversion movements are abrupt and must be refined. All of these considerations were found by Clínica do Dragão while testing the PATD version 1.0.

Therefore, it started by devising a system that would respond to all the most relevant specifications, allowing all the movements in the technical specifications. Next, an exploded view of the created set is shown in order to identify all the components, Figure 17.

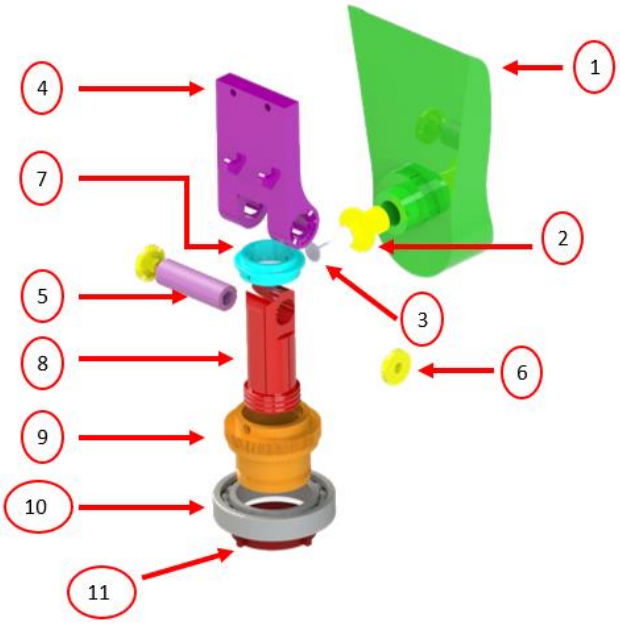

Figure 17- Exploded view of version 2.0 of the PATD.

Table 3- List of components of the 2.0 version of the PATD

Nº of the component	Designation
1	Foot support
2	Bushing
3	Rotation shaft
4	PP connection
5	Fixation shaft
6	Block
7	Cylinder cover
8	Piston
9	Vertical cylinder
10	Polymer bearing
11	Nut

In this way, an angle adjustment was started to be incorporated to allow the regular position of the foot according to the type of examination.

This system consists of parts 5 and 6. Shaft 5 is fixed to piston 8 through the slots. Locks 6, in turn, fit into the extruded hexagon on shaft 5, so they do not rotate either. They only allow adjusting the angle of piece 4, employing its translation. Once a screw crosses the centre of the three parts, and as all

the parts tighten, all the components stand together and find themselves immobilized in the pneumatic cylinder. First the entire system is locked in the desired position, Figure 18.

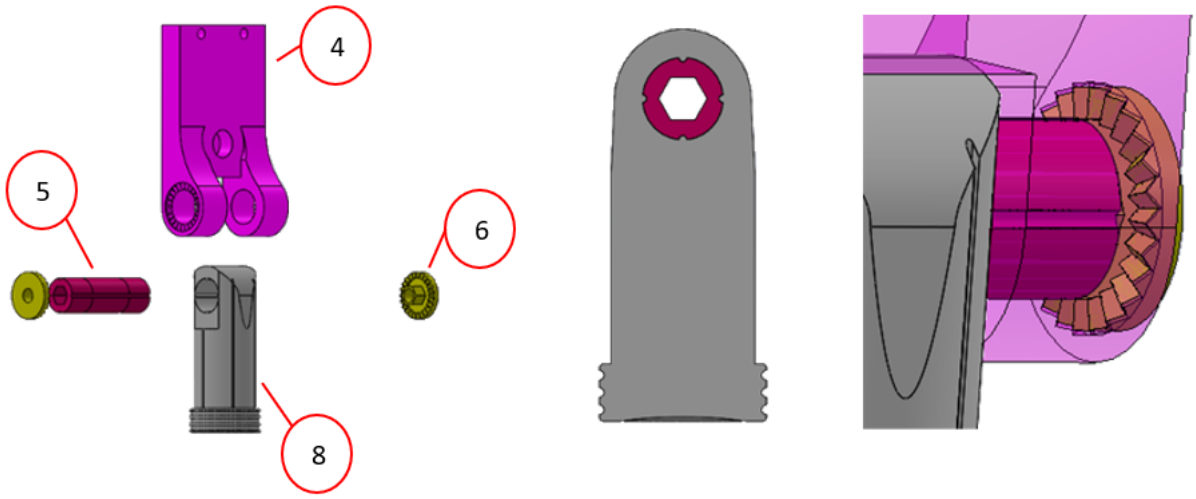

Figure 18- Exploded view of the set that allows angle adjustment (on the left). Cutaway view of the lilac shaft fitted to the cylinder piston (in the centre). Detail of the angle lock system (right).

Then one rotating shaft support was added to the foot support piece so that rotational movement is possible, Figure 19. A sprocket was also added to enable this movement to be driven by a pneumatic cylinder that would be installed later.

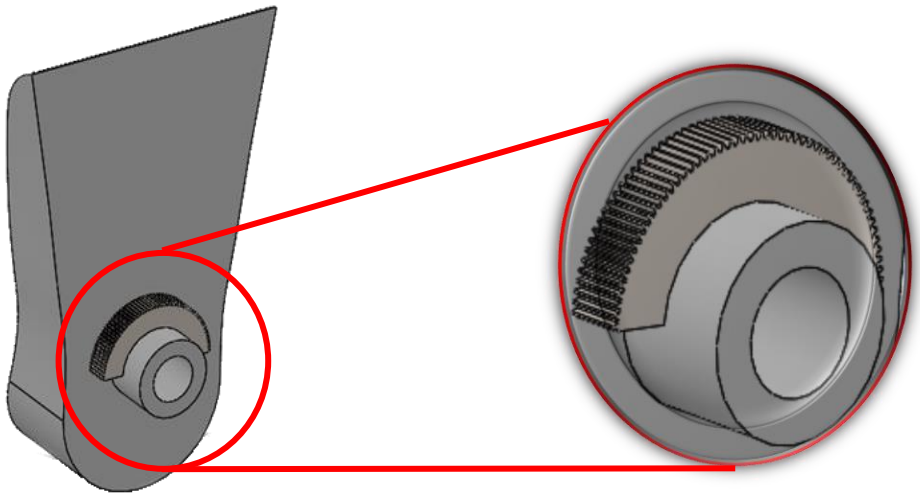

Figure 19- Addition of rotating shaft support and a sprocket.

Finally, a polymeric bearing was added to the cylinder responsible for the anterior translation of the astragalus to smoothen the eversion/inversion movement.

The toothed wheel installed in the cylinder was also modified, decreasing the toothed module and aiming at smoothing this action. The result is PATD version 2.0, Figure 20.

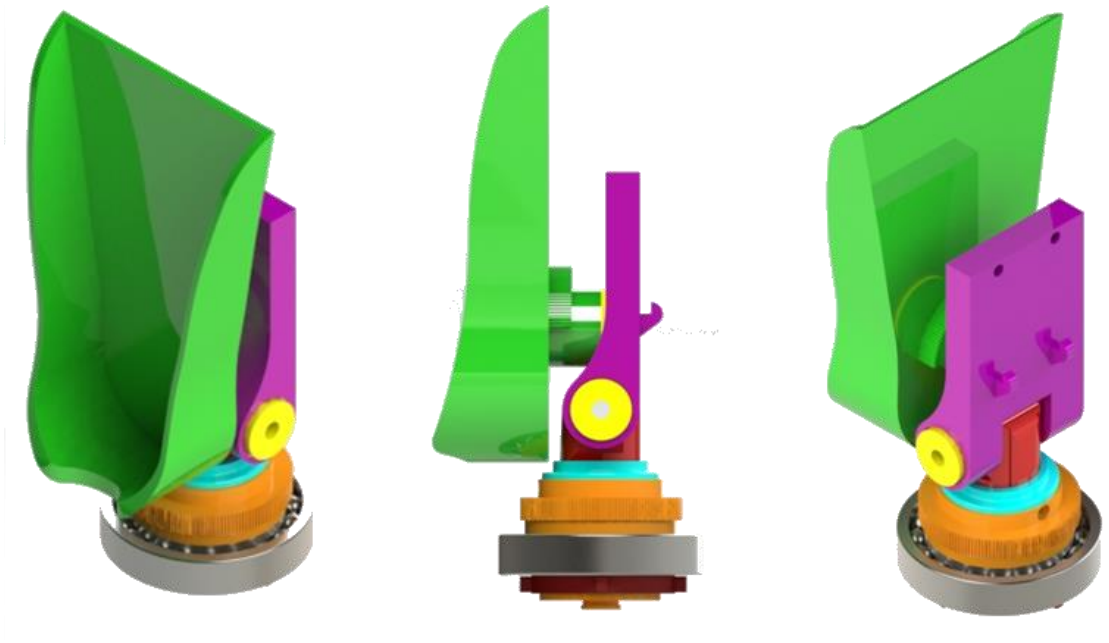

Figure 20- Version 2.0 of the PATD.

This solution has, however, a problem. It does not respect the centre of rotation of the foot located in the ankle area. Thus, foot angle adjustment movements, as well as eversion/inversion, do not cause passive movement of the foot as the movement is not the natural movement of the joint, Figure 5.

Therefore, this limitation was corrected by changing the component that connects the cylinder shaft to the foot support, Figure 21.

Figure 21- Version 2.1 of the PATD.

This solution is similar to the previous one, except for part 4. However, solving the centre of rotation of the eversion/inversion movement does not solve the fact that when adjusting the angle of the foot, it does not move according to the centre of rotation of the foot. This makes the whole leg rise when the foot angle is changed. When the leg goes up, as the tibia is fixed, the patient will feel enormous discomfort which may even worsen the patient's injury.

Therefore, it was necessary to develop an angle adjustment that allows the angle adjustment according to the foot's natural movement. The developed system is based on creating an arc of circumference from the ankle, Figure 22.

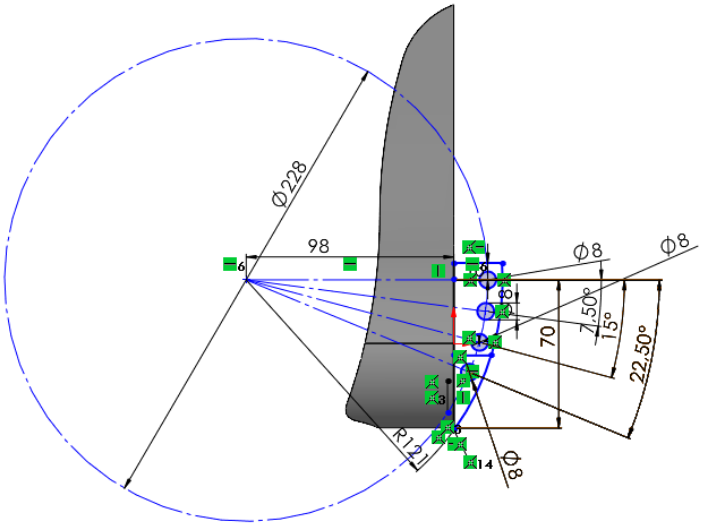

Figure 22- Sketch used to model the foot angle adjustment.

The result is a support with a semi-circular track, and a new component dubbed the 'angle adjustment' also with a semi-circular surface where part 1 slides and allows the adjustment of the foot angle to the angles intended by the examiner, Figure 23.

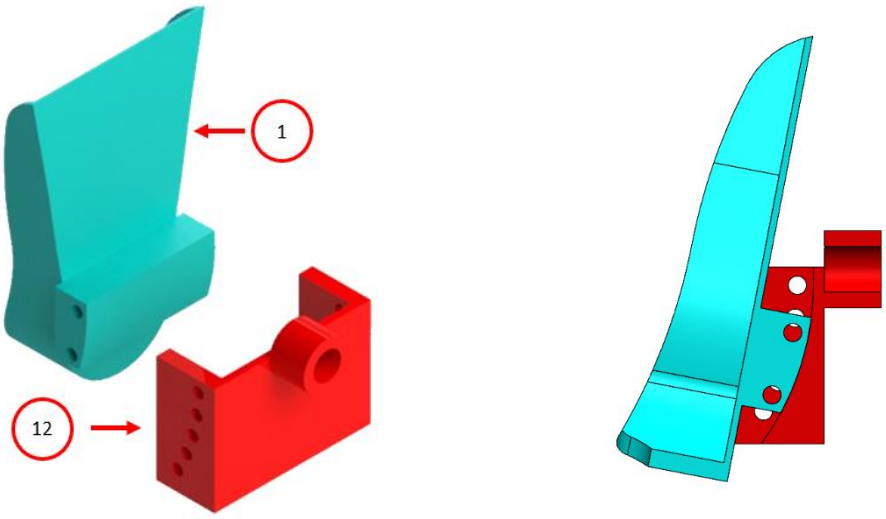

Figure 23- Idealized angle adjustment system.

Table 4- List of components added to version 2.2 of the PATD.

Nº of the component	Designation
1	Foot support
12	Angle adjustment

Thus, component 1 slides over an arc of circumference centred on the ankle and reproduces the joint's natural movement, Figure 23.

This third concept, Figure 23 and Table 4, seems to fulfil all the design specifications. However, it falls short in terms of integration in the PKTD as the foot; therefore, the tibia's support is too high and does not allow mounting on the mentioned device, Figure 24.

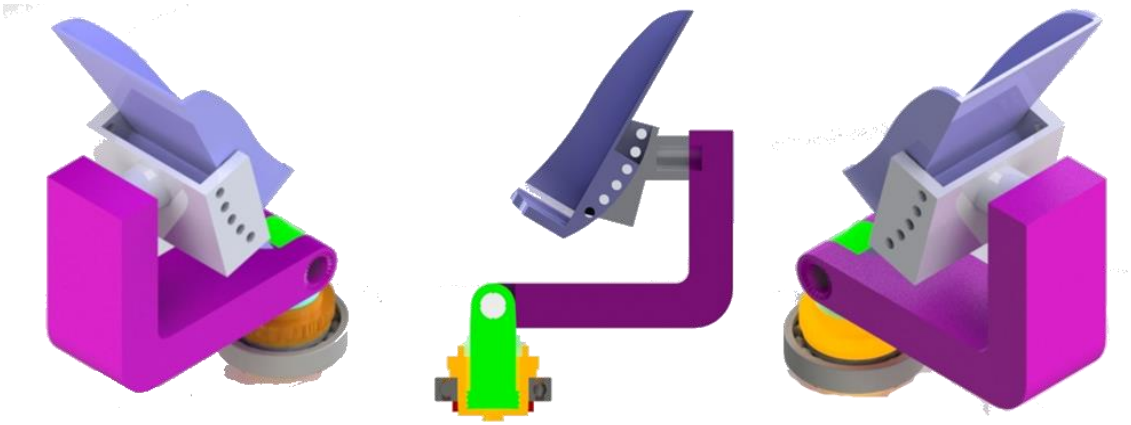

Figure 24- Version 2.3 of the PATD.

In order to respond to the complex set of constraints combined with the movements that the device needs to provide, it was necessary to develop more radical concepts that visually modify significantly the initial device, Figure 24 and Table 5.

Table 5- PATD version 3.0 component list.

Nº of the component	Designation
1	Base
2	Lifting table
3	PP connection
4	Angle adjustment
5	Foot support
6	Vertical cylinder
7	Polymer bearing

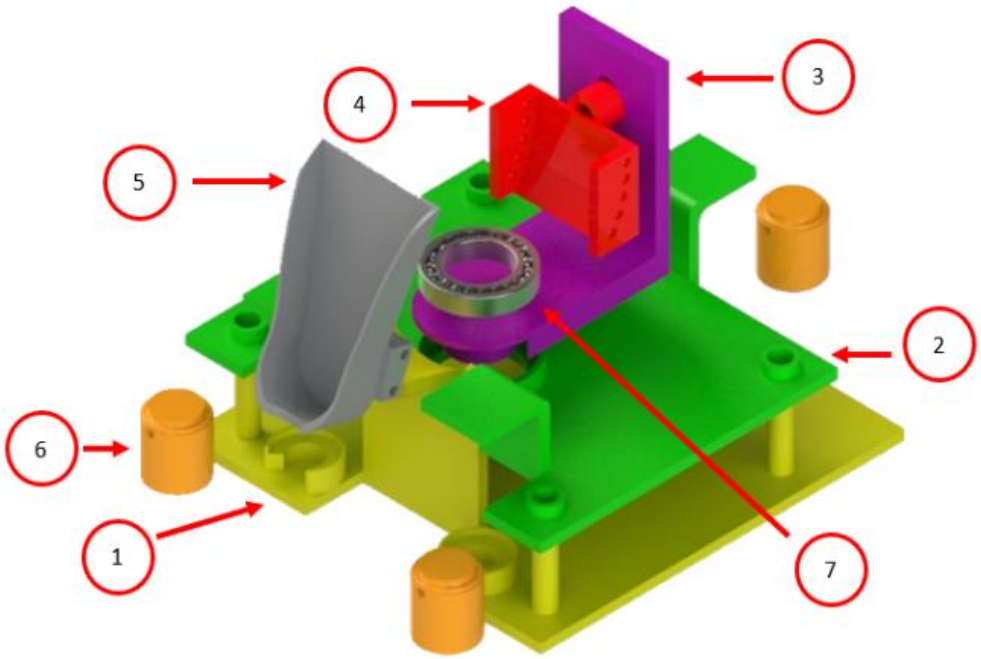

Figure 25- Exploded view of the 3.0 version of the PATD.

This first solution found, which verifies all the design specifications, applies a lift table concept where the remaining movements (rotation and inversion/eversion) are performed on the lift table, Figure 25. This system, fulfilling all the project specifications, is more expensive in terms of material and pneumatics since it uses two more cylinders than strictly necessary, Figure 26.

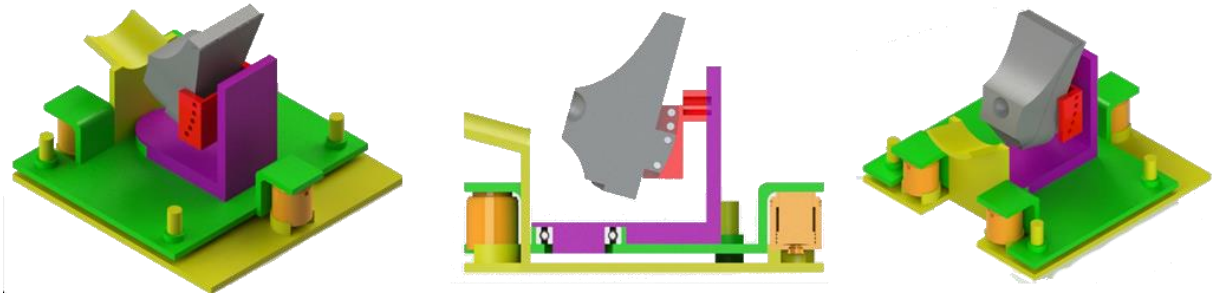

Figure 26- Version 3.0 of the PATD.

For that reason, this solution was simplified to reduce the number of components and the amount of material needed to manufacture the device. This new concept also reduces the number of pneumatic actuators required, reducing costs in the pneumatic system, Figure 27 and Table 6.

This concept fulfils all project requirements as well as all technical specifications. Therefore, this will be the concept to be explored in future works, developing all the components in detail and installing the entire pneumatic circuit that will be responsible for triggering the various necessary movements.

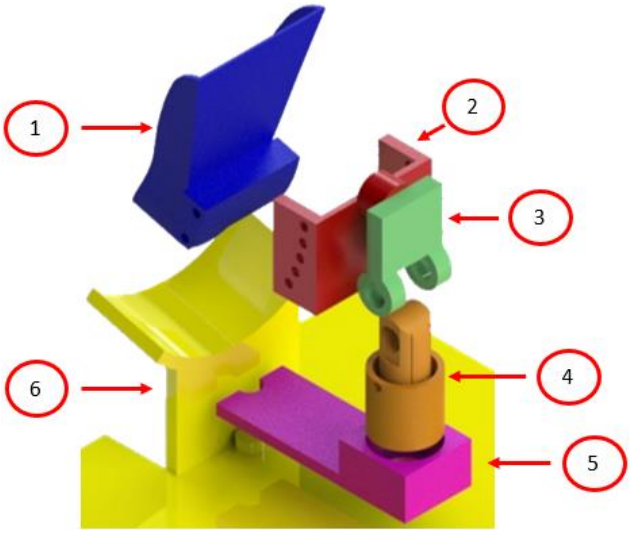

Figure 27- Exploded view of the 4.0 version of the PATD.

Table 6- Component list of the 4.0 version of the PATD.

Nº of the component	Designation
1	Foot support
2	Angle adjustment
3	I connection
4	Vertical cylinder
5	L connection
6	Base

This latest version meets all specifications; however, the technical specifications were changed after the development of this concept, and therefore the translation movement has changed. Before, this movement had a vertical direction. Still, after more orthopaedic specialists observed the concept, they understood that the upward movement has to be carried out parallel to the foot. Therefore component 4, the vertical cylinder, must be positioned at a different angle. This concept supports this change, so this aspect does not become relevant for this stage of development, Figure 28.

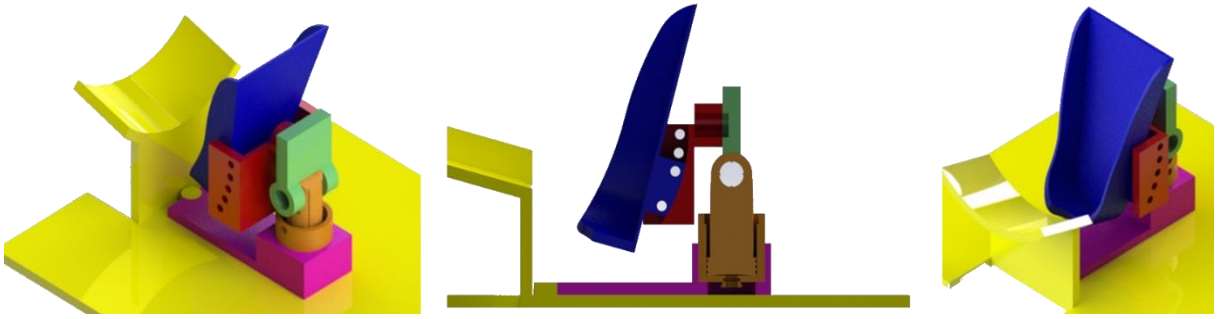

Figure 28- Version 4.0 of the PATD.

The movements contemplated in version 4.0 of the PATD are schematically represented in Figures 29, 30 and 31.

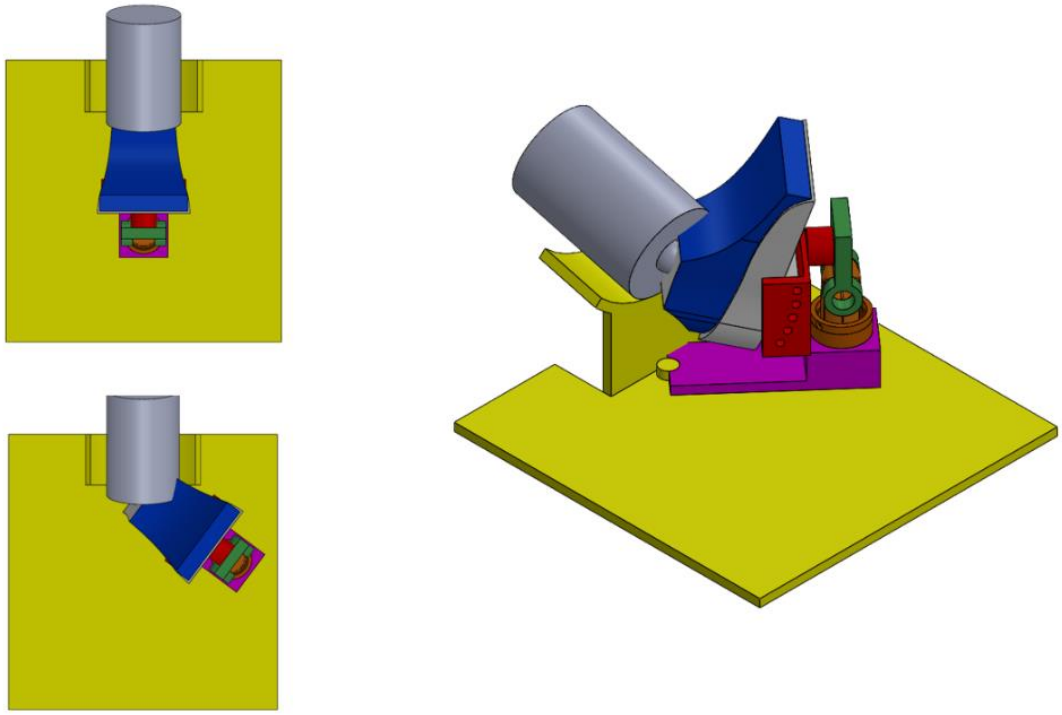

Figure 29- Schematic view of the inversion/eversion movement of PATD version 4.0.

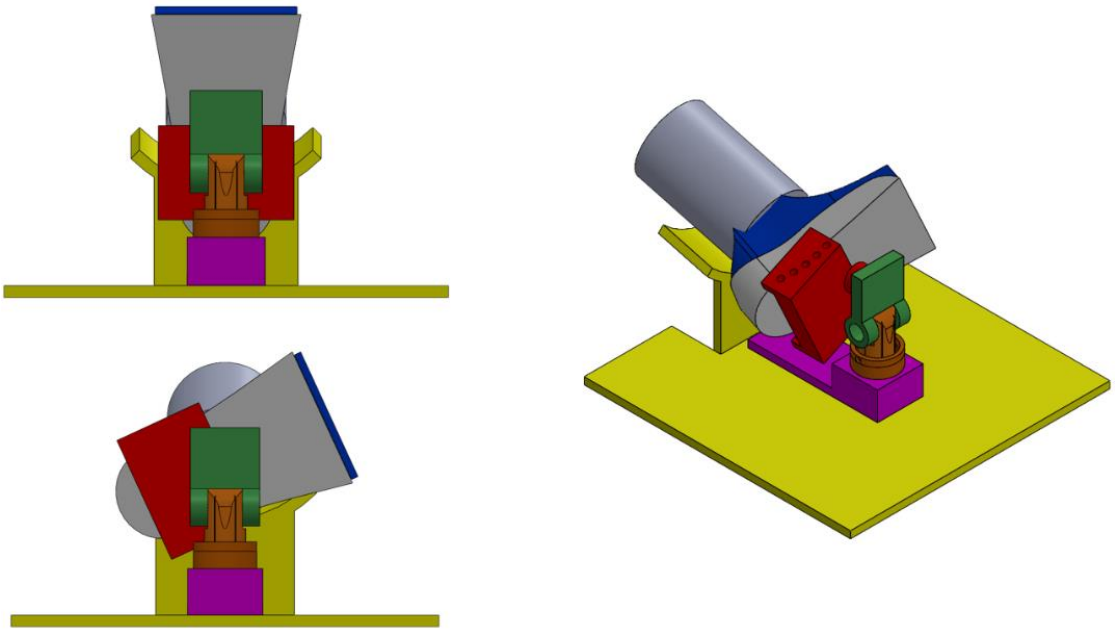

Figure 30- Schematic view of the abduction/adduction movement of PATD version 4.0.

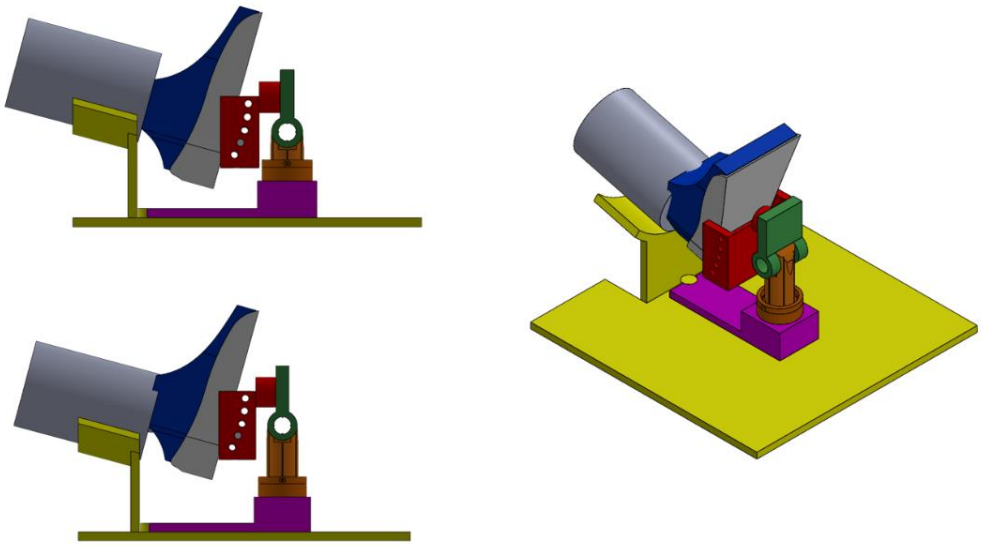

Figure 31- Schematic view of the anterior translation movement of PATD version 4.0.

Another relevant aspect is the fixation of the tibia. For this, the helmet manufacturing industry was used, and the best helmet-tightening systems were verified. It was noticed that the best type of grip is the "Double D", Figure 32.

Figure 32- Fastening belt with "double D" clasp.

It should be mentioned that the closure cannot be magnetic to respect the project specifications.

3.6. PRELIMINARY DESIGN

Having determined the concept, it was necessary to concretize the different components in preliminary parts. This is because after defining the components, it will be necessary to carry out mechanical simulations to verify the deformations and stresses and understand if the various components can withstand the different demands to which they will be subjected.

Initially, it started by designing the base (this model does not contain the tibia support yet, as this has to be positioned according to the exact location of the foot support), which includes the cylinder supports responsible for carrying out the inversion/ eversion movement and a threaded rod to support one bearing. The device's centre of rotation will coincide with an axis concentric with the bearing support since this axis is the axis along which the inversion/eversion movement will be carried out. It should be noted that the bearing will not contact the base except for the ring-shaped around the bearing support rod, Figure 33.

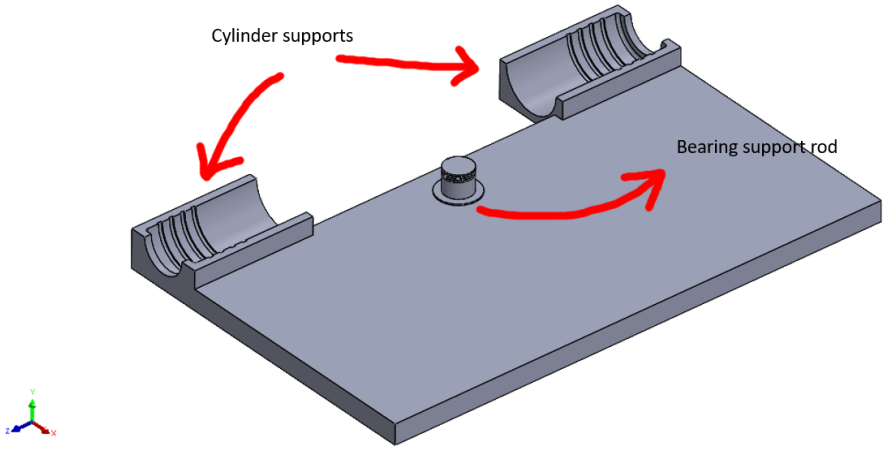

Figure 33- Base component of PATD version 1.4.

Next, the component supporting the cylinder responsible for the translation movement was designed. This part has several component housings, including accommodation for a bearing, four for transfer spheres (only two are visible because the image is a section in the mid-plane of the part) and the housing for the anterior translation cylinder, Figure 34. The angle of this cylinder was adjusted comparatively to the one shown in the final concept according to the indication of the medical panel of *Clínica do Dragão*.

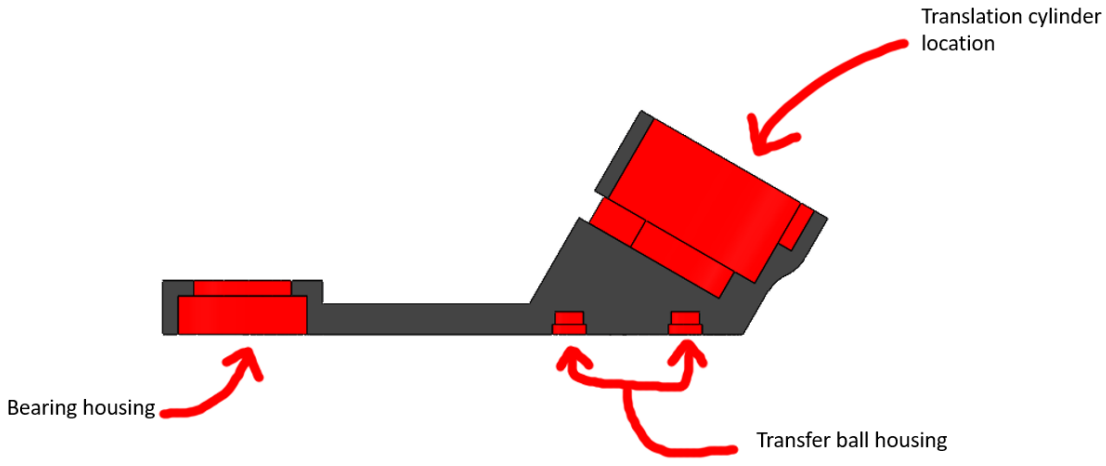

Figure 34- Section view of the L connection of PATD version 4.0.

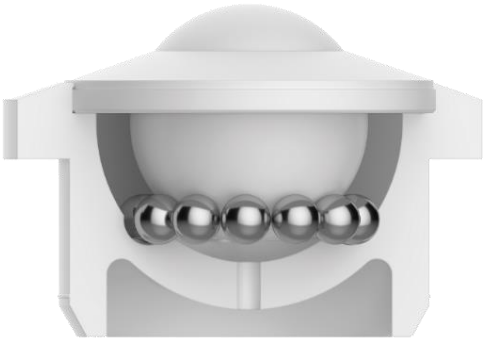

Figure 35- Transfer spheres (section view of the midplane of the part).

Finally, the gear that will allow the inversion/eversion movement was added, Figure 36. The calculation of the gears is shown is Appendix A.

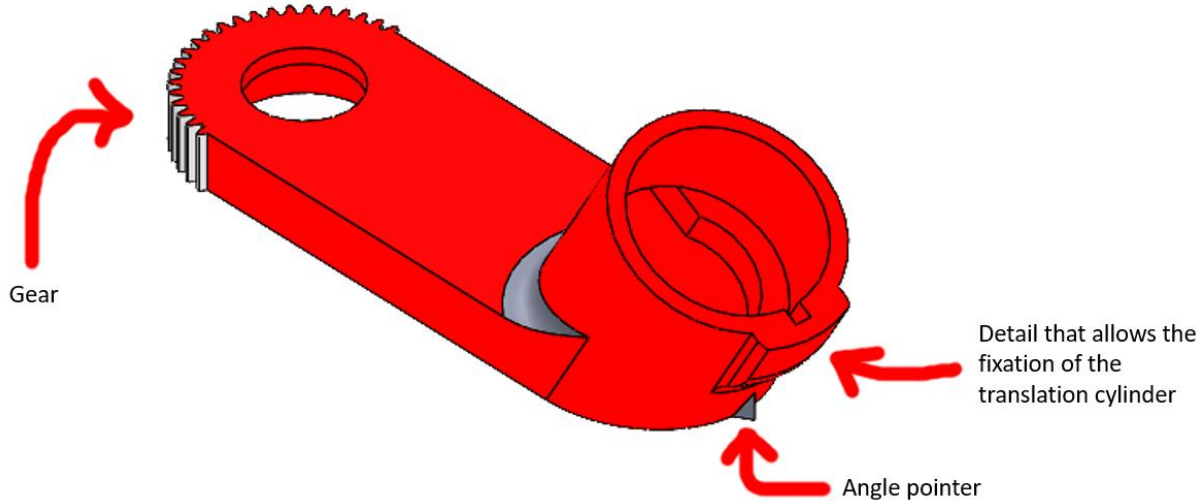

Figure 36- Several functions added to the L connection component of PATD version 4.0.

One detail was added that would serve as an indicator to measure the inversion/eversion angle that the foot will reach, and another detail that will allow the translation cylinder to be fixed so that it does not rotate along its axis during the inversion movement.

Regarding the translation cylinder, only a tiny notch was added to allow immobilization, as described above. Regarding this component, it was tried to minimize the changes made since this component was not designed from scratch but was already in version 1.0.

Subsequently, with the cylinder cover and the piston, no design changes were made, and these components present the geometry shown in version 3.0 of the PATD, Figure 37.

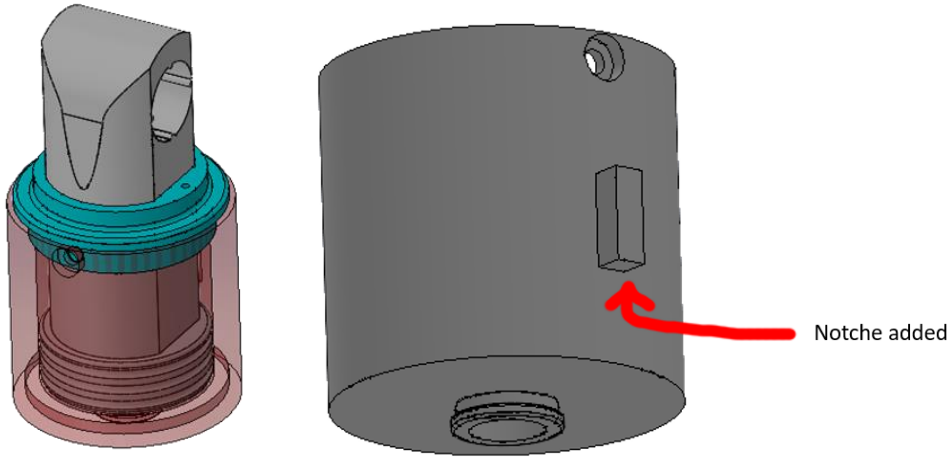

Figure 37- Details of cylinder-cap-piston assembly (left) and notch added to the cylinder (right).

Also, the system, which in the initial versions was for angle adjustment, was kept to connect the piston to connection I. However, this system lost the angle adjustment function.

Regarding Connection I, it underwent several changes throughout the design process. Here the final design will be presented and explained.

First, it was decided that two bearings would be used to support the shaft that will pass through the central hole in order to give more rigidity to the assembly. The choice of bearings was based on the loads that need to be supported, in this case, 200 N. As each bearing supports 140 N, using two guarantees safe use. Two holes and a slot were also created in order to mount a double-acting cylinder that will be presented later, Figure 38.

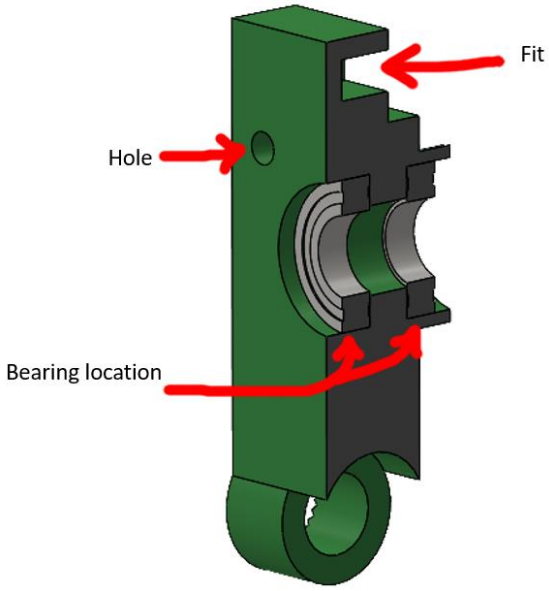

Figure 38- Section view of connection I with the various details added.

After redesigning Connection I, the angle adjustment part was carried out, where this component was reinforced since this component is highly demanded from a mechanical point of view, Figure 39.

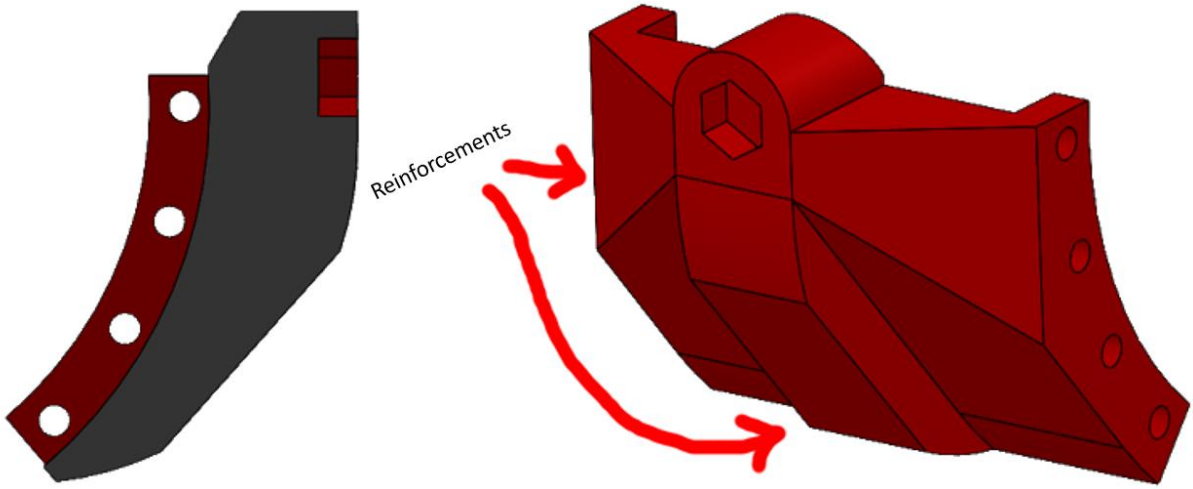

Figure 39- Reinforced angle adjustment component.

The foot support underwent minor changes, namely, to allow the introduction of foot fixation tapes. These rips allow adjustment of the tightness of the fixation of the foot. The part was 3D printed to get these locations, and different areas were marked for different feet. For this, some persons were used in order to have a wide range of foot sizes, Figure 40. After this, the part was 3D printed again with these rips, and in this way, the location of these rips was verified.

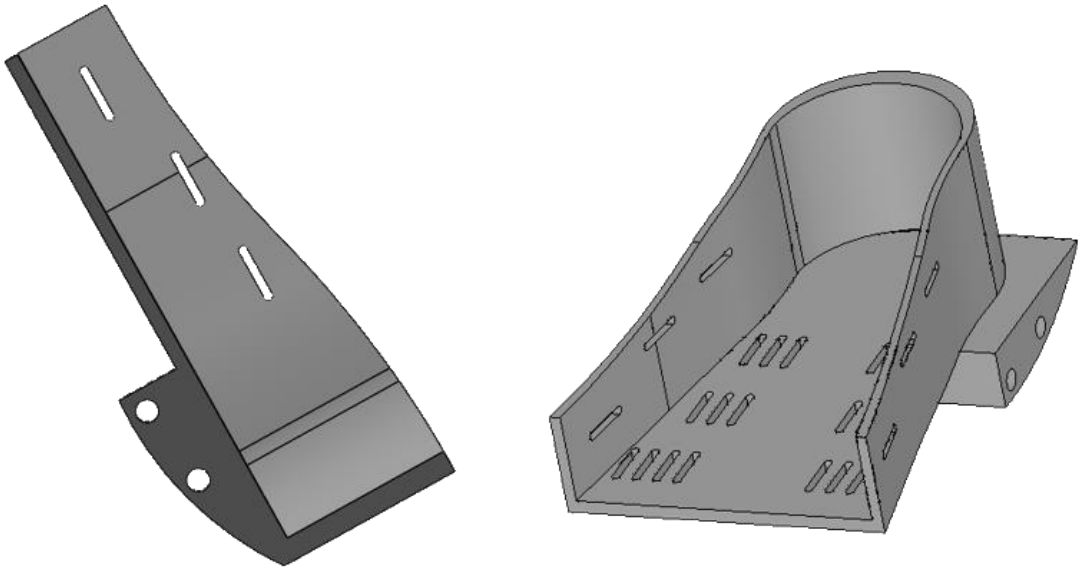

Figure 40- Foot support component of the PATD version 4.0.

Then, the designing of the shaft began, which will be housed in Connection I and will be responsible for the transmission of movement in the rotation movement. This component seems complex. However, its operation is quite simple. The Angle Adjustment Component and the rotation gear will be connected

to the ends of the shaft. The backstop and the thread will allow the shaft to be solidary with the bearings, Figure 41 and Figure 42.

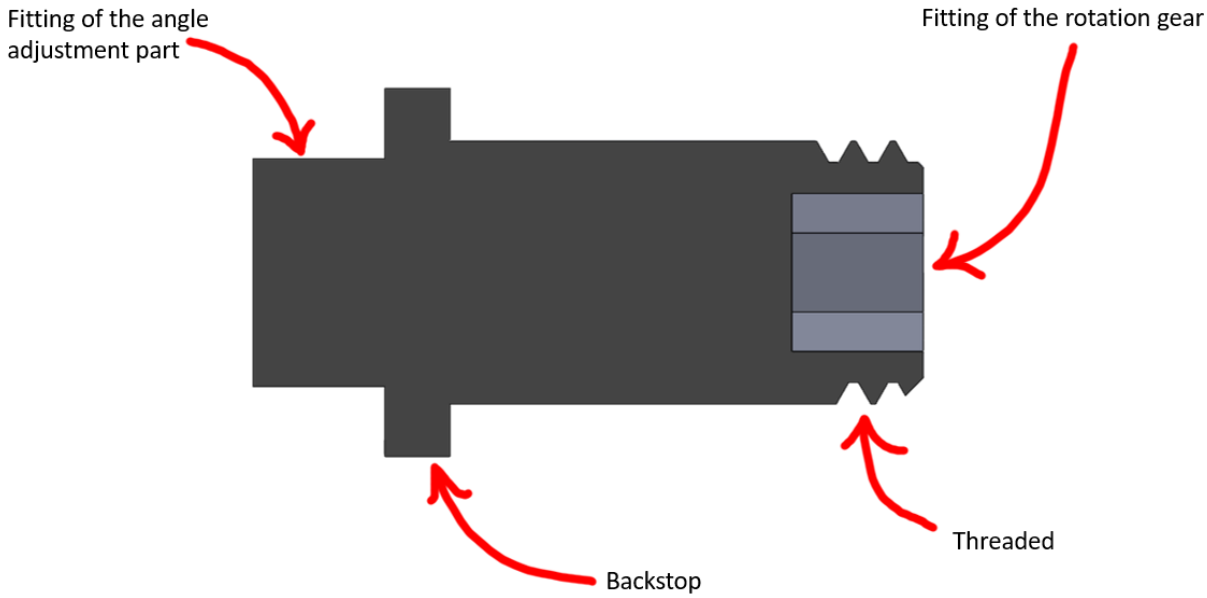

Figure 41- Rotation Shaft Component.

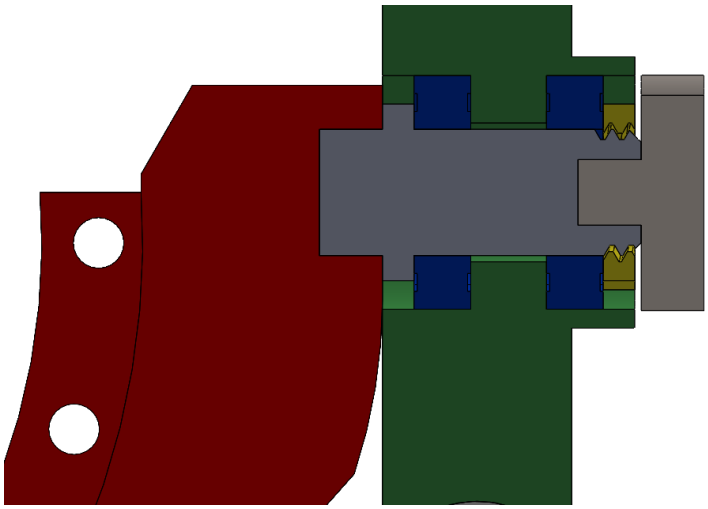

Figure 42- Section view of PATD rotation shaft assembly.

As can be seen, it is a very compact design that maximizes the available space without needing to increase the parts' thickness.

That being said, the pneumatic cylinder responsible for the rotation movement was designed next.

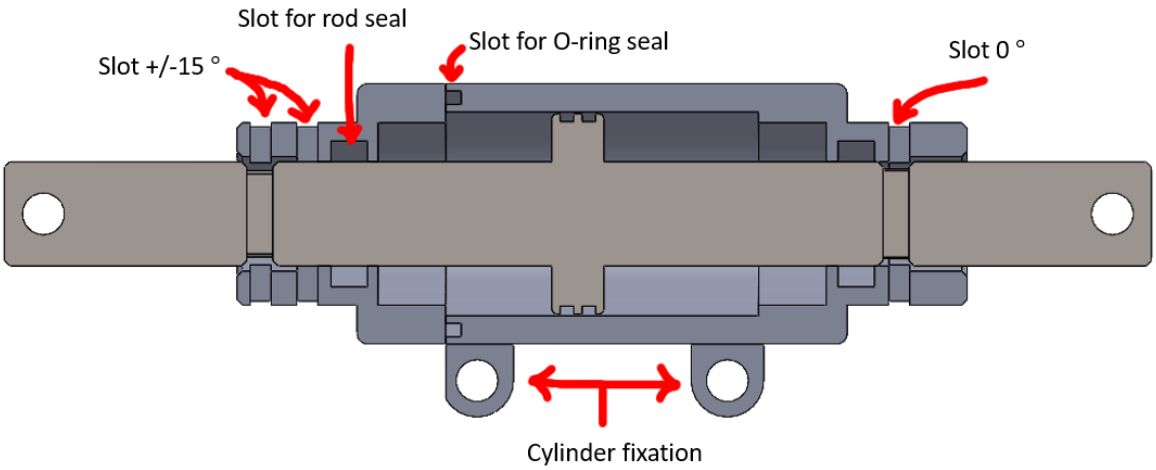

Figure 43- Section view of the double-acting pneumatic cylinder.

The slot for the seal will ensure an efficient seal. In contrast, the slots 0° and +/- 15° allow the foot support to be rotated through these certain angles in order to be able to carry out the translation movement with the foot at these angles and thus eliminate the need for the scaffolds (this was in version 1.0 but it didn't work as intended), Figure 43. There is also a slot for the rod seals so that no air escapes.

Next, the part that will connect to the shaft of the double-acting cylinder and allow the foot rotation, called Rotation Rack Support, was designed, Figure 44.

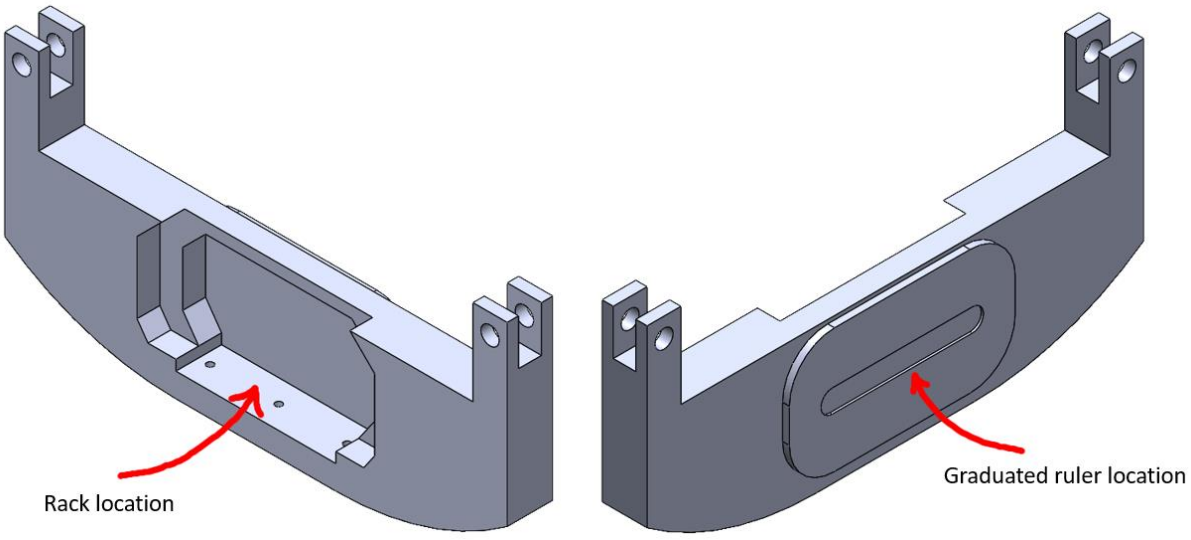

Figure 44- Rotation Rack Support Component.

This component is quite reinforced as it will have to transmit a very high force, which will be applied at a long distance, so the moment created will be very high. The fact that the rack is not in this component is related to the fact that if there is ever any incorrect use that leads to one or more teeth of the rack breaking, the rack can be easily replaced.

Finally, the tibia support was positioned, and the cylinders responsible for the inversion/eversion movement were mounted, Figure 45.

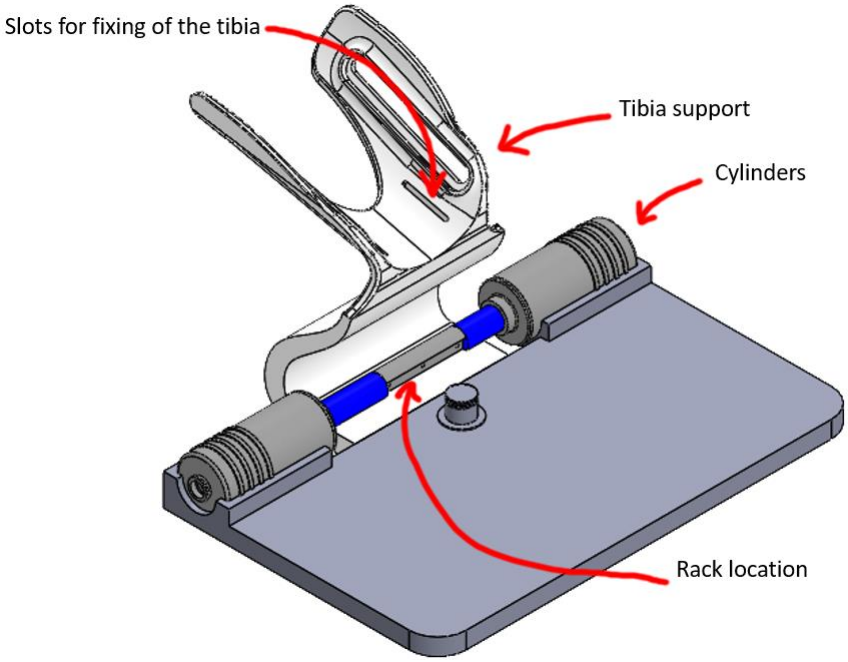

Figure 45- Positioning of the tibia support and pneumatic cylinders.

In the tibia support, slots were built to allow the passage of "Double D" tapes to fix the leg. The eversion cylinders were mounted on the base, and a system similar to the rotation movement was built so that the rack could also be easily replaced. It should be noted that these racks must be made of a less rigid material (lower Young's Modulus) so that any damage occurs to them.

The result of all these changes can be seen in Figure 46.

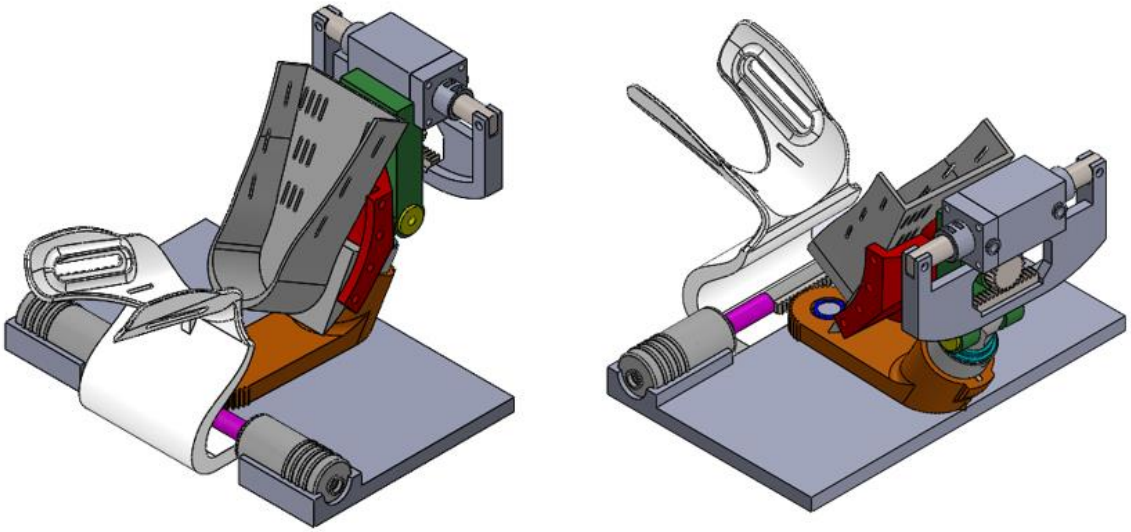

Figure 46- Preliminary Design of the PATD.

This design is a design close to the end design. However, it is necessary to check the various deformations in the different critical components to obtain the mechanism's viability to work correctly. After this phase, some areas will still be included to place markings that will allow the measurement of the various displacements. Either linear or angular.

Material

The material that will be used is a very important parameter and Clínica do Dragão has a few options, all of which are resins of polyurethane, Table 7.

- PR403, which was the material used in the PKTD.
- PR700, which is similar to ABS.
- 8051, with or without adding glass fibre.

Table 7- Different materials available with their main properties

	PR403	**PR700**	**8051**	**8051 w/20% GF**
Yield Strength (MPa)	47	55,9	55,9	70,1
Young Modulus (MPa)	1850	1800	2150	5696

It is obvious that the best material in terms of mechanical resistance would be the 8051 w/20% GF. However, the mechanical simulations that will be carried out will be considered the combination of the worst material properties. This means the properties that will be used for the FEA study will be:

$$\sigma_y = 47\ MPa$$

$$E = 1800\ MPa$$

This is a conservative approach, and it's justified since the material will be chosen after finishing the design process. This means that every choice of material will result in a safe choice. Also, it should be said that the manufacturing process will be casting for the device's production while the prototype will be made by 3D printing.

The technical sheet of each material can be seen in Appendix B.

4. VALIDATION OF THE PRELIMINARY DESIGN

4.1. MECHANICAL VALIDATION

First, it is necessary to determine the critical components that need to be studied. The first components are the gears that will transmit the movement as they need to be stiff and withstand the loads. Secondly, the system responsible for the fixation between the piston and the I connection needs to be studied to prove the robustness of the structure. Finally, a simulation for each of the three types of movement will be performed on the assembly because the device's complexity makes it very difficult to predict how each part will behave relative to the next.

4.1.1. EVERSION/ INVERSION MOVEMENT GEARS

1. Pre-analysis

Before starting the initial phase of the simulation, it is necessary to carry out a pre-analysis. This is intended to perform some calculations by hand in order to verify the simulation results. Remember that since some simplifications will be made, the values calculated here are merely indicative.

As verified by the Ludwig equation, the stress must have the value of:

$$\sigma = \frac{k_v \cdot w_t}{F \cdot m_t \cdot Y} \tag{1}$$

$$\sigma = \frac{1{,}074 \cdot 181{,}82}{10 \cdot 10^{-3} \cdot 1{,}5 \cdot 10^{-3} \cdot 0{,}485} \approx 27\ MPa$$

2. Geometry

The geometry imported into the simulation will be simplified; therefore, only the sprocket and rack will be studied, Figure 47.

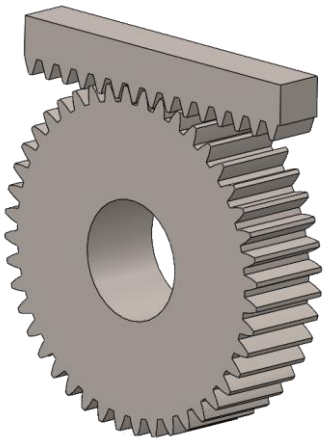

Figure 47- Simplified geometry of the eversion gears.

3. Mesh

This point is one of the most important since a weak discretization of the set will inevitably lead to poor and far from real results. Given the low computational power available, the refinement will be carried out specifically in critical areas. In this case, the contact between the teeth of the rack and the wheel, Figure 48.

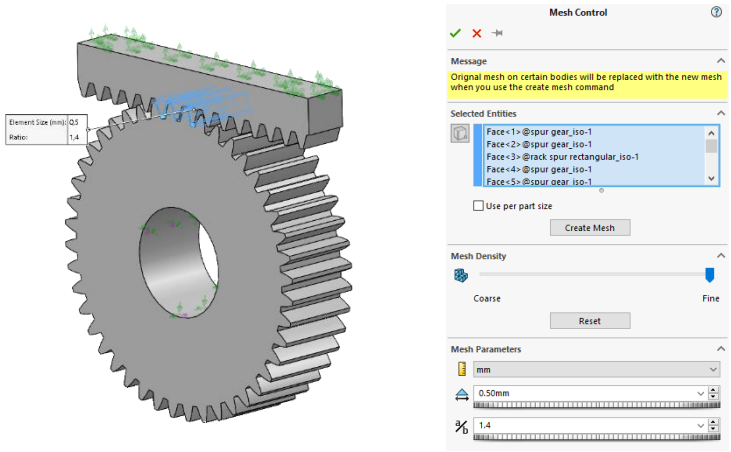

Figure 48- Mesh control used in the eversion gear.

In the remaining areas, a mesh size of 3 mm was used, Figure 49.

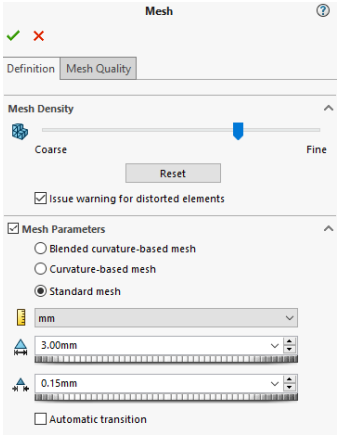

Figure 49- Mesh size used in the eversion gear.

Finally, the quality of the mesh was also verified, and a good mesh must have at least 90% of the elements with an aspect ratio below 5 [61].

In this case, there are only 66 elements with an aspect ratio above 5, so the mesh quality is satisfactory, Figure 50.

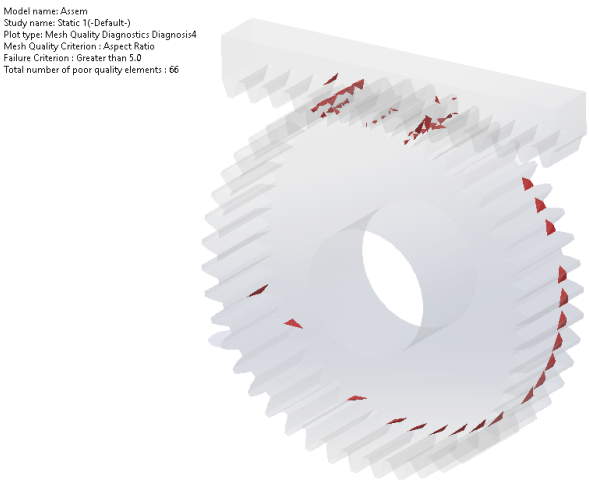

Figure 50- Aspect ratio above 5 of the mesh used in the eversion gear.

4. Model Configuration

In this simulation phase, it is necessary to define the boundary conditions and material properties. Regarding material properties, see Figure 51.

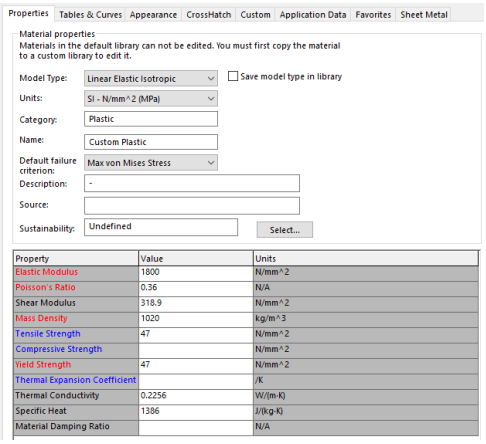

Figure 51- Material Properties.

In terms of boundary conditions, it was defined that the rack would be fixed, and the wheel could only rotate along its axis, Figure 52.

Finally, a torque was applied to the centre of the wheel, Figure 53. Since the eversion/reversion movement is performed with a maximum torque of 4000 Nmm [60], when considering a safety factor of 1.5:

$$T = 4000 \cdot 1{,}5 = 6000\ N \cdot mm$$

The last important aspect is the contact parameters, Figure 54. In this section, it was considered a friction coefficient of 0,4 as it is the highest possible friction coefficient for plastic on plastic [62].

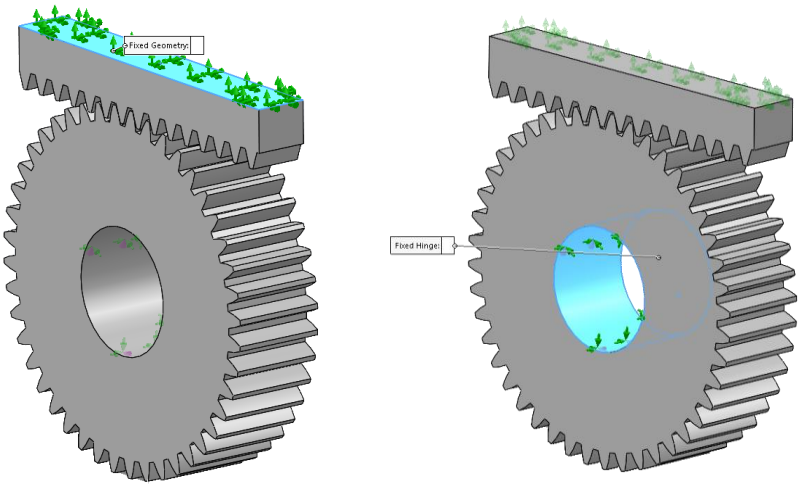

Figure 52- Boundary conditions used in the eversion gear.

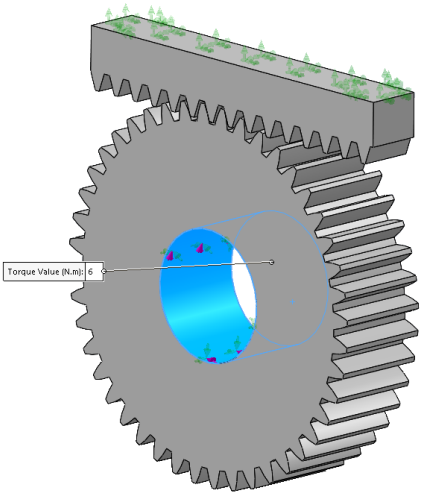

Figure 53- Load applied to the eversion gear.

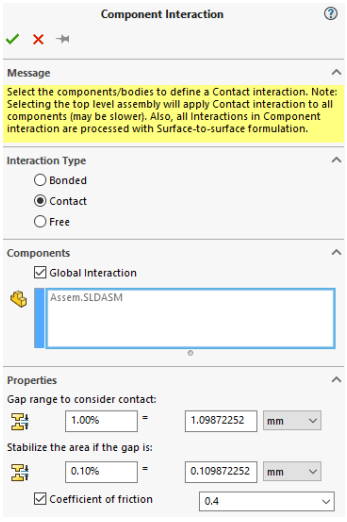

Figure 54- Contact parameters used in the eversion gear.

5. Numerical Solution

In terms of the desired solution, the most important thing is that the stress does not exceed the material's yield stress, and the displacements do not compromise the motion of the different parts of the device, Figure 55.

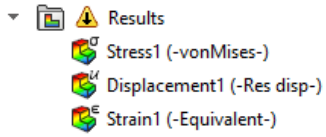

Figure 55- Numerical Results required for the eversion gear.

6. Numerical Results

In the specific case of this simulation, the stress result will only be later verified with the one calculated in the pre-analysis. The displacement values will also be seen, given that high rigidity and reliable equipment are intended. Regarding the results in terms of tension, the maximum value recorded was about 28 MPa, while in terms of displacement, the maximum value found was about 0,07 mm, Figure 56.

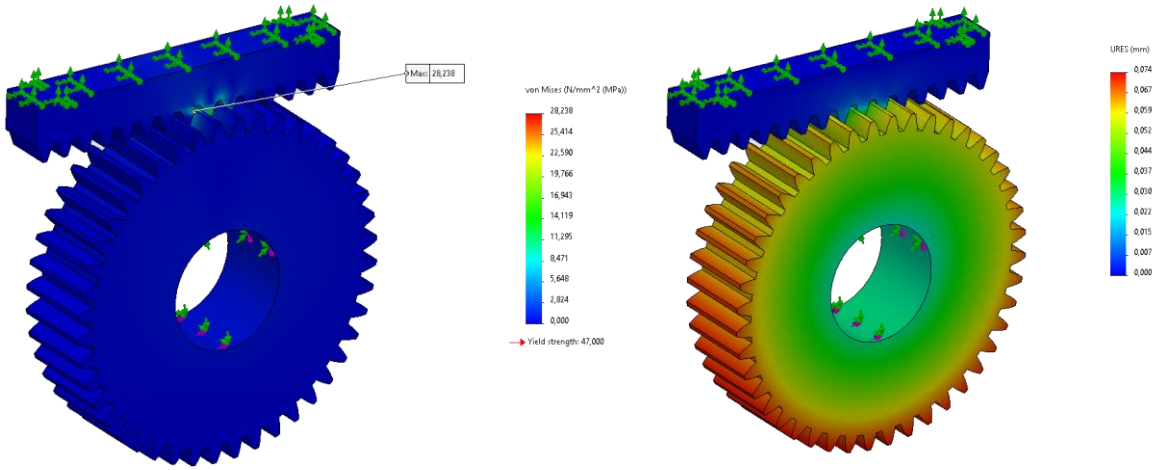

Figure 56- Stress and displacement results of the eversion gear.

7. Verification and/or Validation

In this last step, some checks will be made to verify the simulation's validity. Firstly, the maximum stress value is found at an expected location, at the contact of the teeth, Figure 57.

Regarding the displacement, it seems that the results do not make much sense but looking at the strain, it is clear that although the teeth that are not in contact travel a greater distance, they are not the ones that suffer the most deformation, Figure 58.

Finally, just check the error between the stress value calculated in the pre-analysis and the one obtained in the simulation:

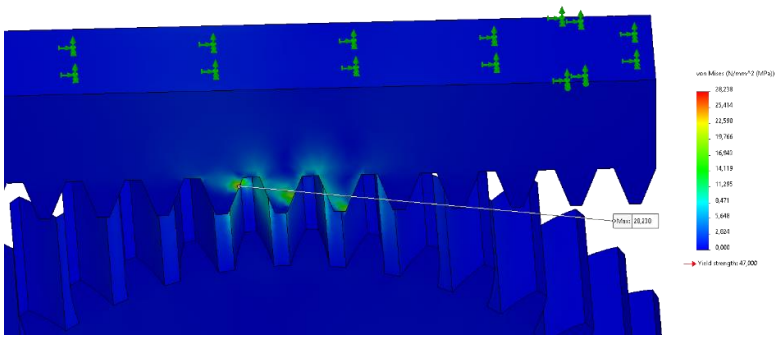

Figure 57- Maximum stress location for the eversion gear.

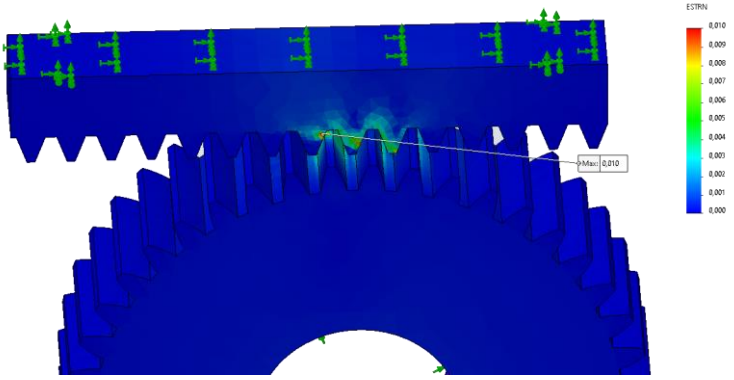

Figure 58- Strain results for the eversion gear.

$$Relative\ Error = \frac{28 - 27}{27} \cdot 100 \approx 4\ \%$$

Although the error is not negligible, given the simplifications of the Ludwig Equation and the fact that the values are very close in absolute terms, the validity of the result is verified.

4.1.2. Abduction and Adduction Movement gears

1. Pre-analysis

Before starting the initial phase of the simulation, it is necessary to carry out a pre-analysis. This is intended to perform some calculations by hand in order to verify the simulation results. Since some simplifications will be made, the values calculated here are merely indicative.

As verified by the Ludwig equation, the stress must have the value of:

$$\sigma = \frac{k_v \cdot w_t}{F \cdot m_t \cdot Y} \tag{1}$$

$$\sigma = \frac{1{,}074 \cdot 333{,}33}{15 \cdot 10^{-3} \cdot 1{,}5 \cdot 10^{-3} \cdot 0{,}485} \approx 33\ MPa$$

In this simulation, the width of the rack and spur gear were increased because previously, the stress was almost the yield stress, and for safety and to ensure the equipment is durable, the width was increased by 5 mm. In the synthesis scope, only the simulation with the increased width will be shown; however, all the steps taken are the same. The only difference is the geometry.

2. Geometry

The geometry imported into the simulation will be simplified; therefore, only the sprocket and rack will be studied, Figure 59.

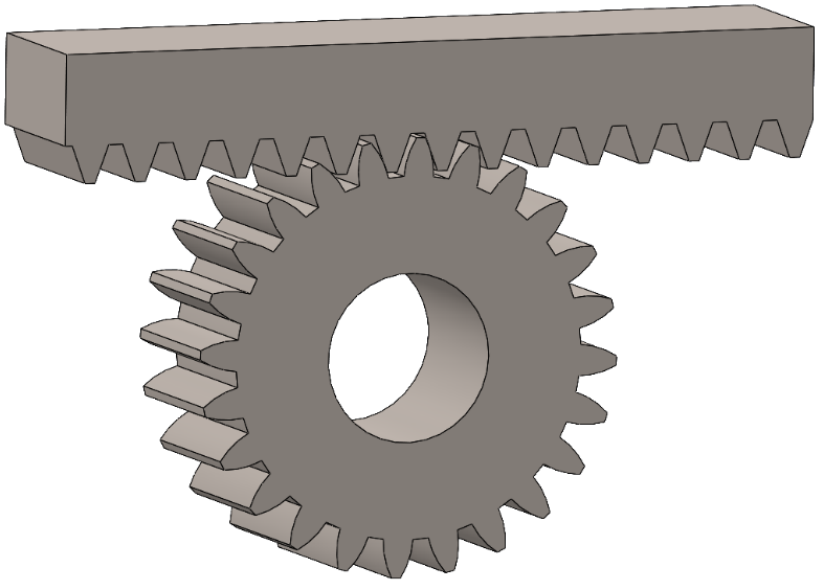

Figure 59- Simplified geometry of the rotation gears

3. Mesh

This point is one of the most important since a weak discretization of the set will inevitably lead to poor and far from real results. Given the low computational power available, the refinement will be carried out specifically in critical areas. In this case, the contact between the teeth of the rack and the wheel, Figure 60. In the remaining areas, a mesh size of 3 mm was used, Figure 61. Also, the quality of the mesh was verified, as was in the previous simulation, Figure 62.

In this case, there are only 103 elements with an aspect ratio above 5, and they are located far from the critical contact zone, so the mesh quality is very satisfactory.

4. Model Configuration

Now, it is necessary to define the boundary conditions and material properties. The material properties are the same for all the simulations and parts because the device will be produced using the same material.

In terms of boundary conditions, they are the same as in the previous simulation, Figure 63.

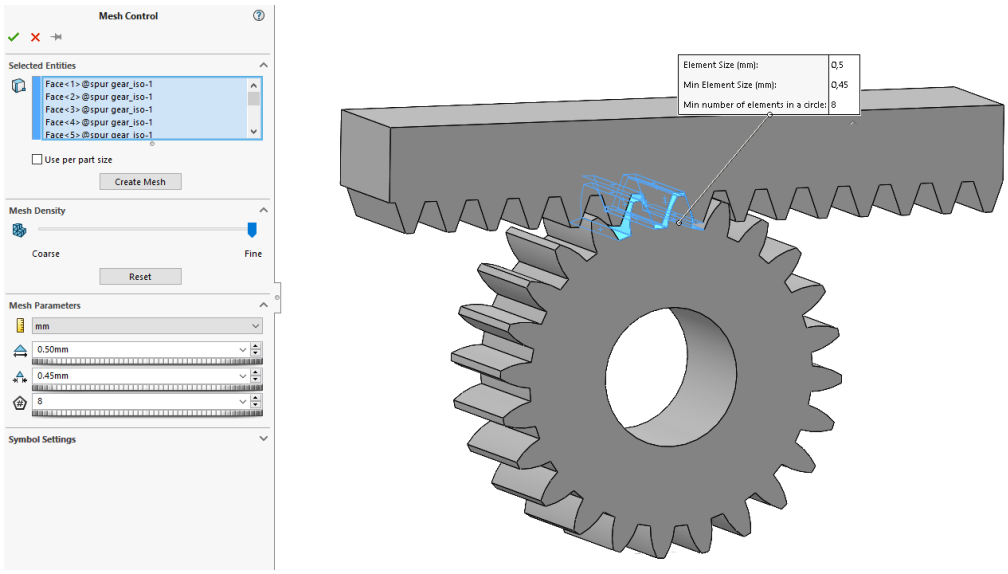

Figure 60- Mesh control used in the rotation gear

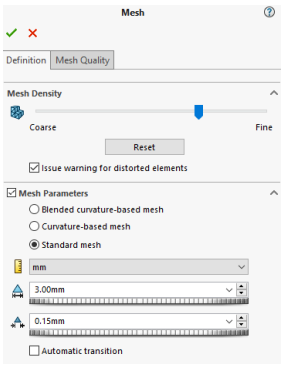

Figure 61- Mesh size used in the rotation gear.

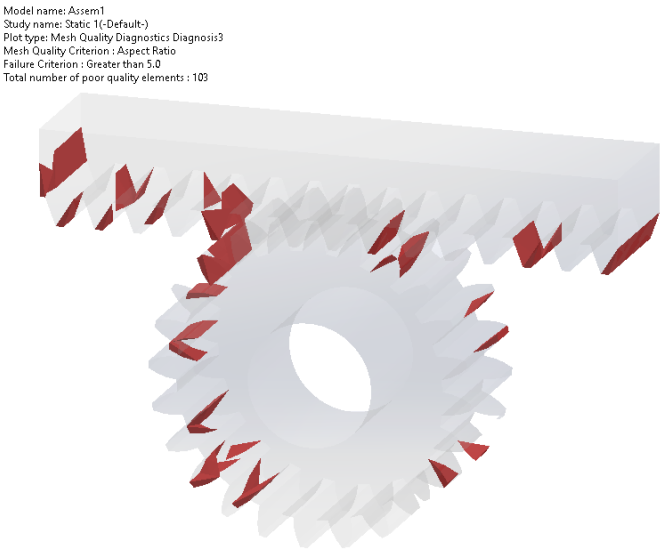

Figure 62- Aspect ratio above 5 of the mesh used in the rotation gear.

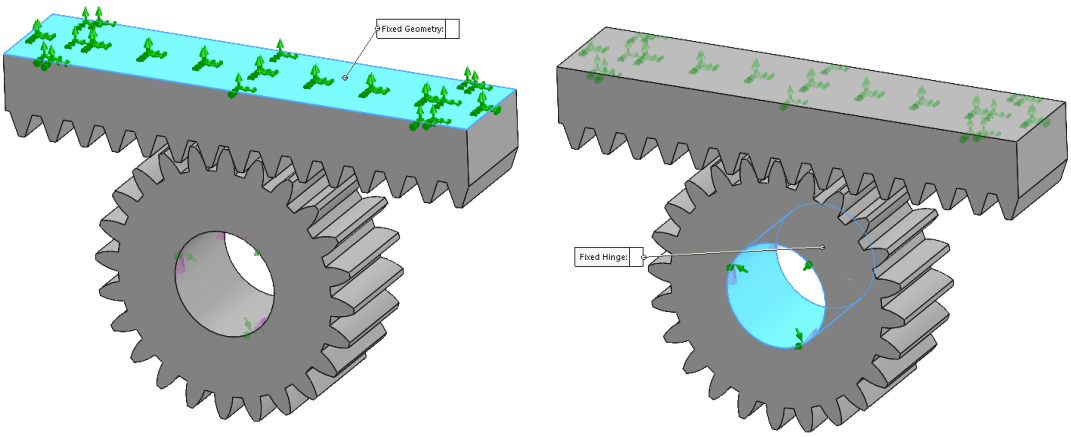

Figure 63- Boundary conditions used in the rotation gear.

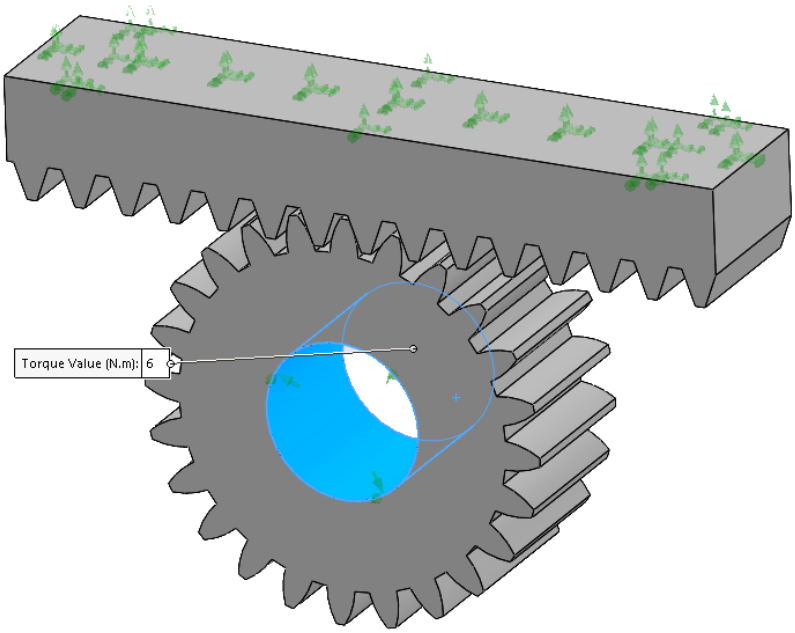

Figure 64- Load applied to the rotation gear.

Finally, a torque was applied to the centre of the wheel, Figure 64. Since there was a lack of information concerning the loads applied in this movement, the same torque as in the previous simulation will be used, considering a safety factor of 1.5:

$$T = 4000 \cdot 1{,}5 = 6000\ N \cdot mm$$

The last aspect, the contact parameters, was the same as for the eversion gear.

5. Numerical Solution

In terms of the desired solution, the most important thing is that the tension does not exceed the material's yield stress, and the displacements do not compromise the motion of the different device parts, Figure 65.

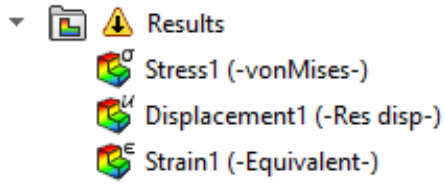

Figure 65- Numerical results required for the rotation gear.

6. Numerical Results

In the specific case of this simulation, the stress result will only be later verified with the one calculated in the pre-analysis. The displacement values will also be seen, given that high stiffness and reliable equipment are intended.

Regarding the results in terms of stress, the maximum value recorded was about 28 MPa, while in terms of displacement, the maximum value found was about 0,14 mm, Figure 66.

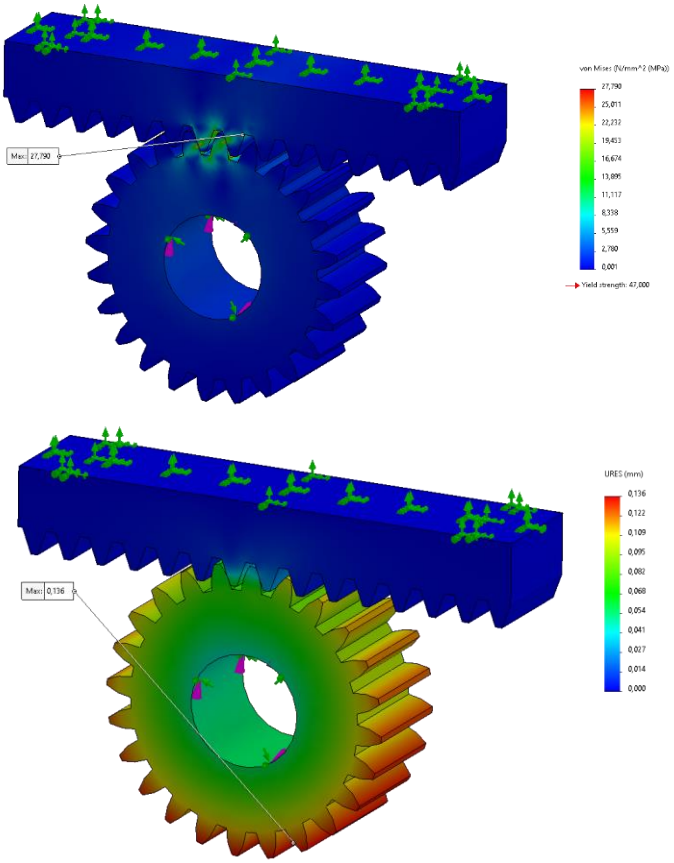

Figure 66- The rotation gear's stress (above) and displacement (behind) results.

7. Verification and/or Validation

In this last step, some checks will be made to verify the simulation's validity. Firstly, the maximum stress value is confirmed at the expected location, in the contact of the teeth, Figure 67.

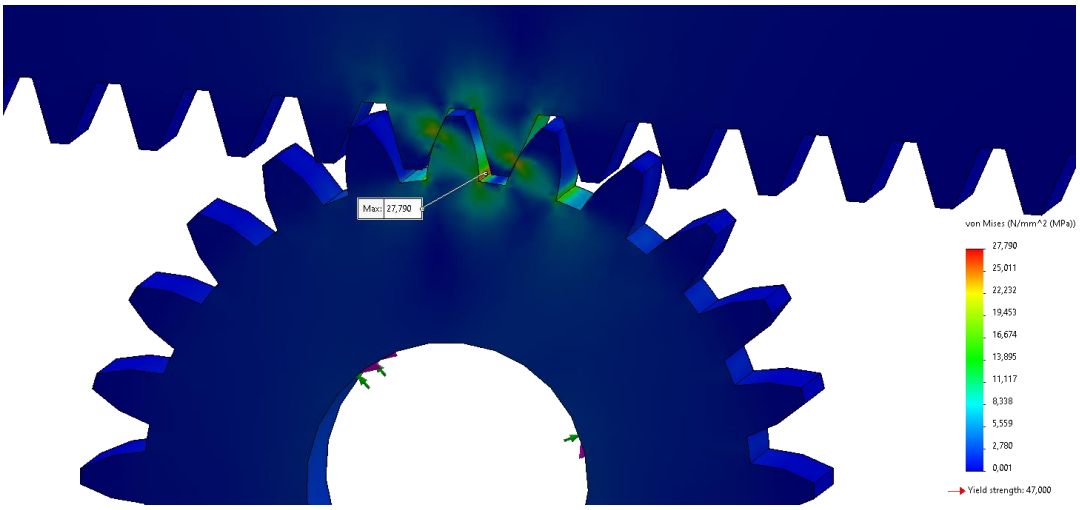

Figure 67- Maximum stress location for the rotation gear.

Regarding the displacement, it seems that the results do not make much sense but looking at the strain, it is clear that although the teeth that are not in contact travel a greater distance, they are not the ones that suffer the most deformation, Figure 68.

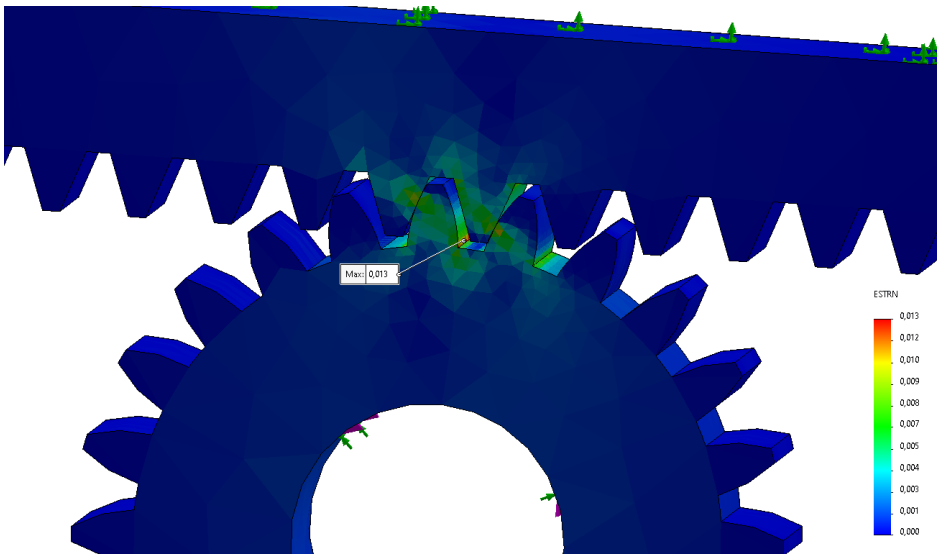

Figure 68- Strain results for the rotation gear.

Finally, just check the error between the stress value calculated in the pre-analysis and the one obtained in the simulation:

$$Relative\ Error = \frac{33 - 28}{33} \cdot 100 \approx 15\ \%$$

Although the error is substantial, given the simplifications of the Ludwig Equation and the fact that the values are very close in absolute terms, the validity of the result is verified. Also, the mesh near the contact probably should be more refined. However, this error will be considered acceptable due to the limitations of the computing power available.

4.1.3. CONNECTION VALIDATION

1. Pre-analysis

Before starting the initial phase of the simulation, it is necessary to carry out a pre-analysis. This is intended to perform some calculations by hand in order to verify the simulation results. Since some simplifications will be made, the values calculated here are merely indicative.

This connection is very complex, with multiple bodies and many contacts, making the analysis very complicated. This means there will be no validation because there will not be any hand calculations in this case.

2. Geometry

The geometry imported into the simulation will be simplified; therefore, only the main components will be inserted, Figure 69. This reduces the number of elements and computational time.

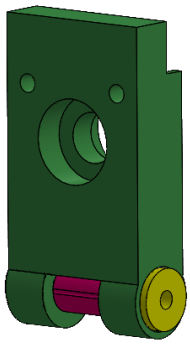

Figure 69- Simplified geometry of the connection.

3. Mesh

This point is one of the most important since a weak discretization of the components will inevitably lead to poor results. Given the low computational power available, the mesh will have a variable size.

Mesh Details

Study name	Static 2 from [Static 1] (-Default-)
Mesh type	Solid Mesh
Mesher Used	Blended curvature-based mesh
Jacobian points for High quality mesh	16 points
Mesh Control	Defined
Max Element Size	2 mm
Min Element Size	0,05 mm
Mesh quality	High
Total nodes	857104
Total elements	576810
Maximum Aspect Ratio	4 112,8
Percentage of elements with Aspect Ratio < 3	98,5
Percentage of elements with Aspect Ratio > 10	0,533
Percentage of distorted elements	0
Number of distorted elements	0
Remesh failed parts independently	Off
Time to complete mesh(hh:mm:ss)	00:00:26
Computer name	

Figure 70- Mesh parameters used in the connection.

The mesh quality was also verified and is very good, as most elements have an aspect ratio below 3, Figure 70.

4. Model Configuration

Now, it is necessary to define the boundary conditions and material properties. The material properties are the same for all the simulations and parts because the device will be produced using the same material.

Firstly, a bolt was inserted to tighten the assembly in terms of boundary conditions, Figure 71.

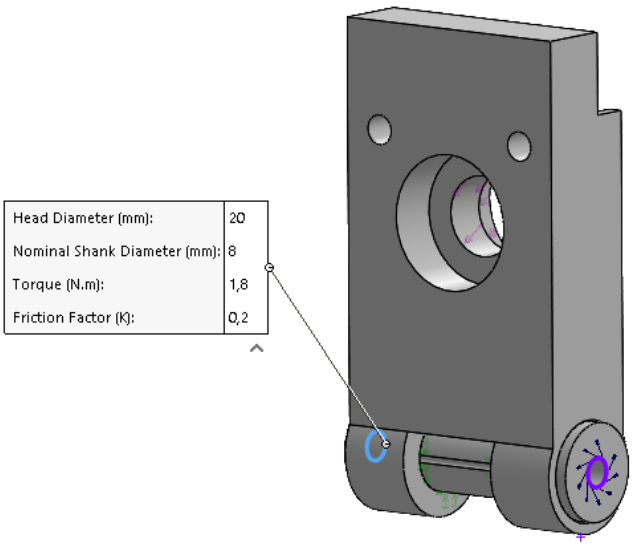

Figure 71- Bolt connector specs used in the connection.

Secondly, the fixation shaft was fixed, and the PP connection part was considered a fixed hinge, only allowing rotation along the fixation shaft axis, Figure 72.

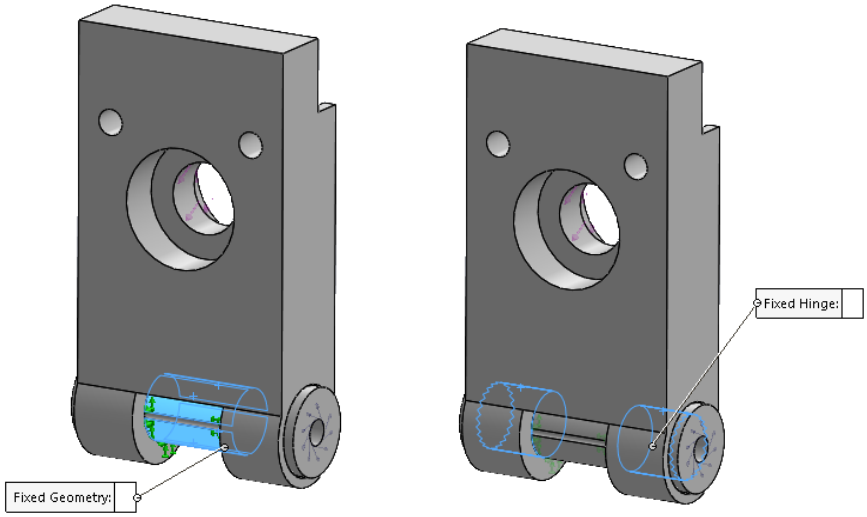

Figure 72- Boundary conditions used in the connection.

Finally, the load was applied [60].

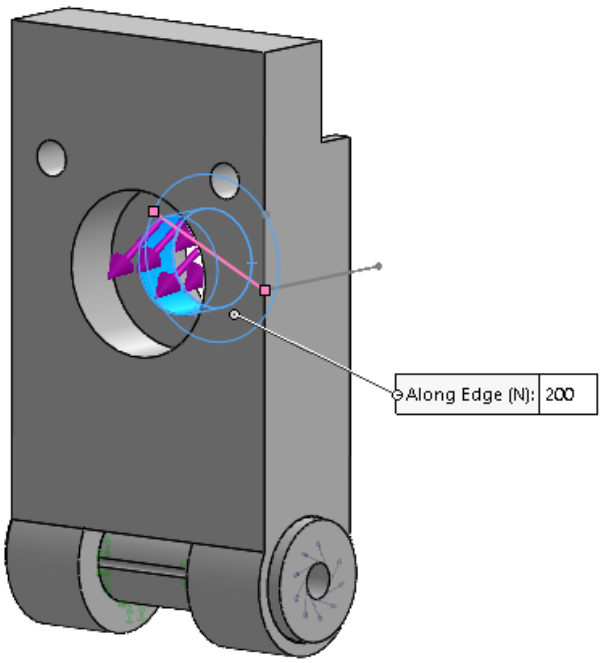

Figure 73- Stress and displacement results of the rotation gear.

In this case, no safety factor was used because there was no pre-analysis made or hand calculations, so the objective is to know the most realistic scenario.

5. Numerical Solution

In terms of the desired solution, the most important thing is that the stress does not exceed the material's yield stress, and the displacements do not compromise the motion of the different parts of the device, Figure 74.

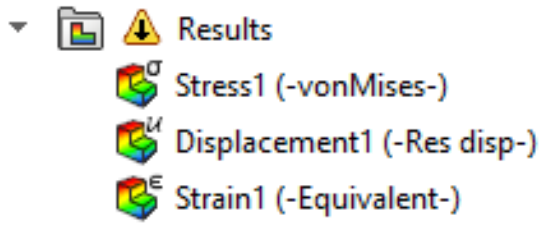

Figure 74- Numerical results required for the connection.

6. Numerical Results

Regarding the results in terms of stress, the maximum value recorded was above the yield strength since there are some stress concentrations. In terms of displacement, the maximum value found was about 2,5 mm, which should be acceptable,

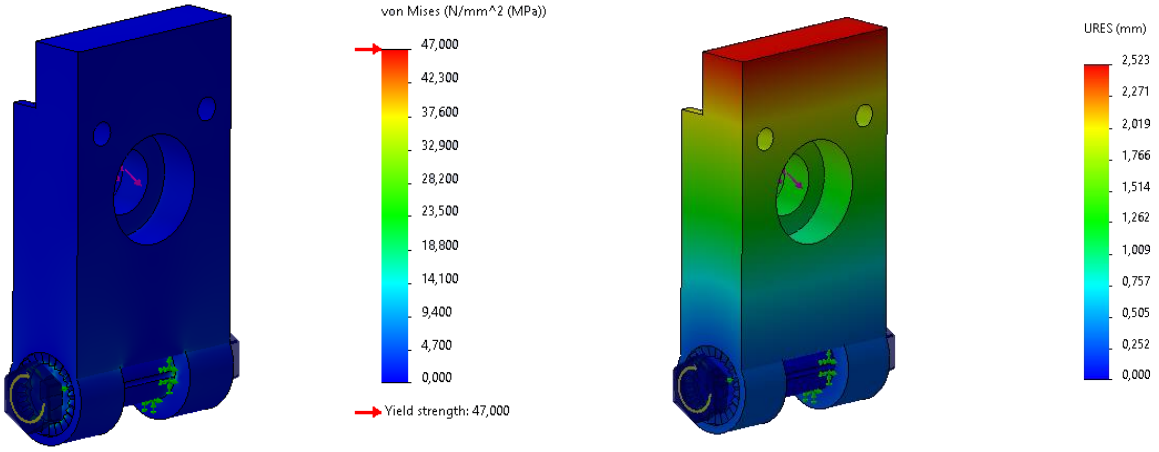

Figure 75- Stress and displacement results for the connection.

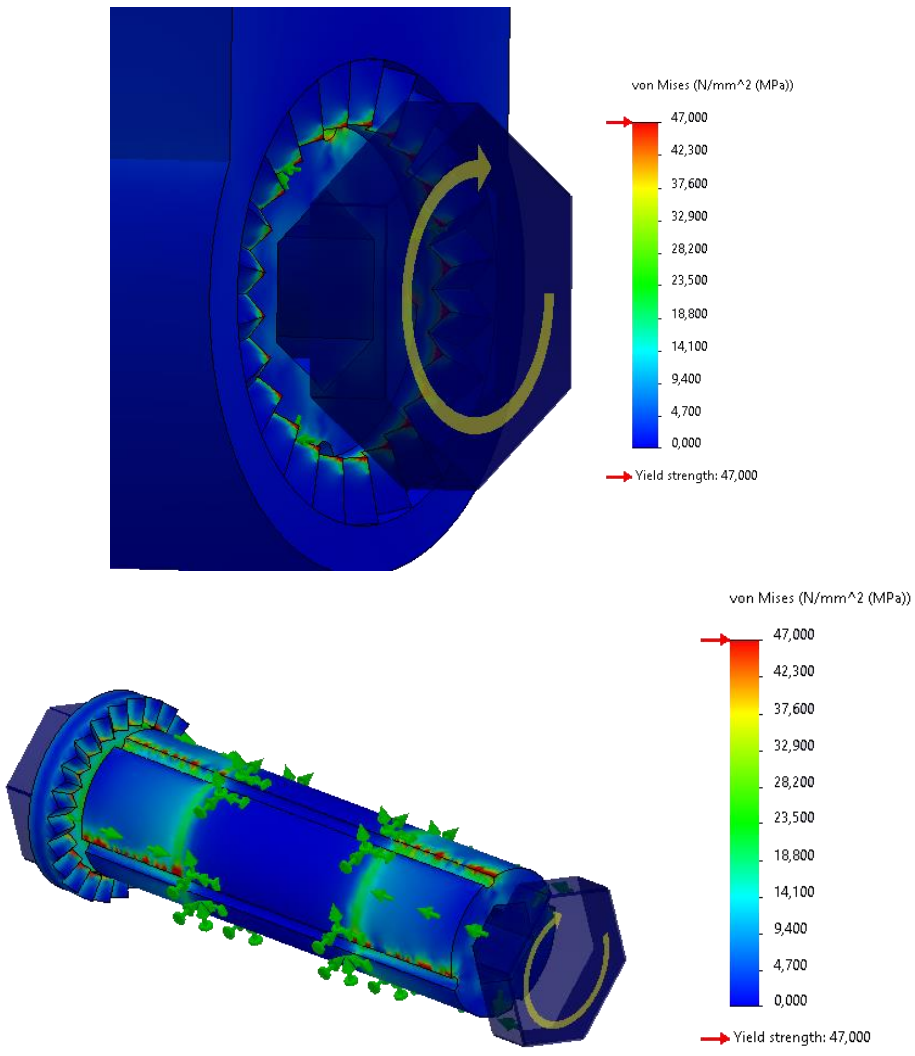

Figure 76- Location of the stress concentration.

7. Verification and/or Validation

In this last step, some checks will be made to verify the simulation's validity. Firstly, the maximum stress value is found at an expected location in the contact of the teeth of the block parts teeth and the PP connection's teeth, Figure 76. Regarding the displacement, the displacement increases with the distance to the bolt axis, Figure 75.

Finally, the fact that the stress surpasses the yield stress should not lead to failure because only some very localized zones enter the plastic regime. These zones have very sharp edges, and that increases the stress locally. Also, the fact that these stresses are compressive means they shouldn't cause cracks. Nonetheless, a more straightforward system will be studied.

4.1.4. Rack Support

1. Pre-analysis

Before starting the initial phase of the simulation, it is necessary to carry out a pre-analysis. This is intended to perform some calculations by hand in order to verify the simulation results.

This part is quite complex because the cross-section area varies a lot, and the geometry would have to be significantly simplified to a point where the hand calculations would be irrelevant to this analysis. This means there will be no validation because there will not be any hand calculations in this case.

2. Geometry

The geometry imported into the simulation will not be simplified since there is not much complexity in this geometry, Figure 77.

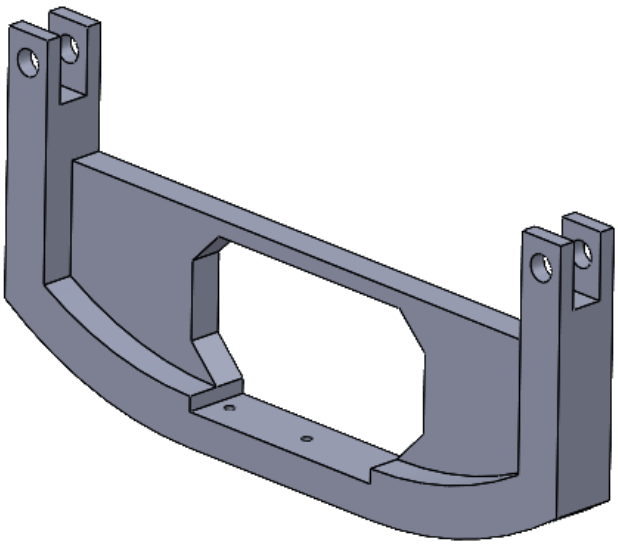

Figure 77- Simplified geometry of the rack support.

3. Mesh

This point is one of the most important since a weak discretization of the components will inevitably lead to poor results.

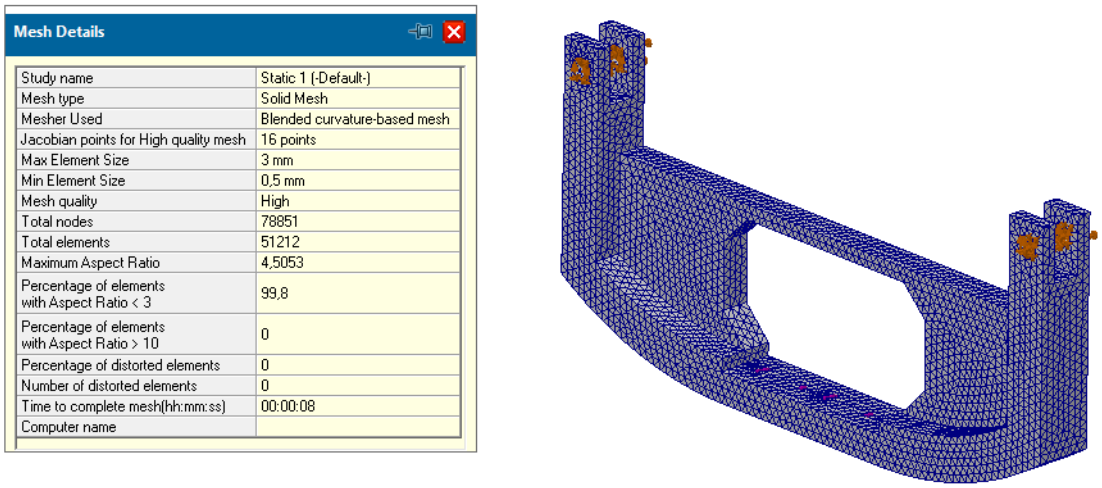

Mesh Details

Study name	Static 1 (-Default-)
Mesh type	Solid Mesh
Mesher Used	Blended curvature-based mesh
Jacobian points for High quality mesh	16 points
Max Element Size	3 mm
Min Element Size	0,5 mm
Mesh quality	High
Total nodes	78851
Total elements	51212
Maximum Aspect Ratio	4,5053
Percentage of elements with Aspect Ratio < 3	99,8
Percentage of elements with Aspect Ratio > 10	0
Percentage of distorted elements	0
Number of distorted elements	0
Time to complete mesh(hh:mm:ss)	00:00:08
Computer name	

Figure 78- Mesh parameters used in the rack support.

The quality of the mesh was also verified, and it is excellent. Almost every element has an aspect ratio below 3, Figure 78.

4. Model Configuration

Now, it is necessary to define the boundary conditions and material properties. The material properties are the same for all the simulations and parts because the device will be produced using the same material.

Regarding boundary conditions, firstly, the rack support was fixed in the connection with the piston shaft, Figure 79.

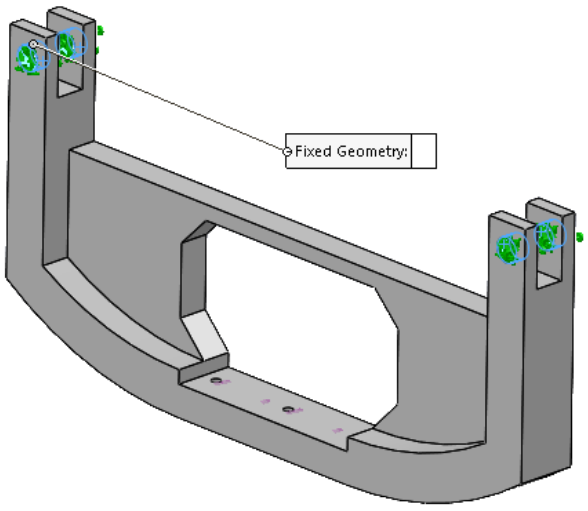

Figure 79- Boundary conditions used in the rack support.

Secondly, the load was applied. Regarding this movement, there weren't any typical load values, so the maximum load available was used and a safety factor of 1,5.

$$F = 200 * 1{,}5 = 300\ N$$

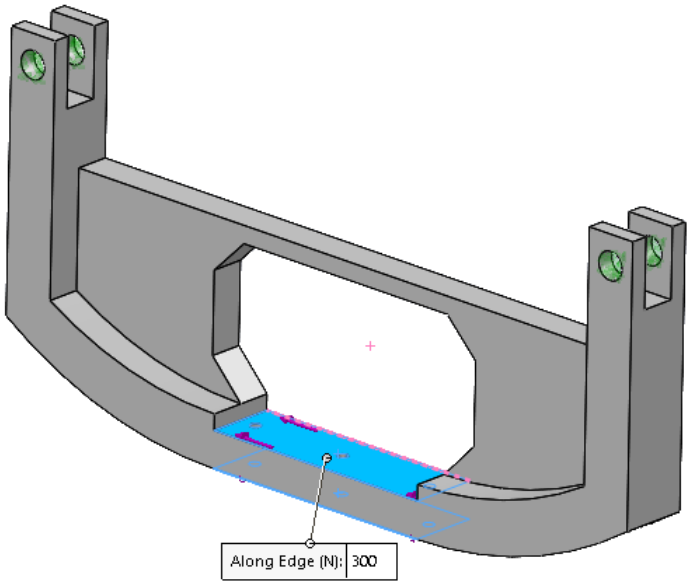

Figure 80- Load applied to the rack support.

5. Numerical Solution

In terms of the desired solution, the most important thing is that the stress does not exceed the material's yield stress, and the displacements do not compromise the motion of the different parts of the device, Figure 81.

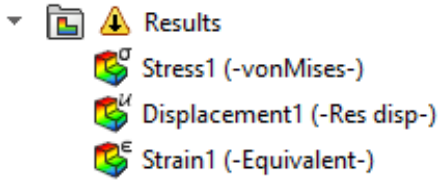

Figure 81- Numerical Results required for the connection.

6. Numerical Results

Regarding the results in terms of stress, the maximum value recorded was below the yield strength, about 39 MPa, Figure 82. In terms of displacement, the maximum value found was about 1,6 mm, Figure 83, but in terms of directions, the maximum was 1,5 mm in the Z direction. In the Y direction was about 0,9 mm, which should be acceptable, Figure 84. Also, the fact that the load is much higher than the real one should be considered.

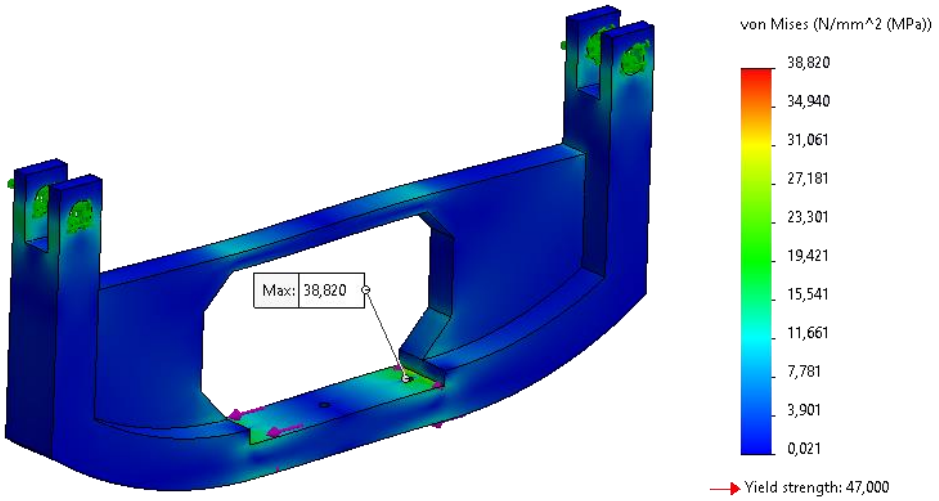

Figure 82- Stress results for the rack support.

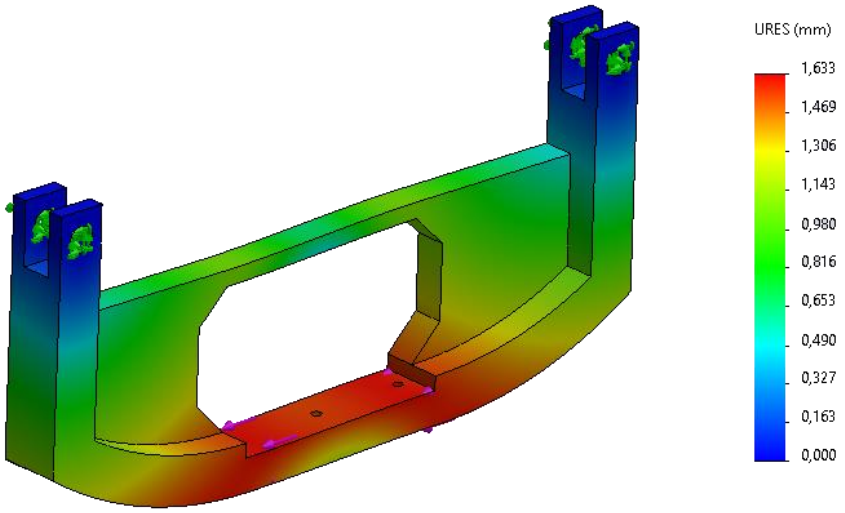

Figure 83- Displacement results for the rack support.

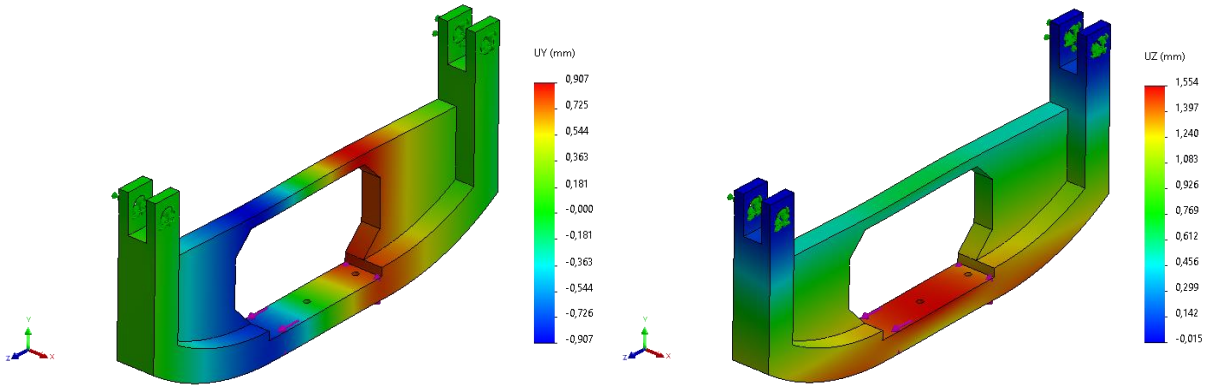

Figure 84- Displacement in Y and Z directions results for the rack support.

7. Verification and/or Validation

In this last step, some checks will be made to verify the validity of the simulation performed. Firstly, the maximum stress value is found at an expected location, at the holes. This is because holes introduce stress concentration that leads to high-stress values. Also, the fact that the component barely deforms in the X direction means the behaviour is the expected one, so the results are verified.

Nonetheless, some changes were made in order to allow this part to have some graduated ruler to measure the joint movement. To accomplish this, the geometry was changed, as seen in Figure 85.

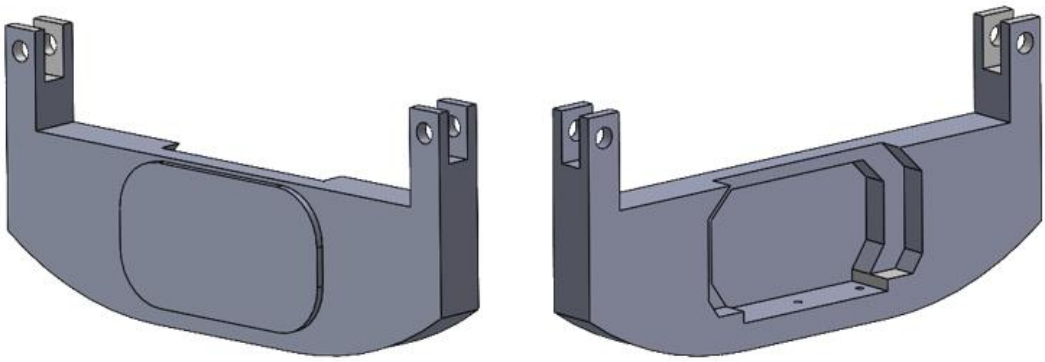

Figure 85- Changed geometry of the rack support that allows for a graduated ruler.

This new design fills the middle void and gives more stiffness to the part while providing a space to put a sticker of a graduated ruler.

The analysis was run with the same parameters as the previous design, so only the results will be shown here.

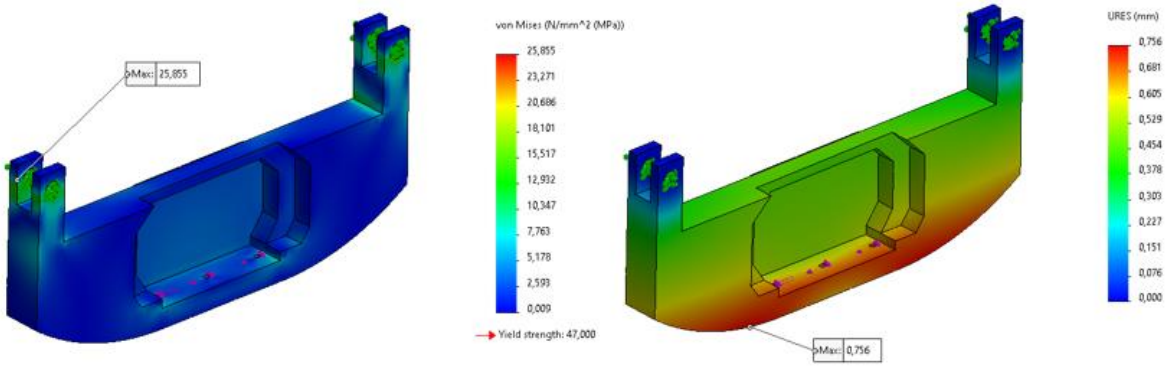

Figure 86- Results in terms of stress and displacement for the new design of the rack support

It can be seen that both the stress and displacements have been reduced significantly, which is very good as this means a stiffer design and a more durable part, Figure 86. In terms of displacements in Y and Z, the results also show an impressive reduction, Figure 87.

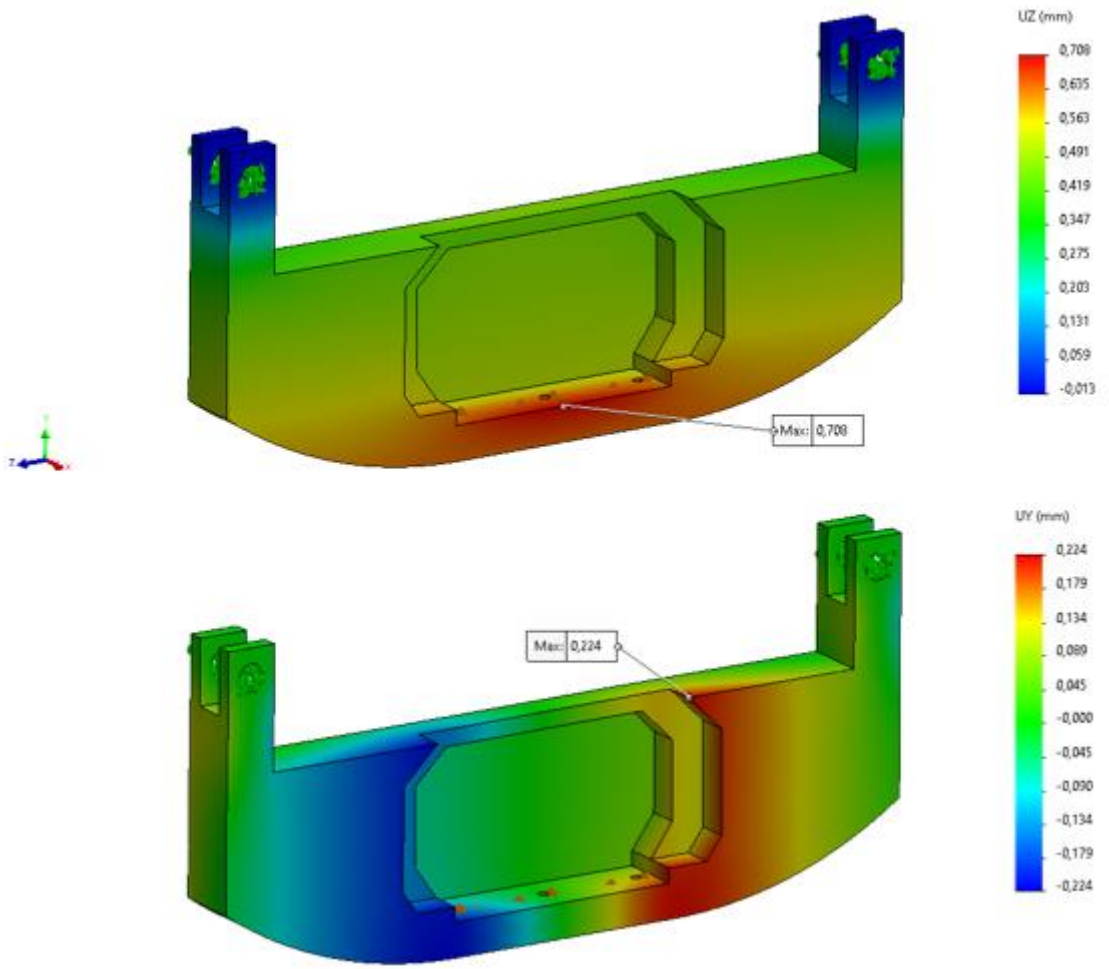

Figure 87- Results in terms of displacements in Y and Z for the new design of the rack support

Now that the simulations of individual parts are finished, there will be shown simulations of the whole device making the three types of movement that it was designed to do. As these simulations involve multiple components, no pre-analysis will be made.

4.1.5. EVERSION MOVEMENT

1. Geometry

Regarding geometry, some irrelevant parts for the analysis were suppressed, such as the base and the double effect cylinder. Also, the fixation system consisting of the block parts was simplified because, in this movement, the connection is not relevant and hasn't got the load-bearing function in this specific move, Figure 88

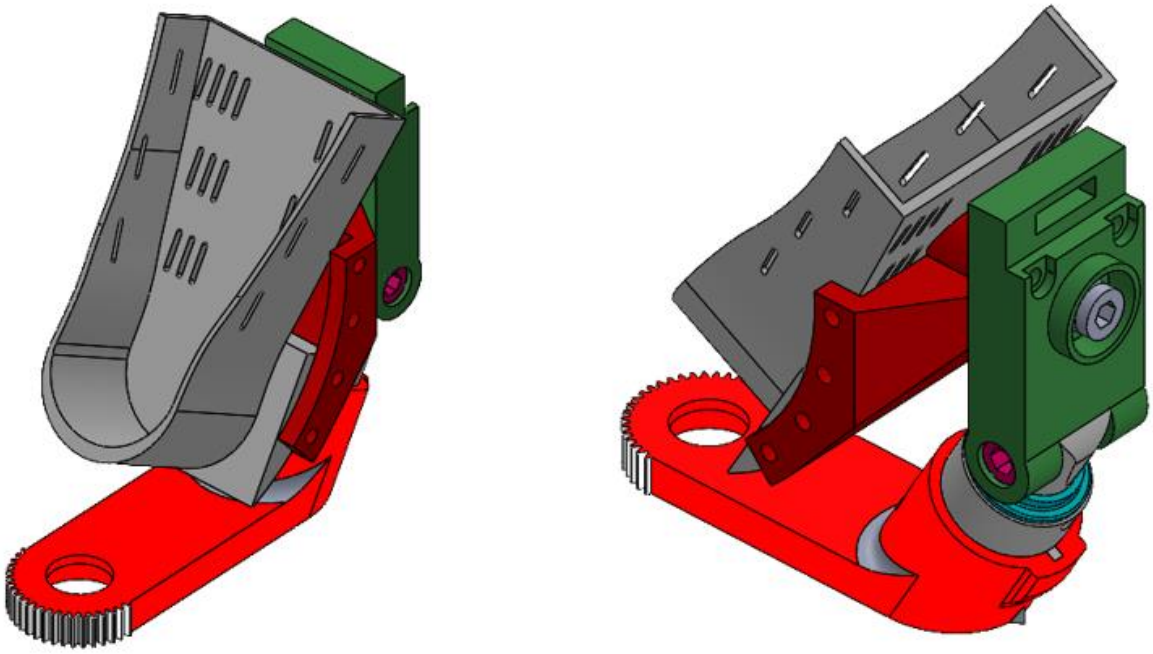

Figure 88- Assembly used for the eversion movement simulation.

2. Mesh

In terms of mesh, a variable mesh size was used with a minimum element size of 0.2 mm and a maximum element size of 5 mm. The mesh quality was verified as very good, as about 97% of the elements have an aspect ratio below three, and there are no distorted elements.

Mesh Details

Study name	Eversão (-Default-)
Mesh type	Solid Mesh
Mesher Used	Blended curvature-based mesh
Jacobian points for High quality mesh	16 points
Max Element Size	5 mm
Min Element Size	0,2 mm
Mesh quality	High
Total nodes	410667
Total elements	252195
Maximum Aspect Ratio	7 506,1
Percentage of elements with Aspect Ratio < 3	96,7
Percentage of elements with Aspect Ratio > 10	0,166
Percentage of distorted elements	0
Number of distorted elements	0
Remesh failed parts independently	Off
Time to complete mesh(hh:mm:ss)	00:00:53
Computer name	

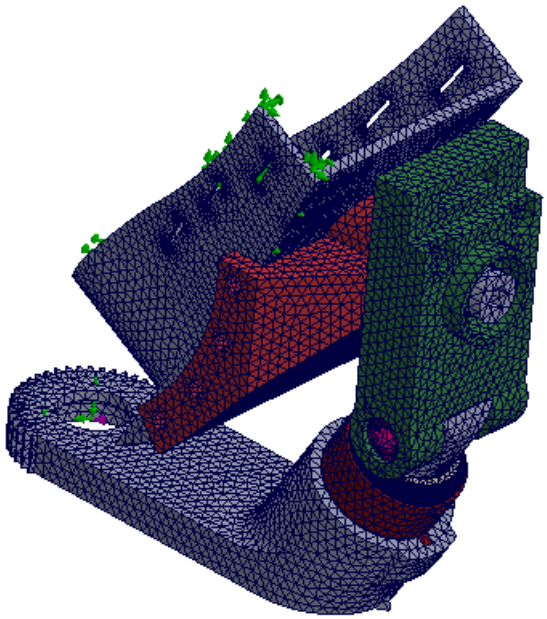

Figure 89- Mesh parameters used in the assembly of the eversion movement simulation.

3. Model Configuration

Now the boundary conditions, contact parameters and connectors need to be defined. Firstly, it was added two pin connectors, Figure 90.

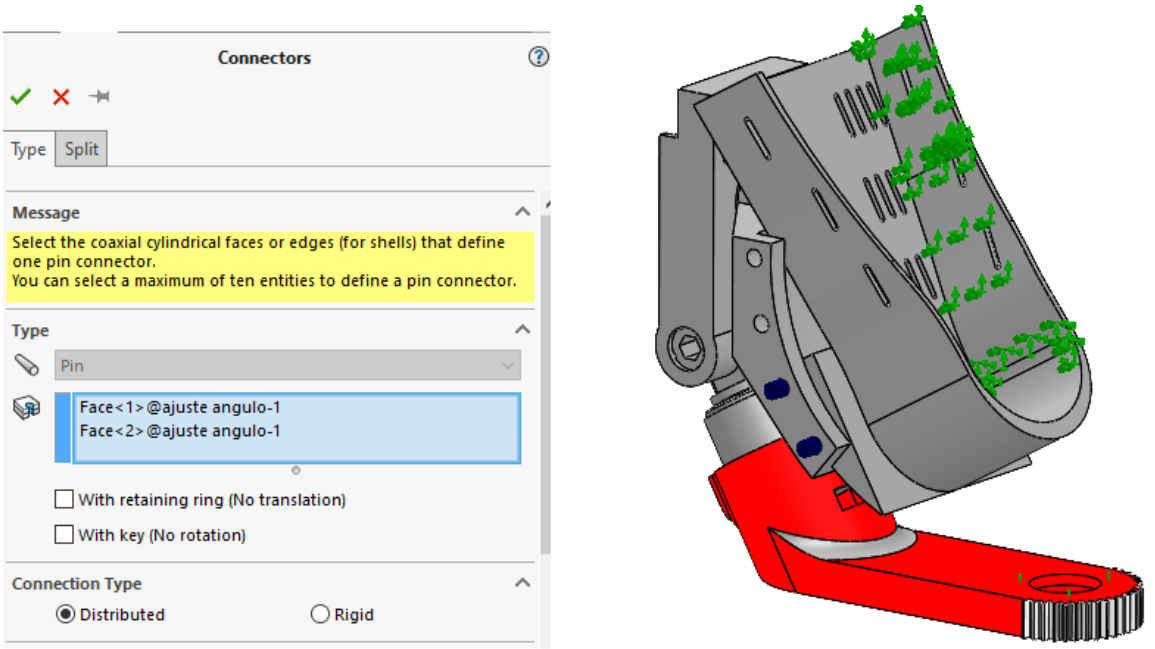

Figure 90- Pin connector parameters.

Next, the contact parameters were imposed. In this stage, it was defined the only contact relevant for this analysis in this stage was between the foot support and the angle adjustment part, Figure 91. This is because the rest of the parts were designed to be static concerning themselves in this movement.

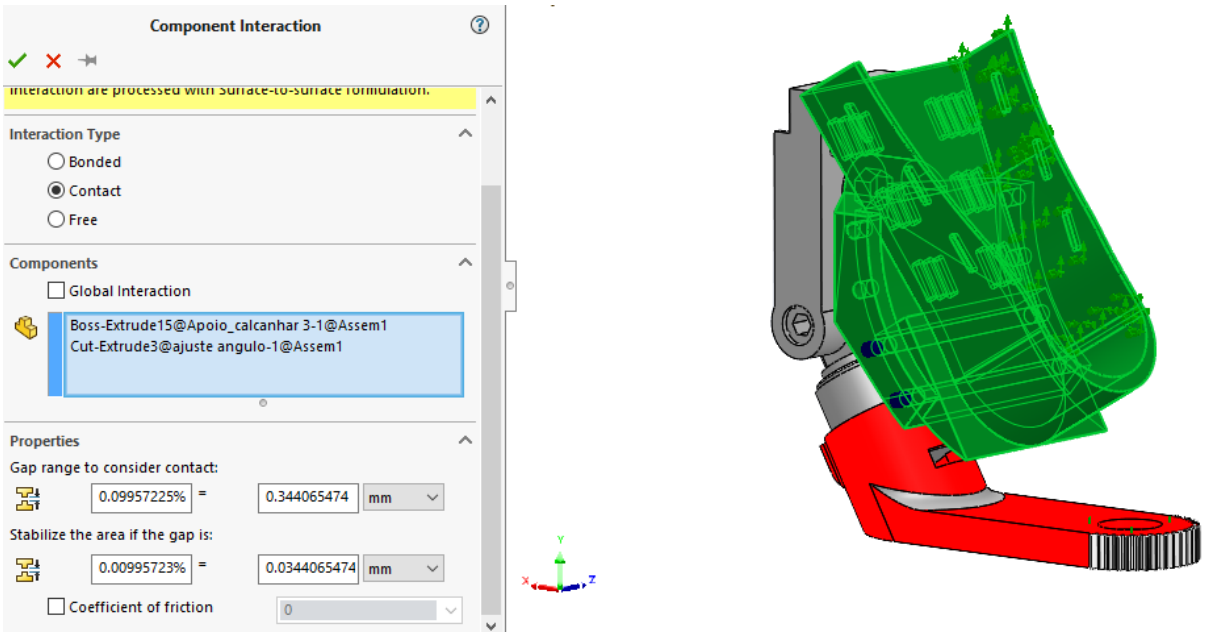

Figure 91- Contact parameters used in the assembly of the eversion movement.

Finally, the boundary conditions were defined. The foot support was fixed on one side, and torque was applied at the location of the eversion bearing. The value of this torque was 6000 Nmm, as in the eversion gears movement simulation, Figure 92.

Also, the location of the bearing was considered a fixed hinge and the location of the transfer spheres was designated as a roller/slider, Figure 93.

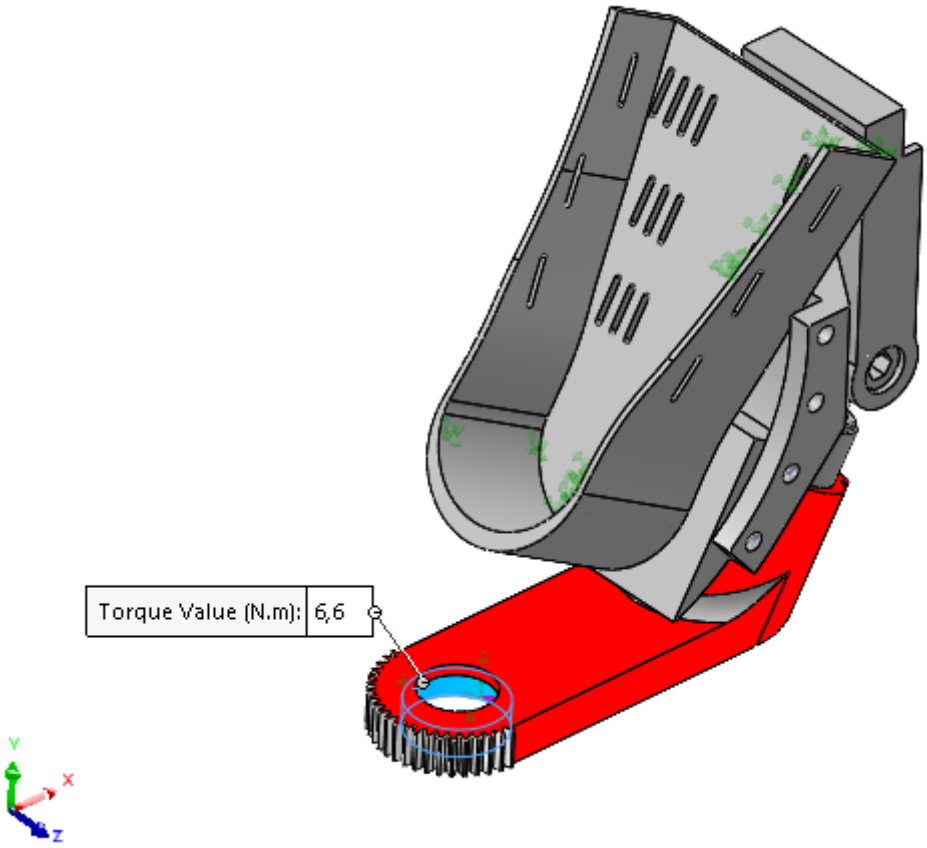

Figure 92- Load applied to the assembly of the eversion movement simulation.

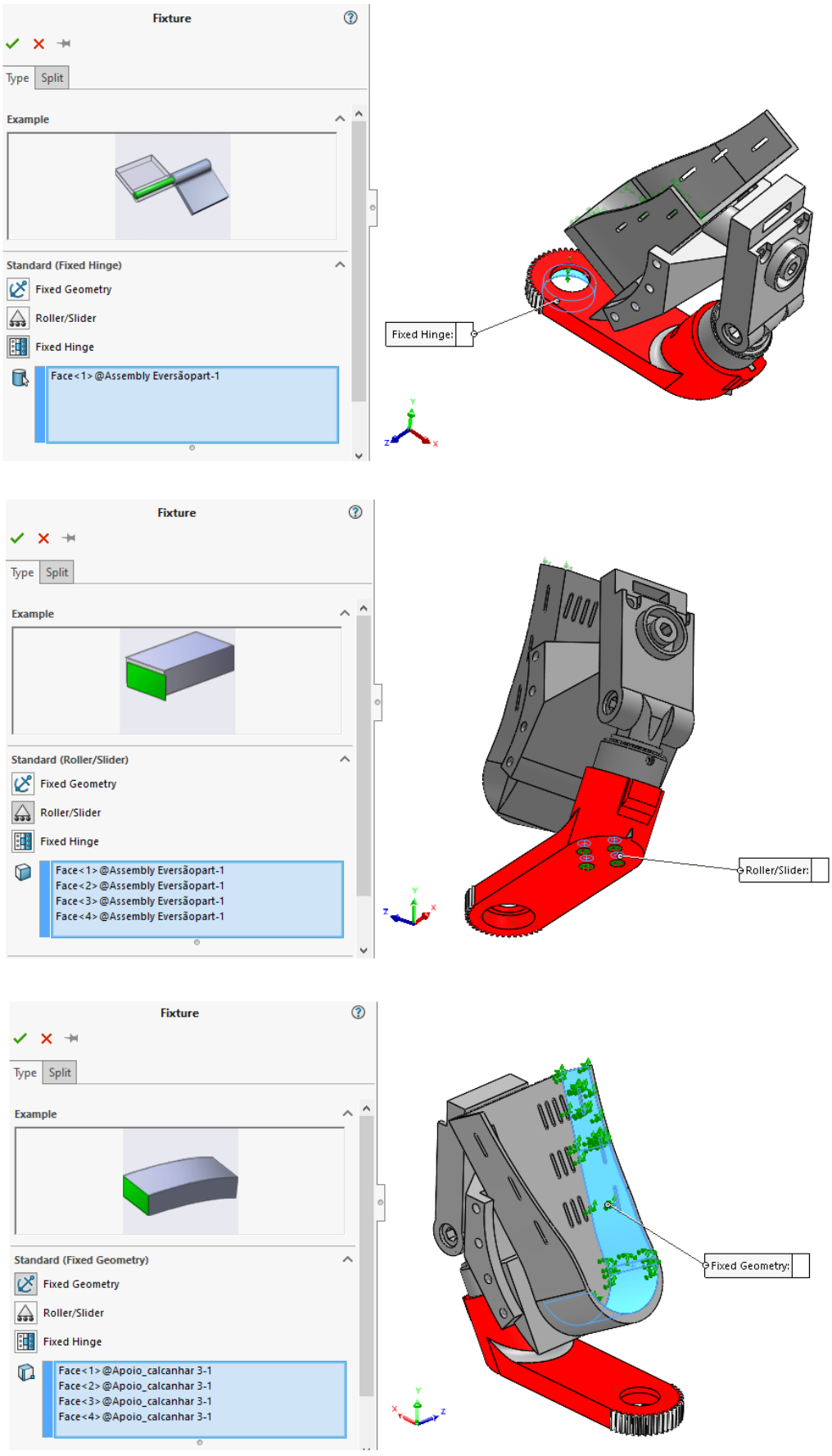

Figure 93- Boundary conditions applied to the assembly of the eversion movement simulation.

4. Numerical Solution

In terms of the desired solution, the most important thing is that the stress does not exceed the material's yield stress, and the displacements do not compromise the motion of the different parts of the device, Figure 94.

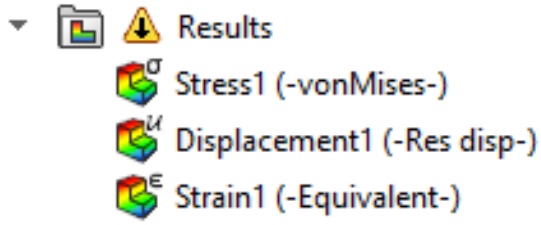

Figure 94- Numerical Results required for the assembly of the eversion movement simulation.

5. Numerical Results

Regarding the results in terms of stress, the maximum value recorded was well below the yield strength, about 3 MPa, Figure 95. In terms of displacement, the maximum value found was about 0,3 mm, which is an excellent result, Figure 96.

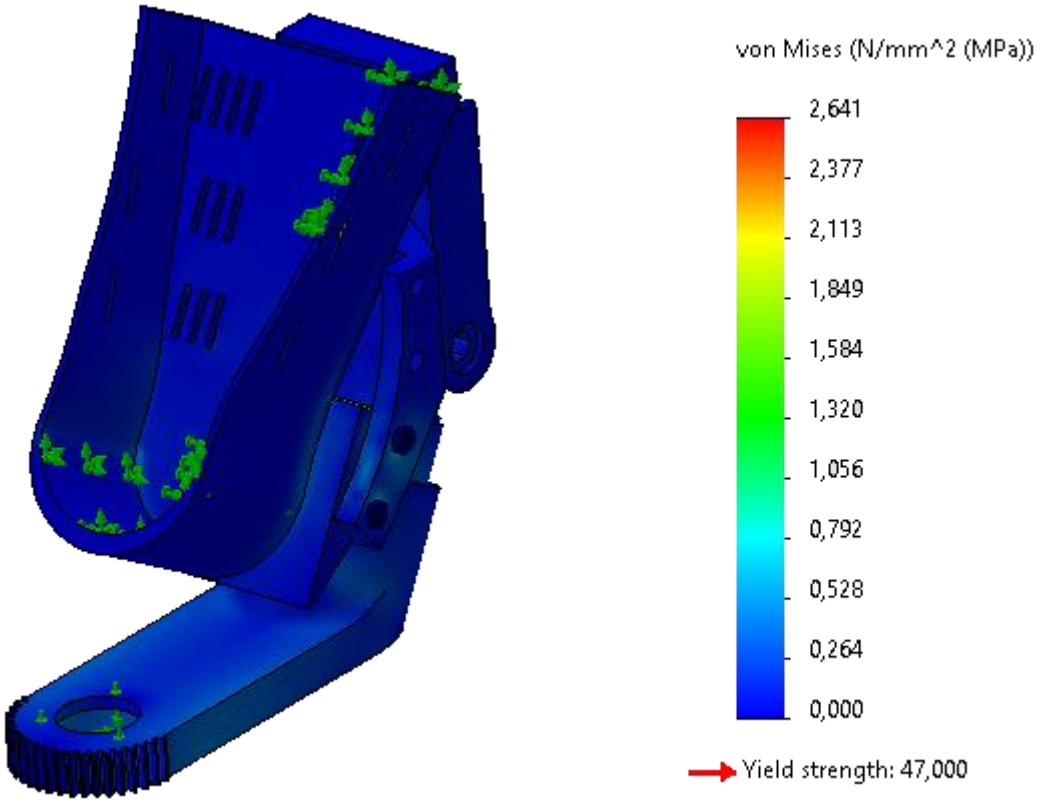

Figure 95- Results in terms of stress for the assembly of the eversion movement simulation.

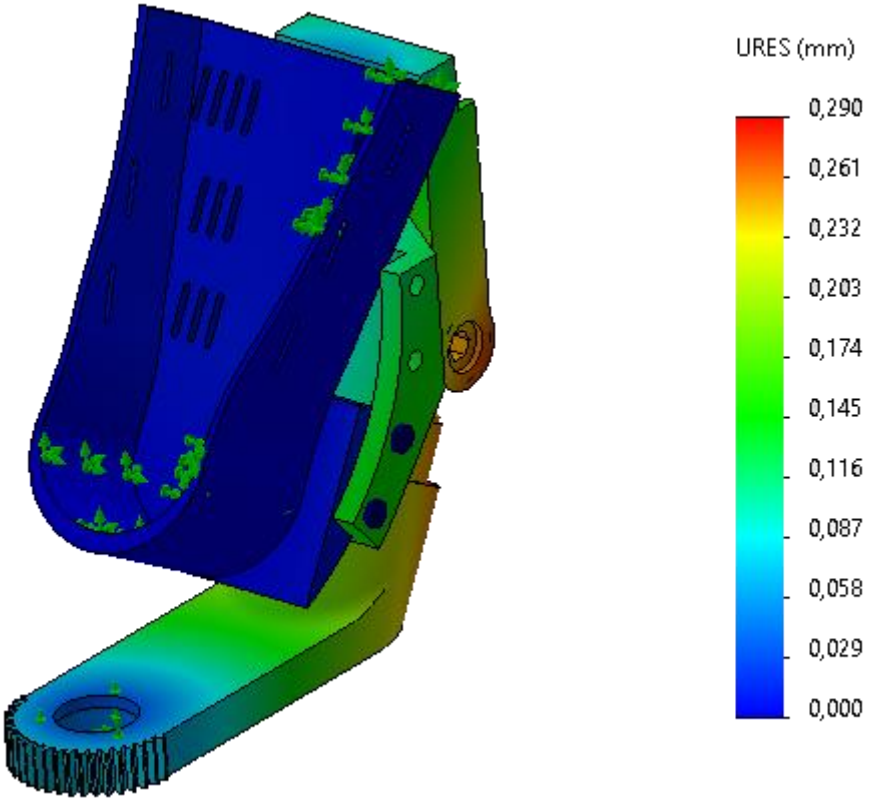

Figure 96- Results in terms of displacement for the assembly of the eversion movement simulation.

6. Verification and/ or Validation

This step is complicated in assemblies with multiple components because the location of the maximum stress or the maximum displacement is very difficult to predict. Nonetheless, as expected, this movement is not the hardest to do from the mechanical point of view, as in version 1.0, this movement was performed relatively easily.

4.1.6. ABDUCTION MOVEMENT

1. Geometry

In terms of geometry, some parts irrelevant to the analysis were suppressed, and only the foot support, the angle adjustment and the rotation shaft were considered, Figure 97. Also, the shaft faces were cut in order to impose the boundary conditions where the bearings will be installed.

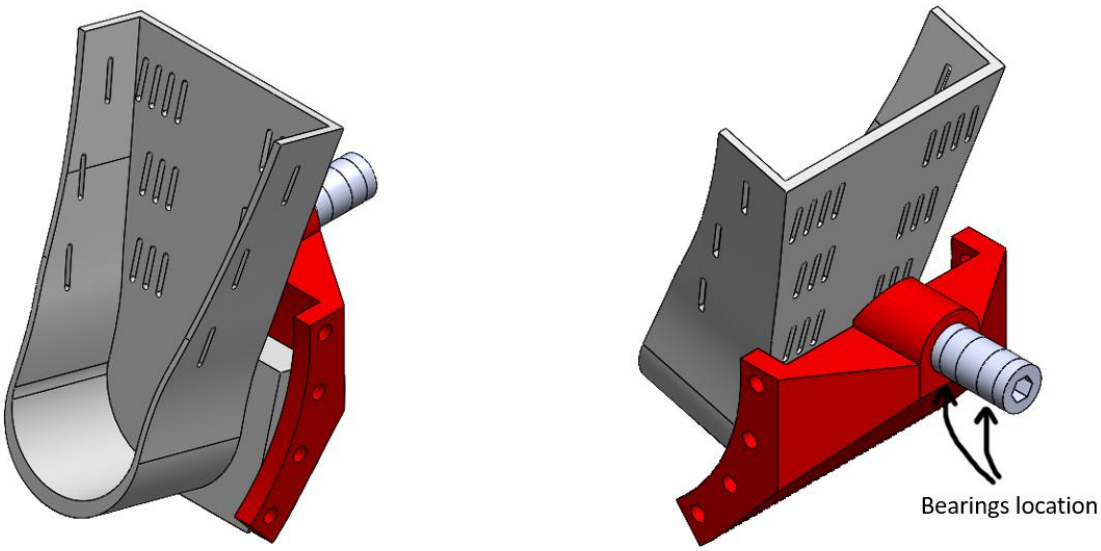

Figure 97- Assembly used for the abduction movement simulation.

2. Mesh

In terms of mesh, a variable mesh size was used with a minimum element size of 0.2 mm and a maximum element size of 5 mm. The mesh quality was verified as very good, as about 97% of the elements have an aspect ratio below three, and there are no distorted elements, Figure 98.

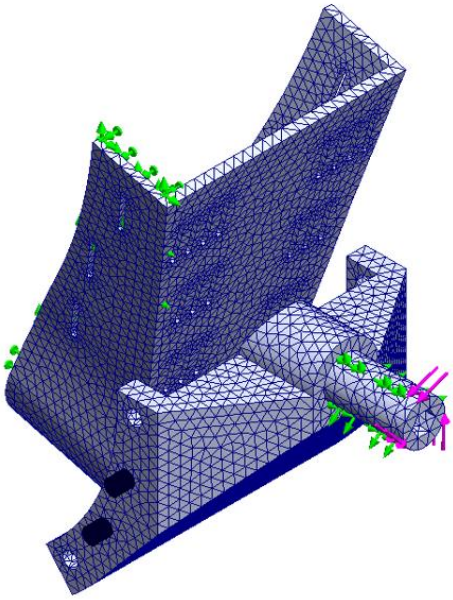

Mesh Details

Study name	Static 1 (-Default-)
Mesh type	Solid Mesh
Mesher Used	Blended curvature-based mesh
Jacobian points for High quality mesh	16 points
Max Element Size	5 mm
Min Element Size	2 mm
Mesh quality	High
Total nodes	95725
Total elements	57689
Maximum Aspect Ratio	314,04
Percentage of elements with Aspect Ratio < 3	98,8
Percentage of elements with Aspect Ratio > 10	0,156
Percentage of distorted elements	0
Number of distorted elements	0
Remesh failed parts independently	Off
Time to complete mesh(hh:mm:ss)	00:00:16
Computer name	TOMAS14CORREIA

Figure 98- Mesh parameters used in the assembly of the abduction movement simulation.

3. Model Configuration

Now the boundary conditions, contact parameters and connectors need to be defined. Firstly, it was added two pin connectors, Figure 99.

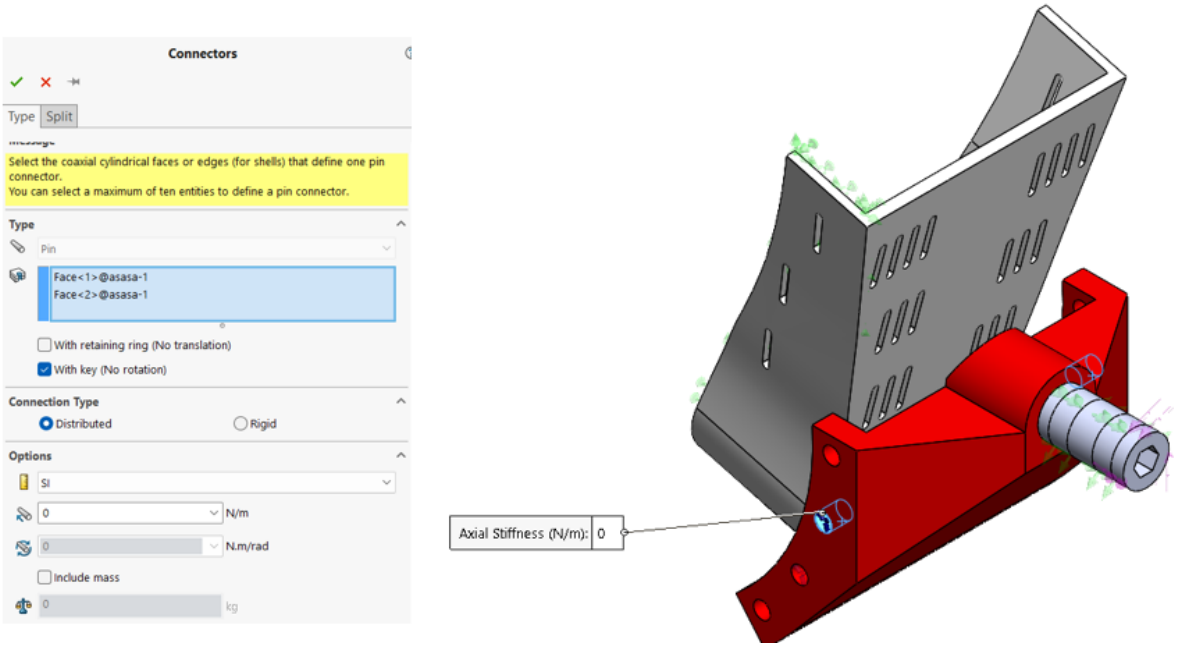

Figure 99- Pin connector parameters used for the abduction movement simulation.

Next, the contact parameters were imposed. In this stage, the global interaction between the components was defined with contact, Figure 100. No friction coefficient was considered in order to simplify the simulation.

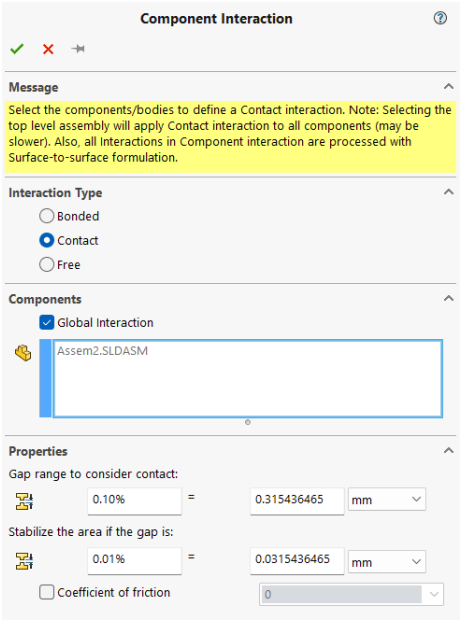

Figure 100- Contact parameters used for the abduction movement simulation

Finally, the boundary conditions were defined. The foot support was fixed on one side, and torque was applied to one end of the rotation shaft. The value of this torque was 6000 Nmm, as in the rotation gears movement simulation, Figure 101.

Also, the location of the bearings was considered a fixed hinge, Figure 102.

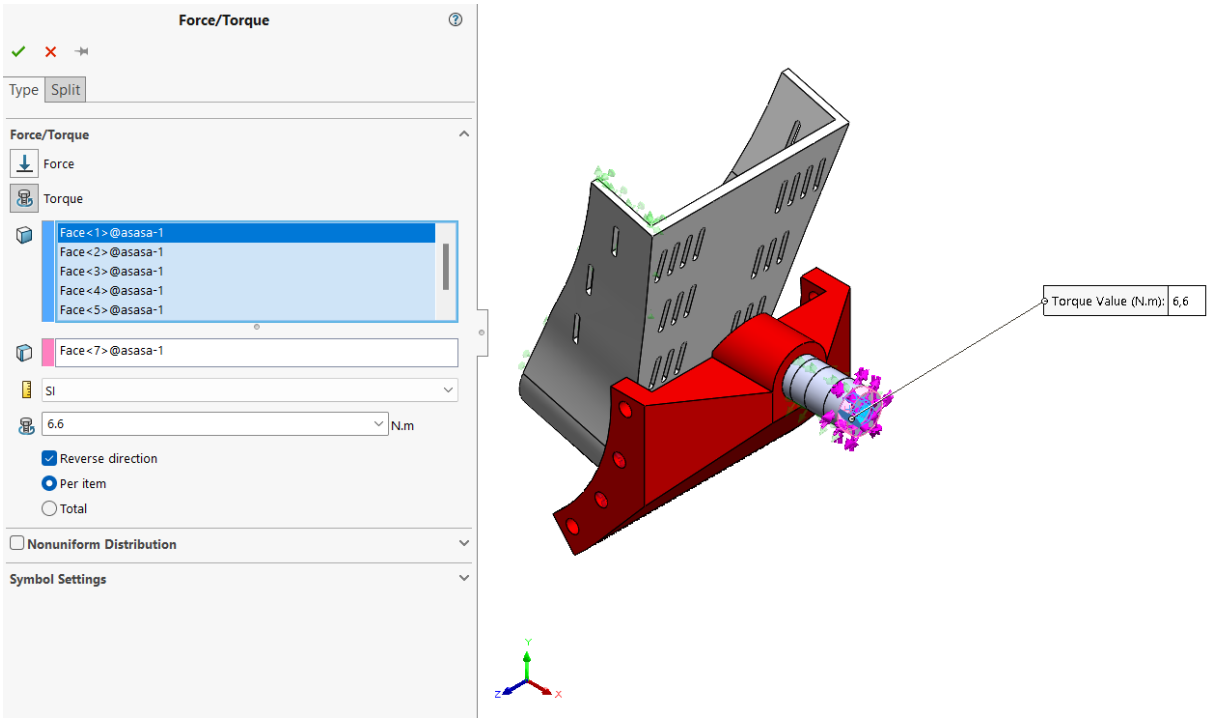

Figure 101- Load applied to the assembly of the eversion movement simulation.

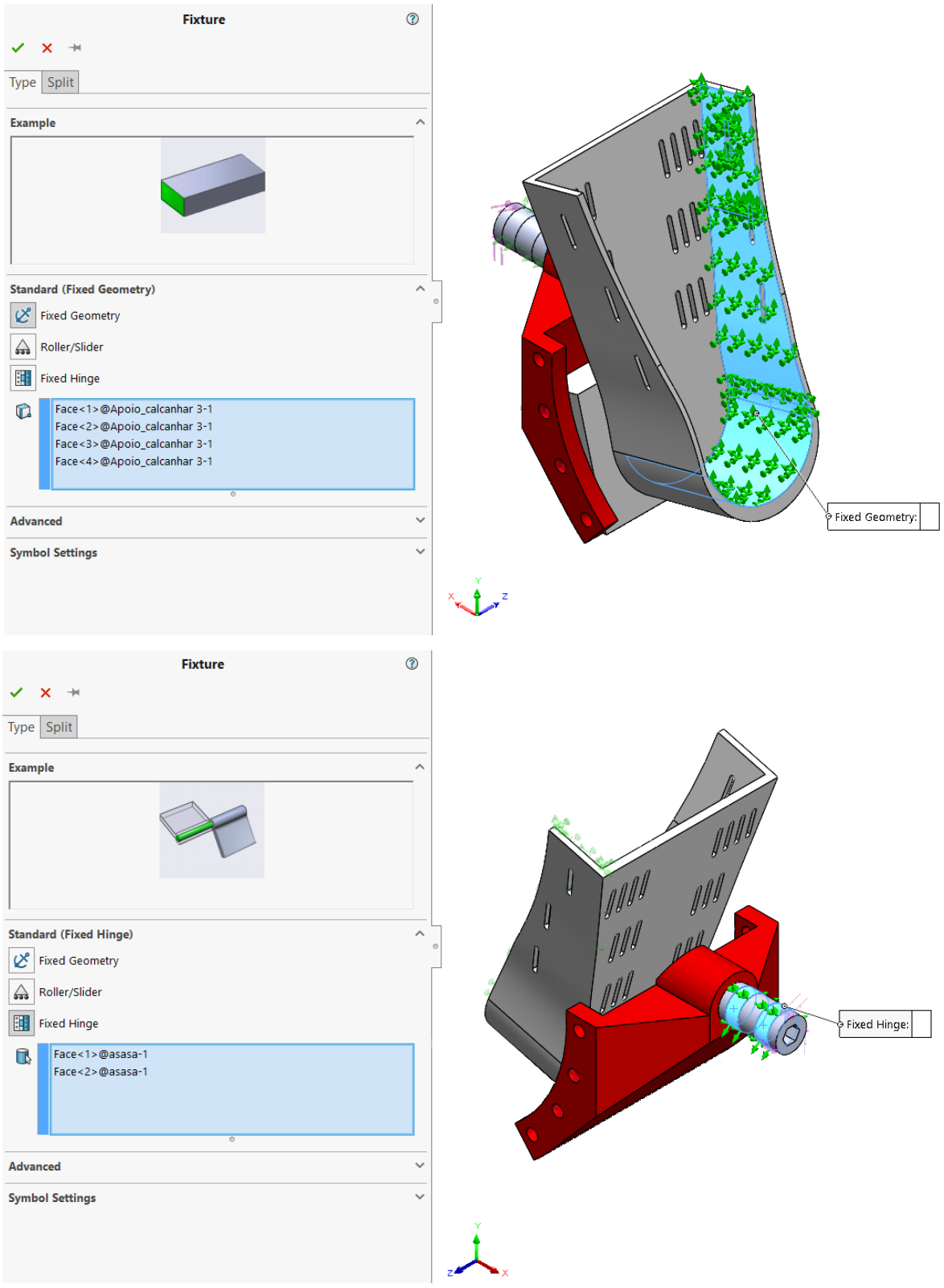

Figure 102- Boundary conditions applied to the assembly of the abduction movement simulation.

4. Numerical Solution

In terms of the desired solution, the most important thing is that the stress does not exceed the material's yield stress, and the displacements do not compromise the motion of the different parts of the device, Figure 103.

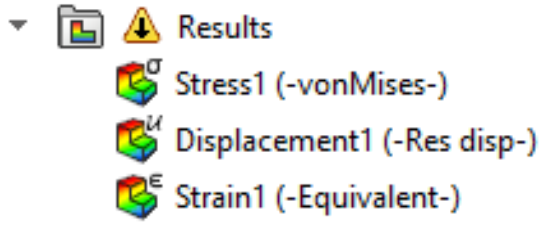

Figure 103- Numerical Results required for the assembly of the abduction movement simulation.

5. Numerical Results

Regarding the results in terms of stress, the maximum value recorded was below the yield strength, about 42 MPa, Figure 104. The maximum value found in displacement was about 1.2 mm, which is a solid result, Figure 105.

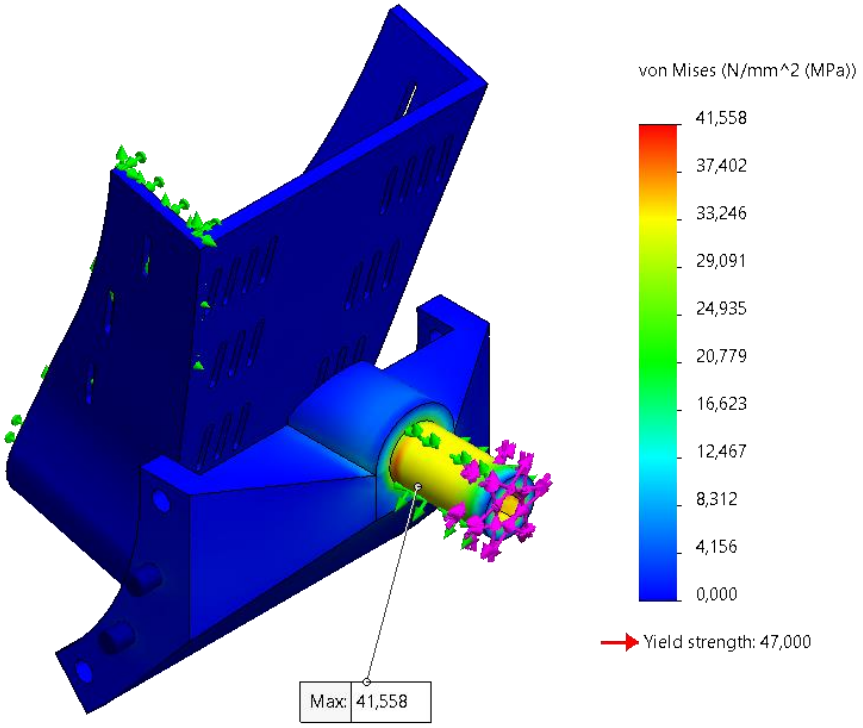

Figure 104- Results in terms of stress for the assembly of the abduction movement simulation.

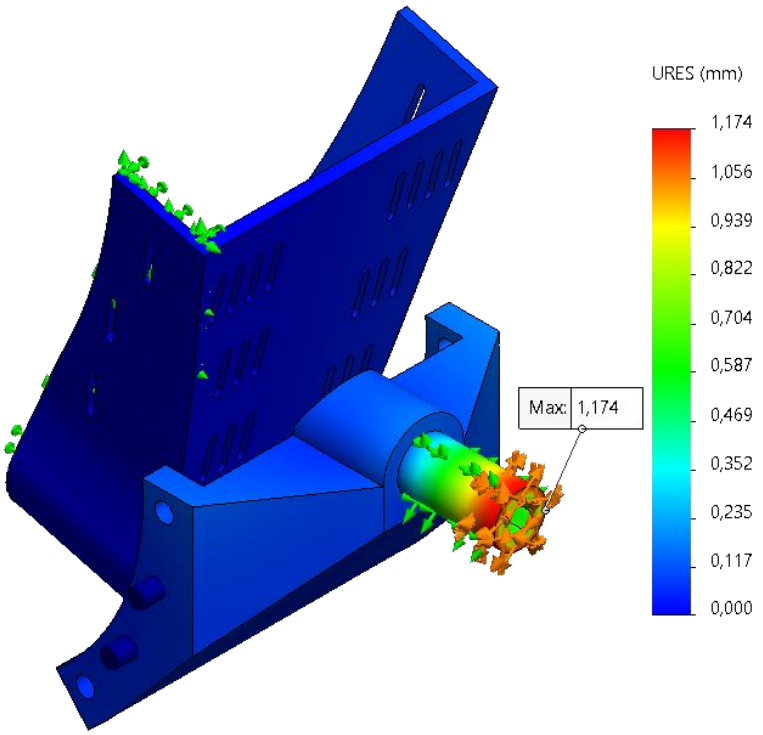

Figure 105- Results in terms of displacement for the assembly of the abduction movement simulation.

6. Verification and/ or Validation

This step is quite tricky in assemblies with multiple components because the location of the maximum stress or the maximum displacement is very difficult to predict. Nonetheless, as expected, the maximum stress is located in the contact of the shaft and the adjustment angle part, as in this zone, there are sharp edges which lead to some stress concentrations.

4.1.7. ANTERIOR TRANSLATION MOVEMENT

This simulation is quite tricky due to the complex parts in the connection between the piston and the fixation shaft, as seen in the Connection Validation phase. This simulation doesn't pretend to validate this connection but simplifies it and, at the same time, gets rid of the stress concentrations and complex parts while still improving the stiffness of the assembly.

1. Geometry

In terms of geometry, firstly, it explored one where the connection is made through a hexagonal pin, Figure 106.

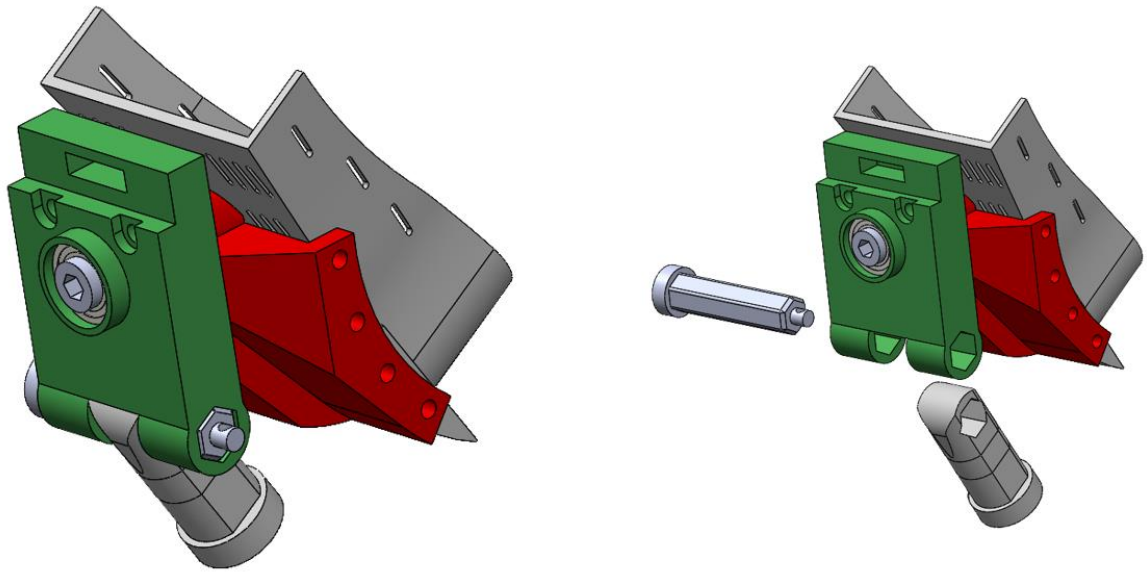

Figure 106- First geometry used for the anterior translation movement simulation (left). Exploded view (right).

2. Mesh

In terms of mesh, a variable mesh size was used with a minimum element size of 0.5 mm and a maximum element size of 3 mm. The mesh quality was verified as very good, as about 99% of the elements have an aspect ratio below three, and there are no distorted elements, Figure 107.

Mesh Details

Study name	Static 1 (-Default-)
Mesh type	Solid Mesh
Mesher Used	Standard mesh
Automatic Transition	Off
Include Mesh Auto Loops	Off
Jacobian points for High quality mesh	16 points
Element size	3 mm
Tolerance	0,5 mm
Mesh quality	High
Total nodes	402898
Total elements	261196
Maximum Aspect Ratio	8,3921
Percentage of elements with Aspect Ratio < 3	99,6
Percentage of elements with Aspect Ratio > 10	0
Percentage of distorted elements	0
Number of distorted elements	0
Remesh failed parts independently	Off
Time to complete mesh(hh:mm:ss)	00:00:26
Computer name	TOMAS14CORREIA

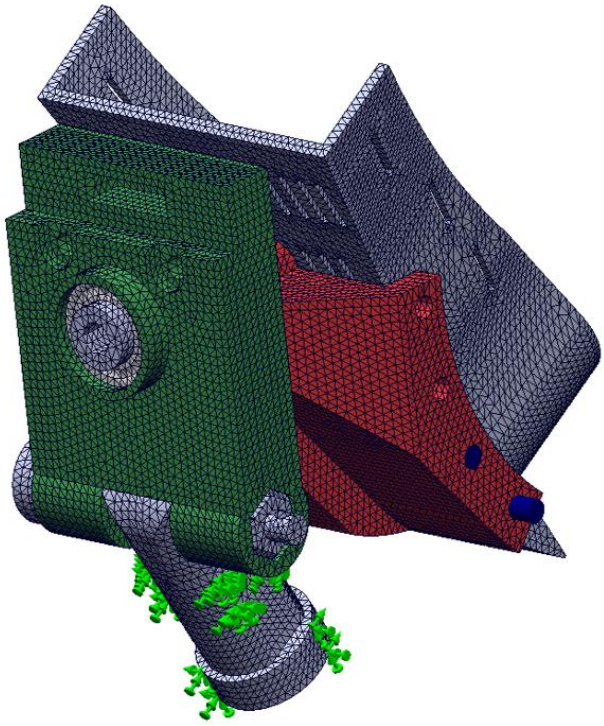

Figure 107- Mesh parameters used in the first geometry iteration of the assembly of the anterior translation movement simulation.

3. Model Configuration

Now the boundary conditions, contact parameters and connectors need to be defined. Firstly, two pin connectors were added, Figure 108.

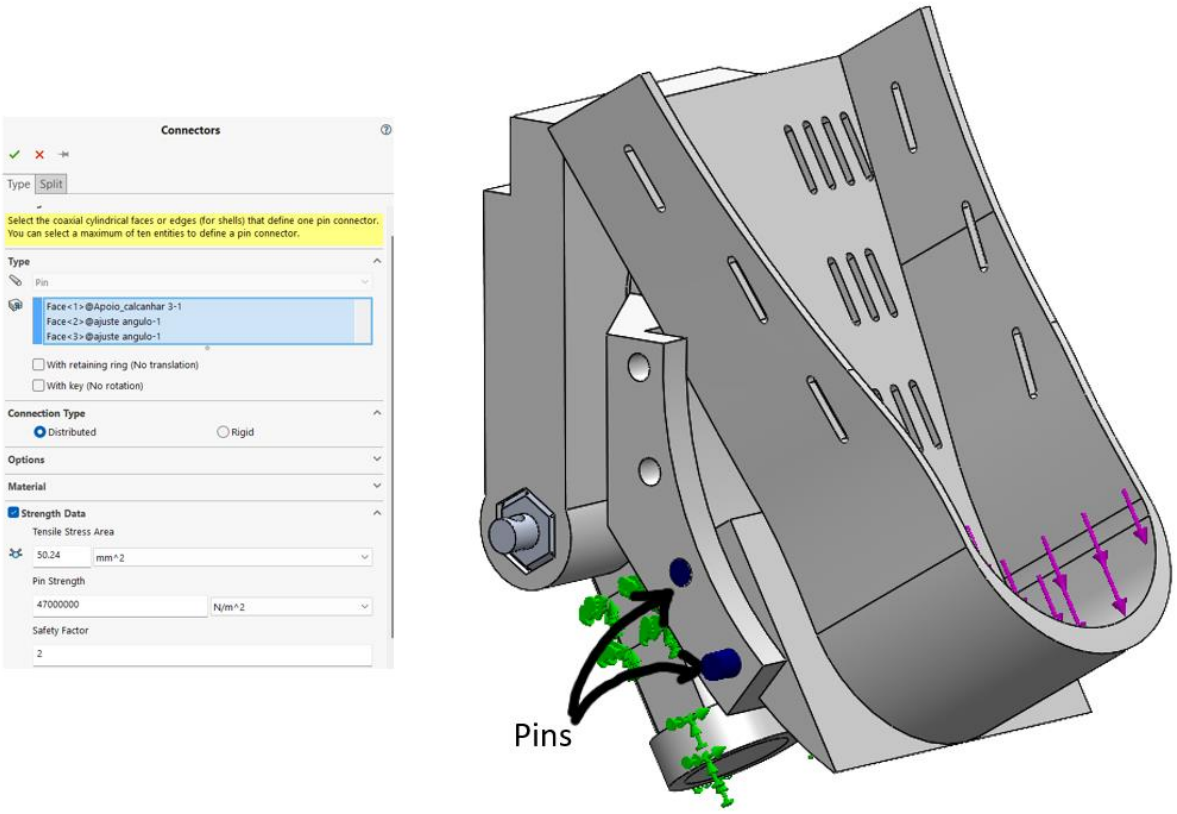

Figure 108- Pin connector parameters used in the first geometry iteration of the assembly of the anterior translation movement simulation.

Next, the contact parameters were imposed. In this stage, three different contacts were defined. The first was to describe the contact between some components, Figure 109.

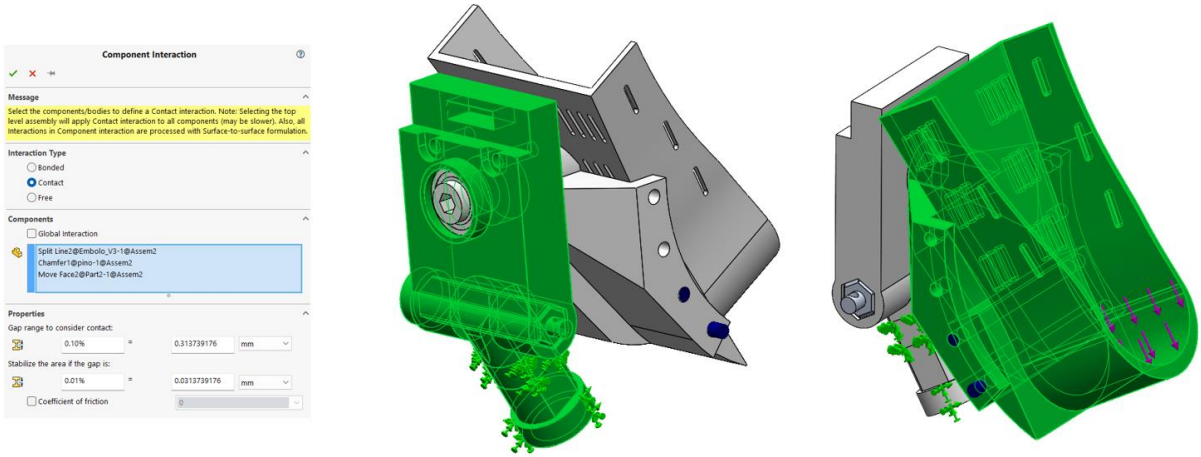

Figure 109- First contact parameters used in the first geometry iteration of the assembly of the anterior translation movement simulation.

The second one considered that the rotation shaft, the bearings and the I connection are bonded as the contact between these parts is irrelevant. This consideration simplifies the simulation, Figure 110.

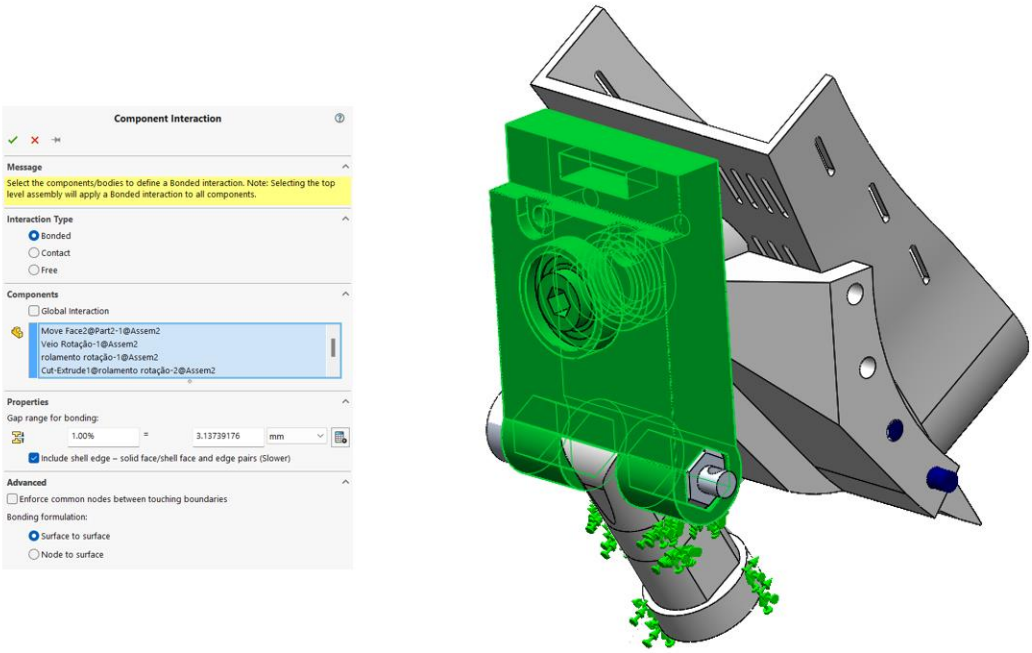

Figure 110- Second contact parameters used in the first geometry iteration of the assembly of the anterior translation movement simulation.

The third and last one considered that the rotation shaft and the angle adjustment part are bonded, enforcing common nodes between touching boundaries, Figure 111.

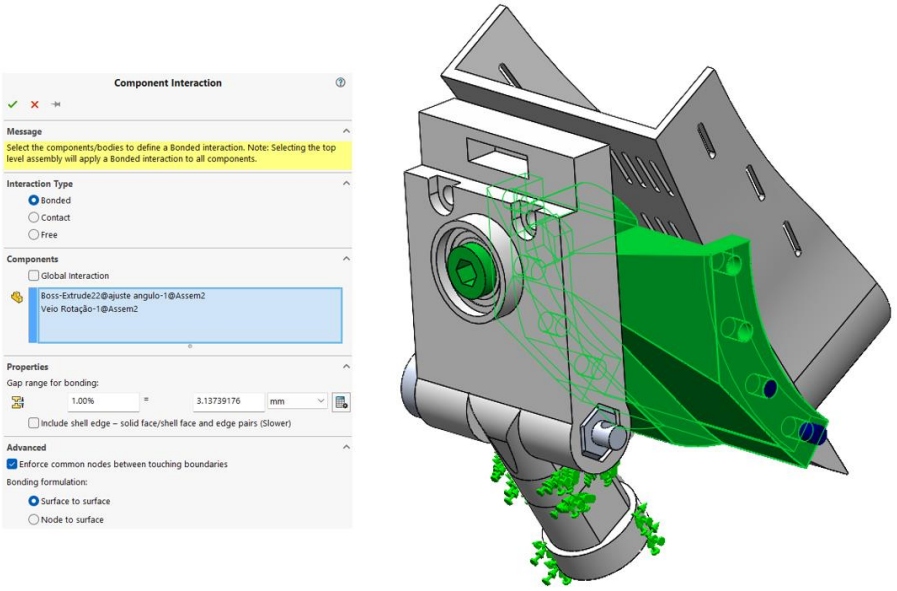

Figure 111- Third contact parameters used in the first geometry iteration of the assembly of the anterior translation movement simulation.

Finally, the boundary conditions were defined. The cylinder shaft was fixed, and a force was applied to the foot support, Figure 112 and Figure 113. The value of this force was 200 N, but it was considered a safety factor of 1,5, so the force applied has a value of 300 N.

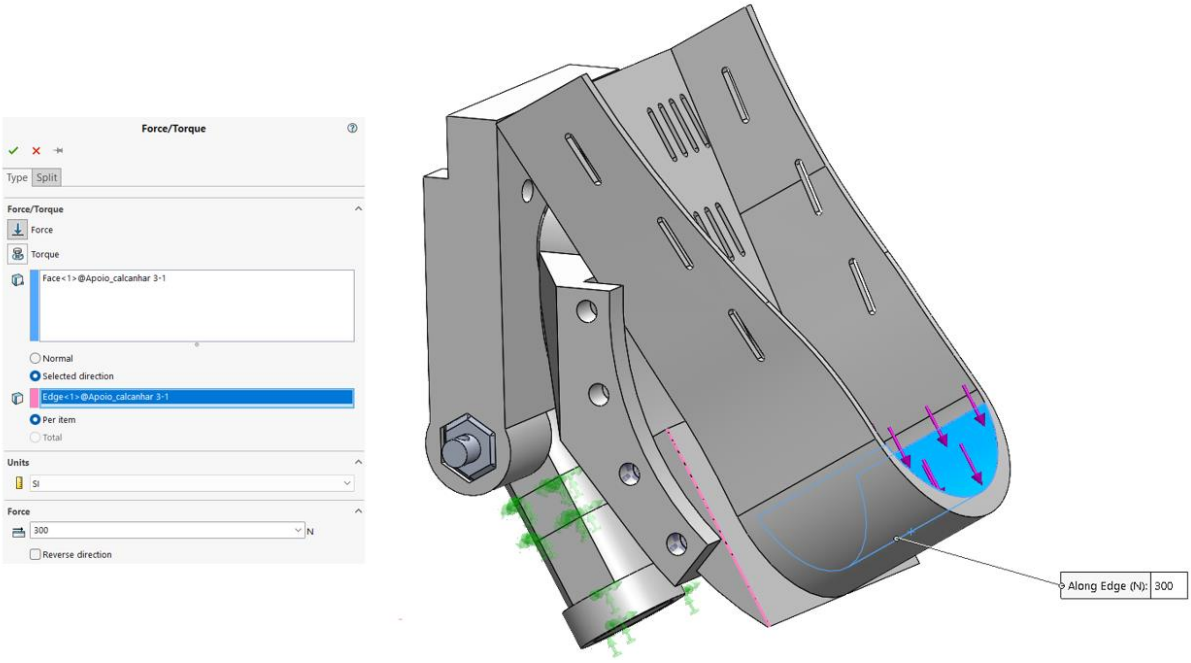

Figure 112- Load applied in the first geometry iteration of the assembly of the anterior translation movement simulation.

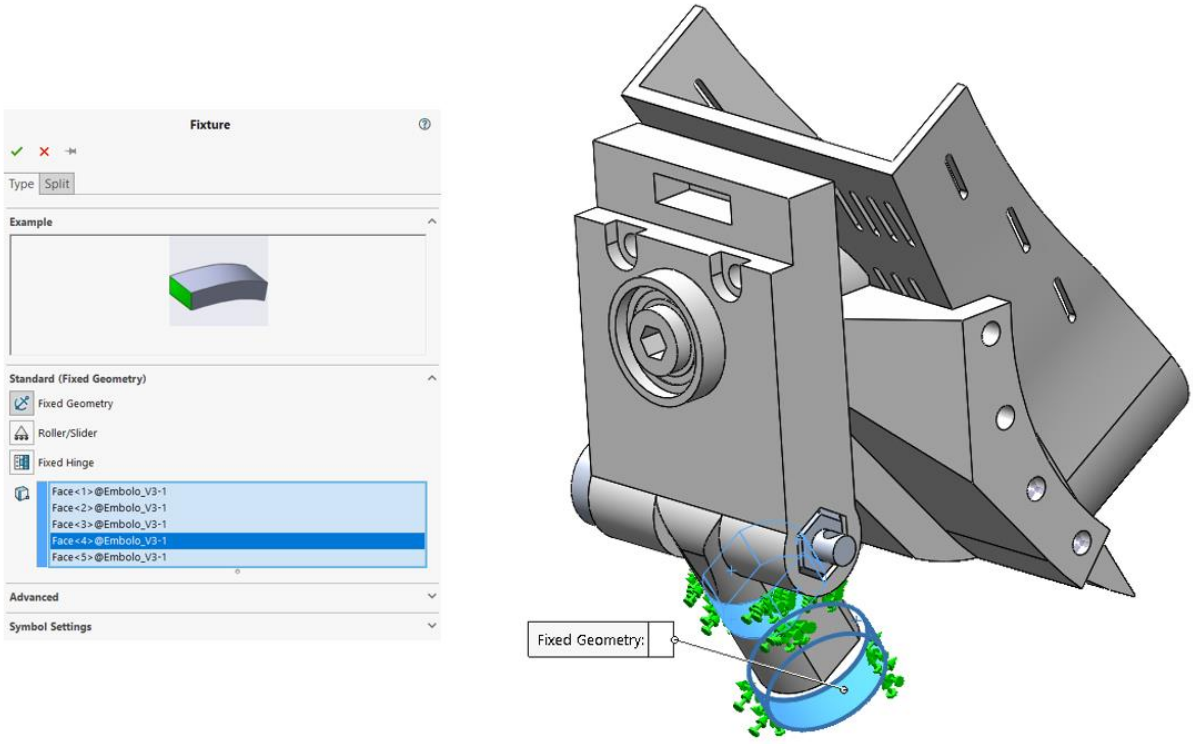

Figure 113- Boundary conditions applied to the anterior translation movement simulation assembly.

4. Numerical Solution

In terms of the desired solution, the most important thing is that the stress does not exceed the material's yield stress, and the displacements do not compromise the motion of the different parts of the device, Figure 114.

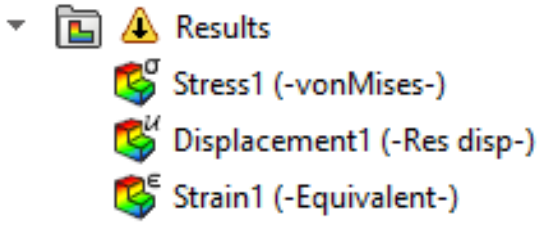

Figure 114- Numerical Results required for the first geometry iteration of the assembly of the anterior translation movement simulation.

5. Numerical Results

Regarding the results in terms of stress, the maximum value recorded was almost the yield strength of about 46 MPa, Figure 115. In terms of displacement, the maximum value found was about 15 mm, which is a non-satisfactory result, Figure 116. For this reason, a new solution was studied with another type of connection.

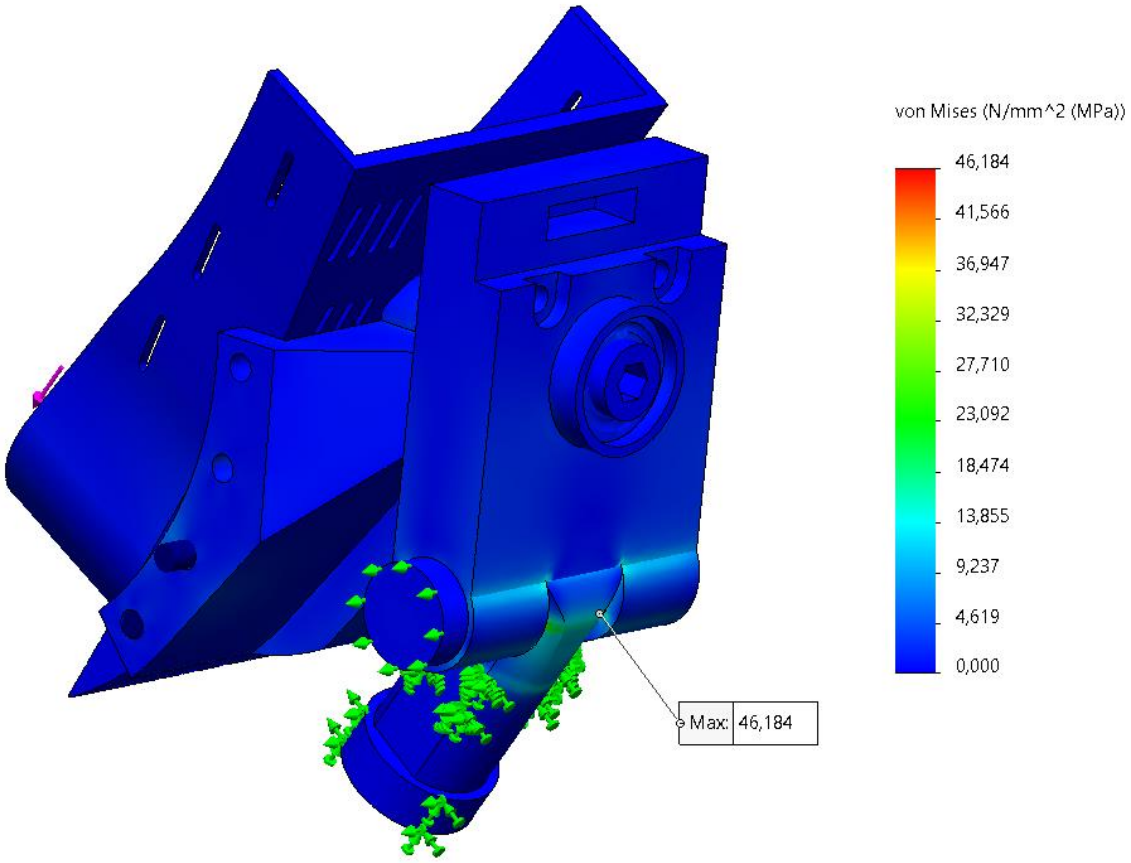

Figure 115- Results in terms of stress for the assembly of the anterior translation movement simulation.

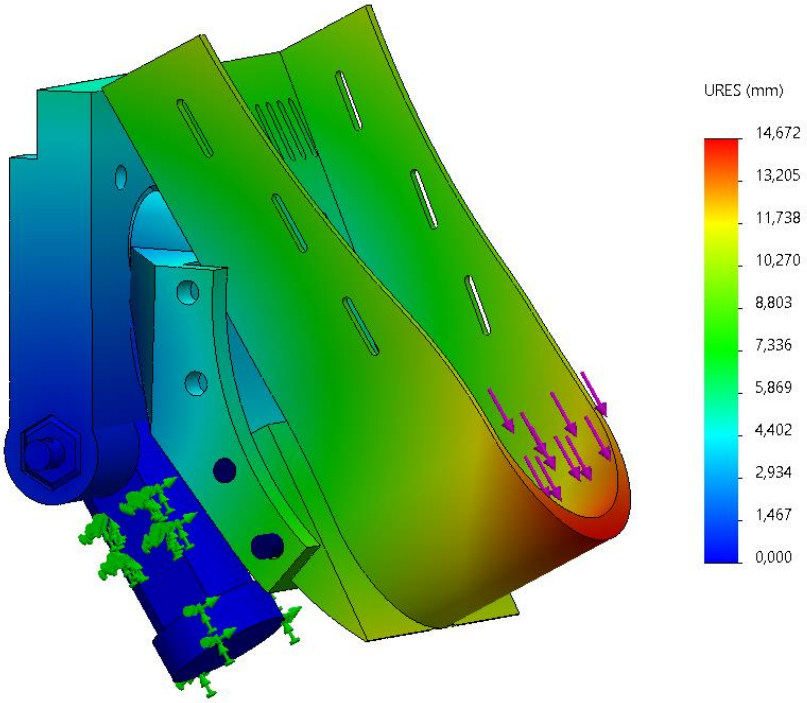

Figure 116- Results in terms of displacement for the assembly of the anterior translation movement simulation.

6. New Geometry

Once the first iteration wasn't worked the expected way, a new solution was studied. This new one uses two pins instead of only one, Figure 117. This allows the load to be supported in shear and not in torsion, as the material has much more load-bearing capacity in this way. For this reason, the expected stiffness should be much higher. Also, the fact that the pins are circular shouldn't create stress concentrations like the previous hexagonal pin.

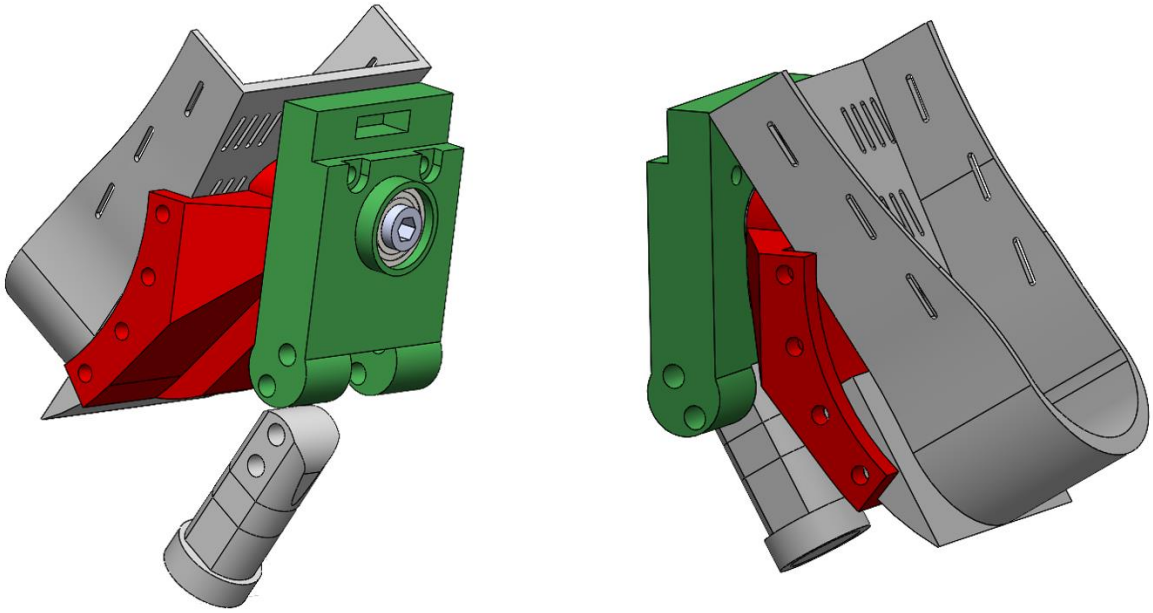

Figure 117- New assembly geometry for the anterior translation movement simulation.

The mesh and the simulation configurations are precisely the same as in the initial geometry. The only difference was the two pins added in the connection, Figure 118.

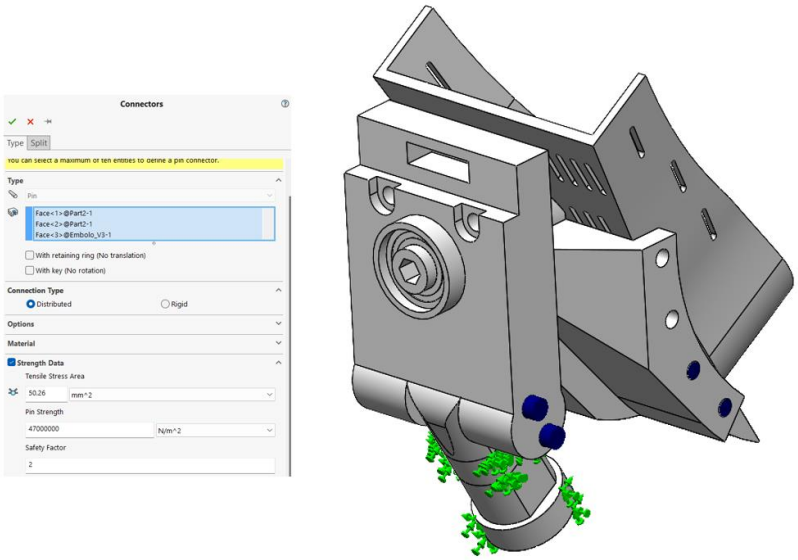

Figure 118- Pins added to the new geometry.

Also, the same results will be checked in terms of numerical results.

5. Results

Regarding the results in terms of stress, the maximum value recorded was below the yield strength, about 26 MPa, Figure 119. The maximum value found in displacement was about 6 mm, which is a very interesting result, Figure 120.

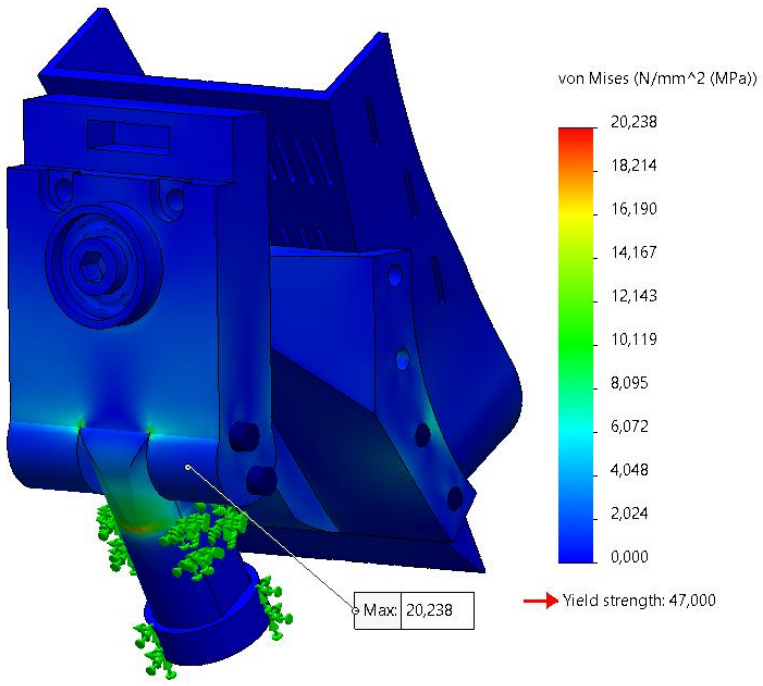

Figure 119- Results in terms of stress for the new geometry.

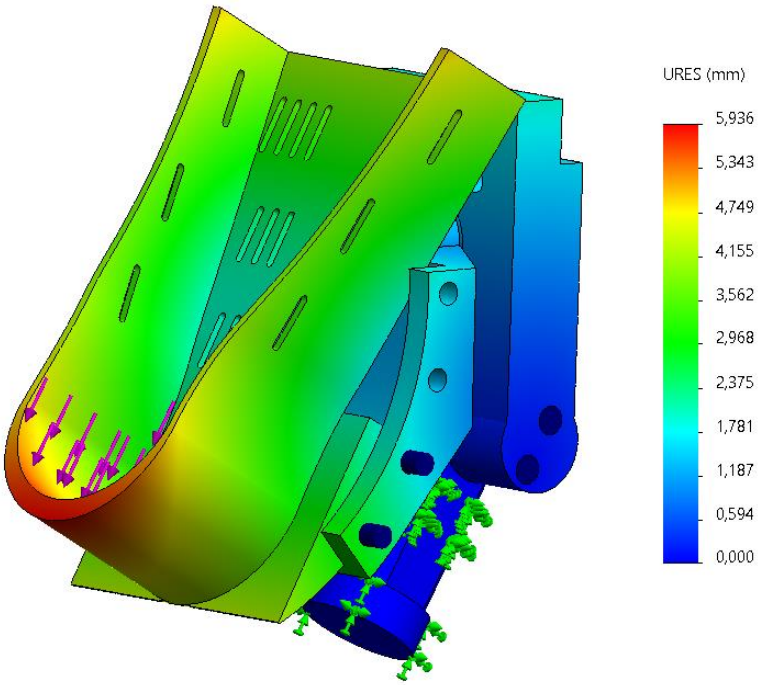

Figure 120- Results in terms of displacement for the new geometry.

Considering that the load is much higher than the real load and that the displacement that truly matters is the one that is in the direction of the movement next, this directional displacement will be shown in Figure 121.

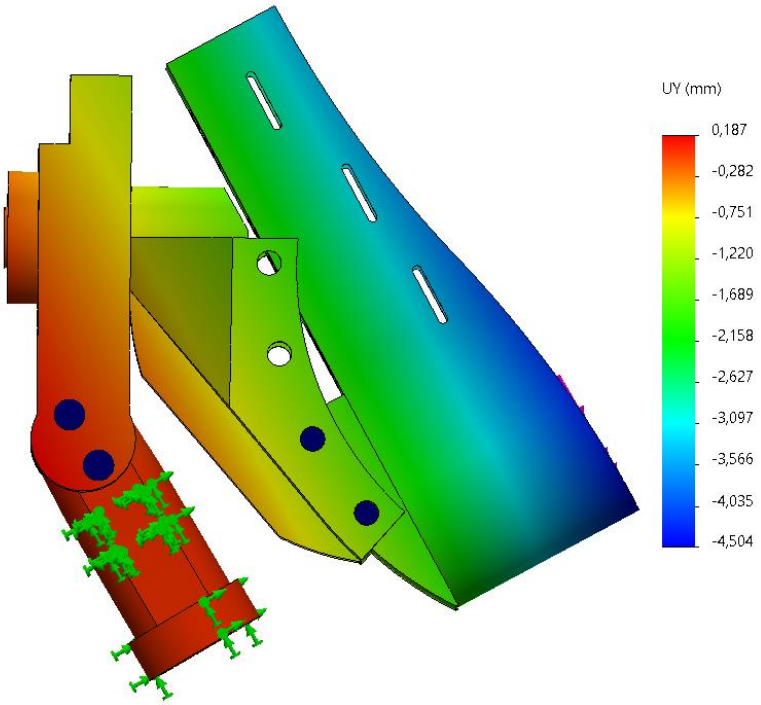

Figure 121- Results in terms of directional displacement for the new geometry.

This is an acceptable result. However, it should be noted that considering a linear behaviour (which is a very reasonable assumption), the expected displacement for the real load (200 N) is:

$$Real\ displacement = \frac{4{,}5 \times 200}{300} = 3\ mm$$

This is a very respectful result as the load is very high and the materials used are not properly load-bearing. Also, keeping the linear behaviour consideration if the material with the highest Young Modulus is used, then the displacement becomes:

$$Real\ displacement = \frac{3 \times 1800}{5696} \approx 1\ mm$$

Keeping this in mind, it is advised to use the material with the highest mechanical properties because even this material doesn't present properties of a load-bearing material; however, it is the best option available.

4.1.8. TIBIA SUPPORT

1. Pre-analysis

Before starting the initial phase of the simulation, it is necessary to carry out a pre-analysis. This is intended to perform some calculations by hand in order to verify the simulation results. Since the geometry is very complicated, there will not be any pre-analysis as the results would be far from reality due to the simplifications used.

2. Geometry

The geometry imported into the simulation will be simplified; therefore, only the sprocket and rack will be studied, Figure 122.

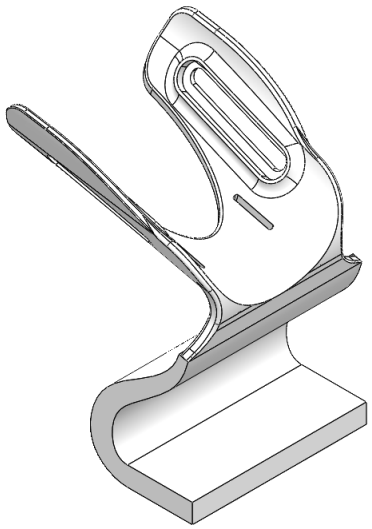

Figure 122- Simplified geometry of the tibia support.

3. Mesh

This point is one of the most important since a weak discretization of the set will inevitably lead to poor and far from real results. A mesh size of 3 mm was used, Figure 123.

The mesh quality is very satisfactory as 99,6% of all the elements have an aspect ratio below 3.

Mesh Details

Study name	Static 1 (-Default-)
Mesh type	Solid Mesh
Mesher Used	Standard mesh
Automatic Transition	Off
Include Mesh Auto Loops	Off
Jacobian points for High quality mesh	16 points
Element size	3 mm
Tolerance	1 mm
Mesh quality	High
Total nodes	175571
Total elements	113452
Maximum Aspect Ratio	106,56
Percentage of elements with Aspect Ratio < 3	99,6
Percentage of elements with Aspect Ratio > 10	0,00176
Percentage of distorted elements	0
Number of distorted elements	0
Time to complete mesh(hh:mm:ss)	00:00:15
Computer name	TOMAS14CORREIA

Figure 123- Mesh parameters used in the tibia support.

4. Model Configuration

Now, it is necessary to define the boundary conditions and material properties. The material properties are the same for all the simulations and parts because the device will be produced using the same material.

In terms of boundary conditions, see Figure 124.

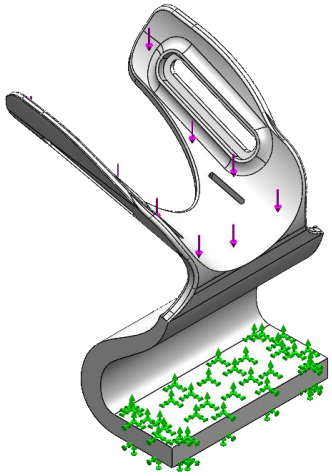

Figure 124- Boundary conditions and force applied to the tibia support.

The base was considered fixed, while in the zone where the tibia seats, a force of 200 N was applied.

5. Numerical Solution

In terms of the desired solution, the most important thing is that the stress does not exceed the material's yield stress, and the displacements do not compromise the motion of the different parts of the device, Figure 125.

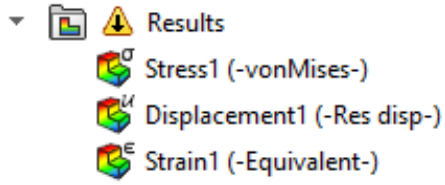

Figure 125- Numerical results required for the tibia support.

6. Numerical Results

Regarding the results in terms of stress, the maximum value recorded was about 18 MPa, while in terms of displacement, the maximum value found was about 10 mm, Figure 126.

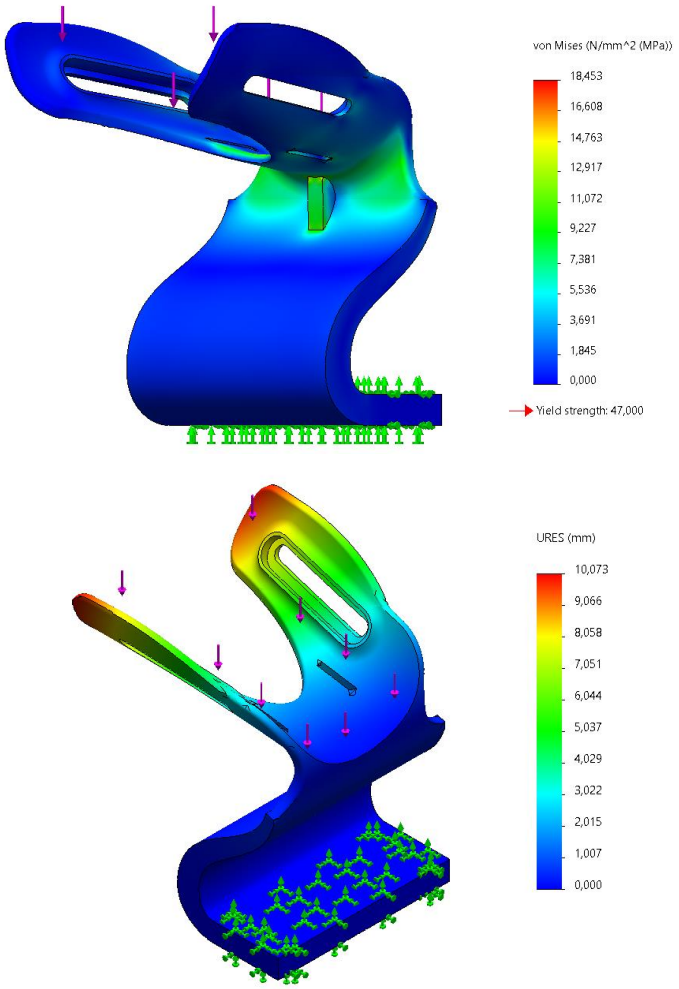

Figure 126- Stress (above) and displacement (behind) results of the tibia support.

7. Verification and/or Validation

In this last step, some checks will be made to verify the simulation's validity. Firstly, the maximum stress value is found at the expected location in the reinforcement backbone, Figure 127.

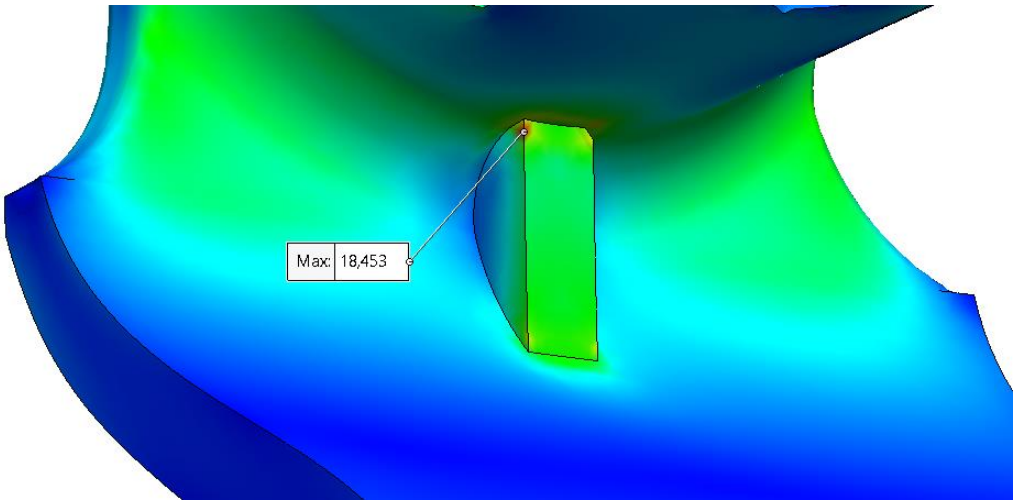

Figure 127- Maximum stress location for the tibia support.

Regarding the displacement, it seems that 10 mm is a lot; however, this is the maximum value. If we look at the zone where the tibia is supported, it is noticeable that the displacement results are satisfying, Figure 128.

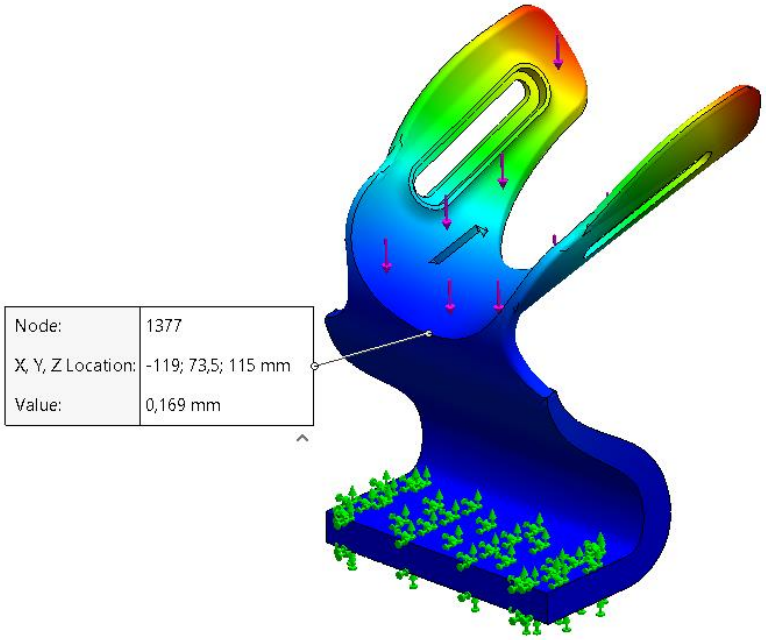

Figure 128- Displacement detail for the tibia support.

4.2. KINEMATIC VALIDATION

Having the device validated from the mechanical point of view will now be validated from the cinematic point of view so that every movement can be realized without any interference. In this chapter, the Motion Study feature of Solidworks was used.

Eversion Movement

Firstly, the eversion/ inversion movement was performed. This was accomplished as expected for an angle of 60°, Figure 129.

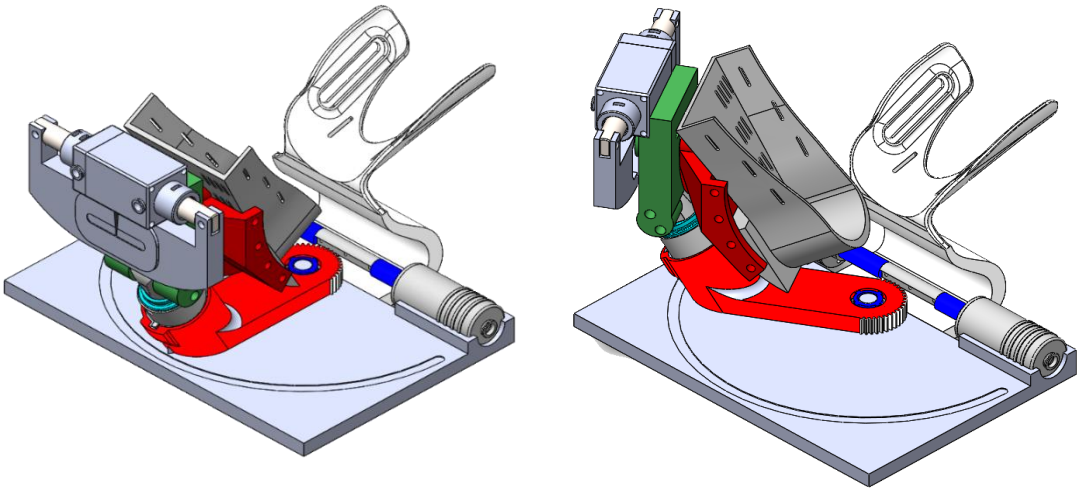

Figure 129- Motion simulation of the eversion/ inversion movement.

Abduction Movement

Secondly, the abduction/ adduction movement was simulated. Once again, and as expected, the motion was completed without any hiccups due to the same analysis performed on the concept, Figure 130.

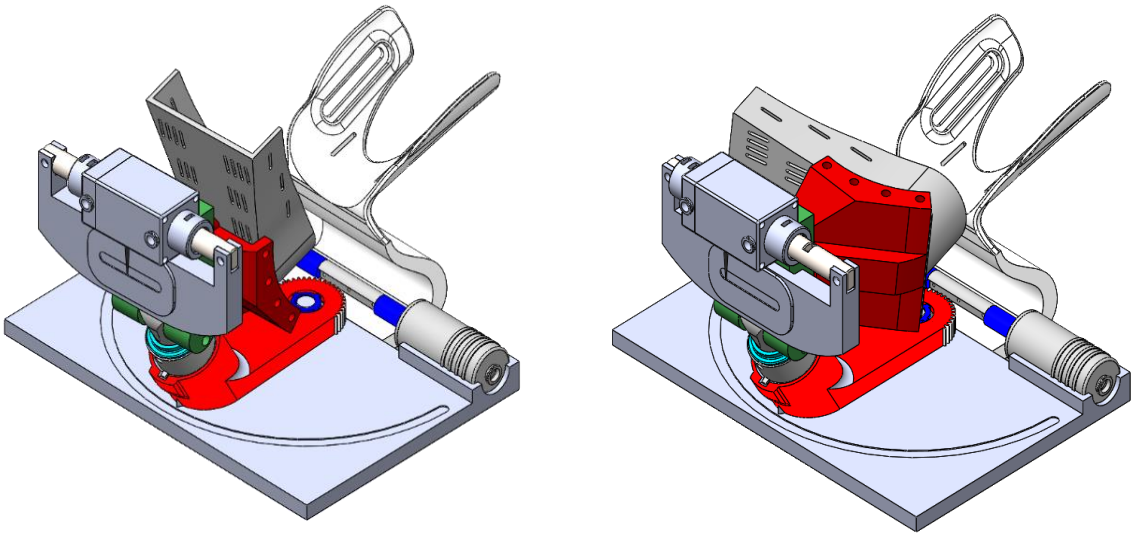

Figure 130- Motion simulation of the abduction/ adduction movement.

Anterior Translation Movement

Finally, the anterior translation movement was simulated. As expected, this movement was performed correctly. This was expected as this was the movement better performed in the original device, Figure 131.

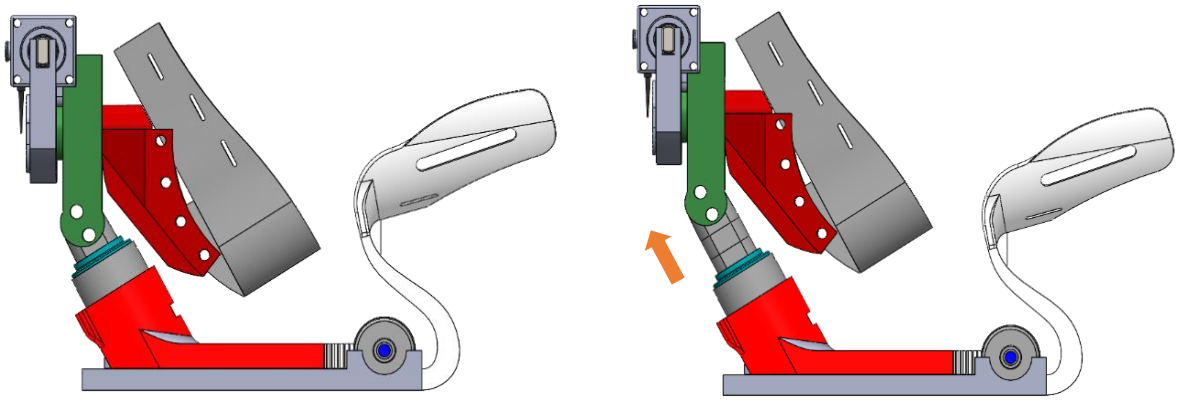

Figure 131- Motion simulation of the anterior translation movement.

5. PNEUMATIC SYSTEM

Once the device is validated, the actuating system needs to be designed. Firstly, this system is a pneumatic one, and the components must operate in the MRI environment. Therefore, they cannot have metals or any magnetic materials in their composition. This means that some of the system's main components may need to be designed.

First, it should be understood what the main goals of this system are:

- No need to connect/ disconnect the actuators from the supply each time the health technician changes the movement.
- Reduce the exam duration and simplify the overall process.

To accomplish these goals, the idealized system must have a pneumatic reservoir with the necessary volume to realize the exam. This reservoir is filled outside the MRI room with a compressor and should then be connected to the PATD.

There are three cylinders to actuate: the eversion, the abduction and the anterior translation cylinder. The first two are bi-directional, meaning they must always be actuated. The final one only needs to actuate in one motion. The retreat doesn't need to be actuated. Also, the cylinders' movement should be smooth, so a flow controller is necessary, Figure 132.

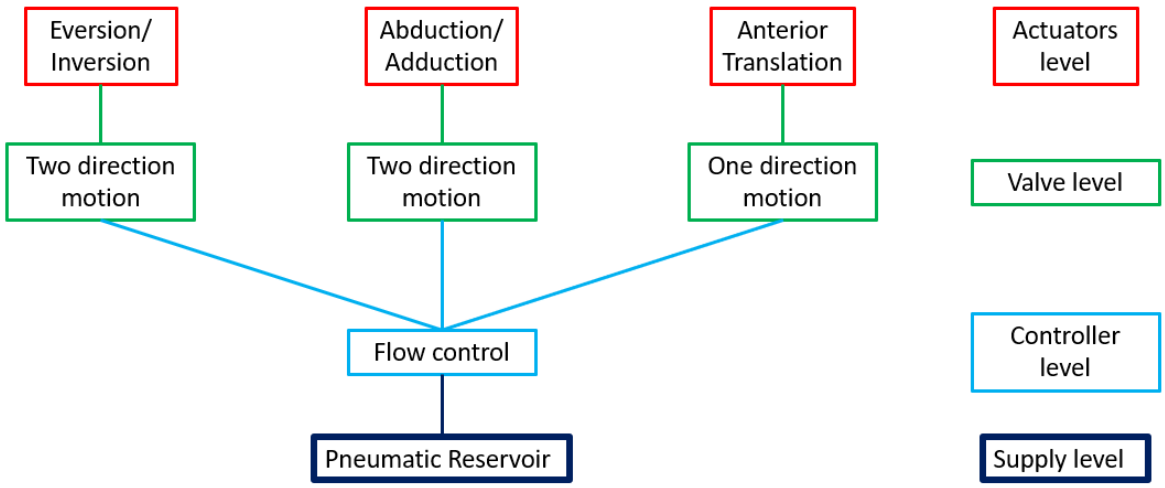

Figure 132- Scheme of the pneumatic system needed.

Using the FluidSim software, the following system was designed: two 4-way valves and one 3-way valve. They control the eversion and abduction cylinders, respectively, while the last valve controls the translation cylinder. Also, instead of one flow control and three faucets, it was used three flow controls,

Figure 133. This way allows for a reduction in the number of components and also the space needed to allocate the pneumatic system.

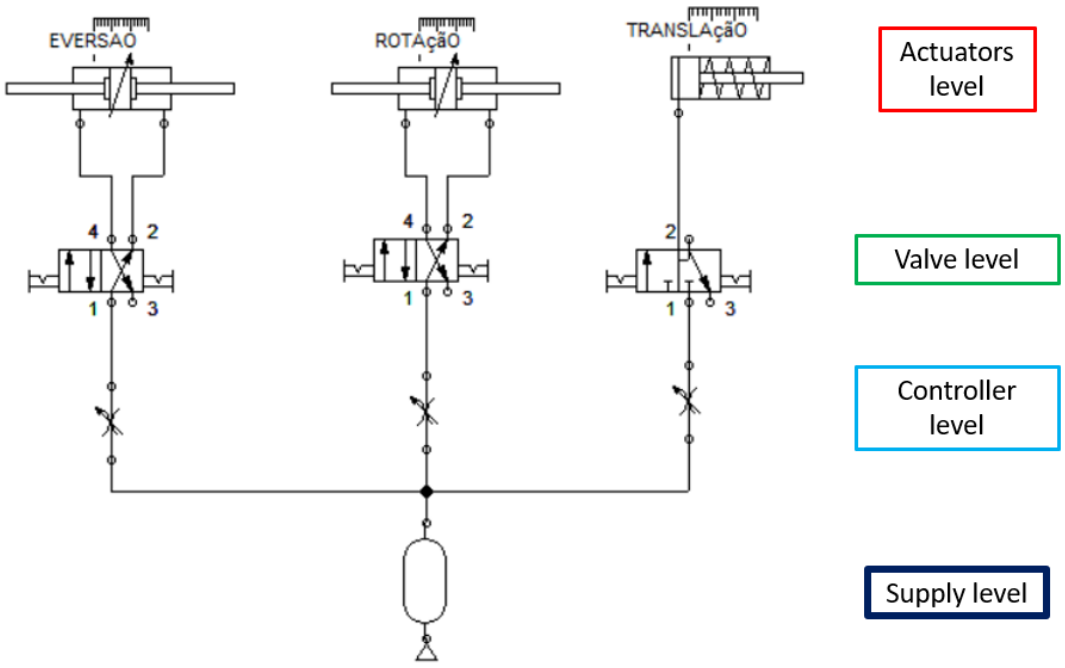

Figure 133- Pneumatic system designed in FluidSim.

Because the cylinders are already designed, the valves are the first components to design in this section.

5.1. Valve Design

A valve is a simple component that consists of two bodies, the main valve (red) and the spool (black), that moves and allows the user to select which hole the air is going to, Figure 134.

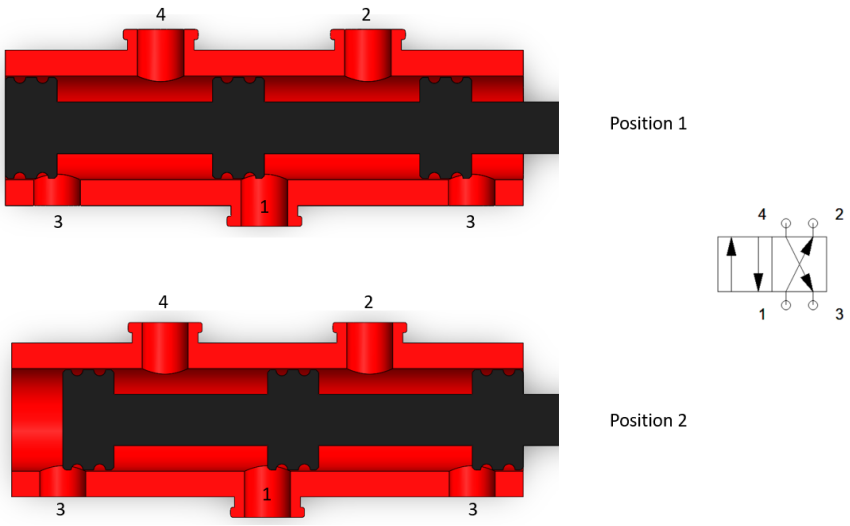

Figure 134- 4-way valve, section view.

The spool has six slots for O-rings to prevent the pressurized air from escaping at the contact between the spool and the main body. In position 1, the pressurized air enters hole number 1 and is directed to hole number 2 while the air in the cylinder gets out to the environment through holes 4 to 3. In position 2, the pressurized air enters hole number 1 and is directed to hole number 4 while the air in the cylinder gets out to the environment through holes 2 to 3. The final design can be seen in Figure 135.

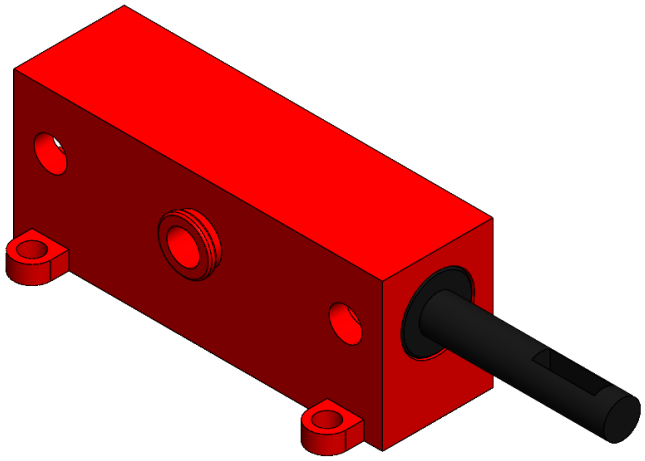

Figure 135- 4-way valve final design.

Next, the 3-way valve was designed. This valve is simpler as it only has 3 ways and, for that reason, 3 holes, and the spool is much shorter than the previous one, Figure 136.

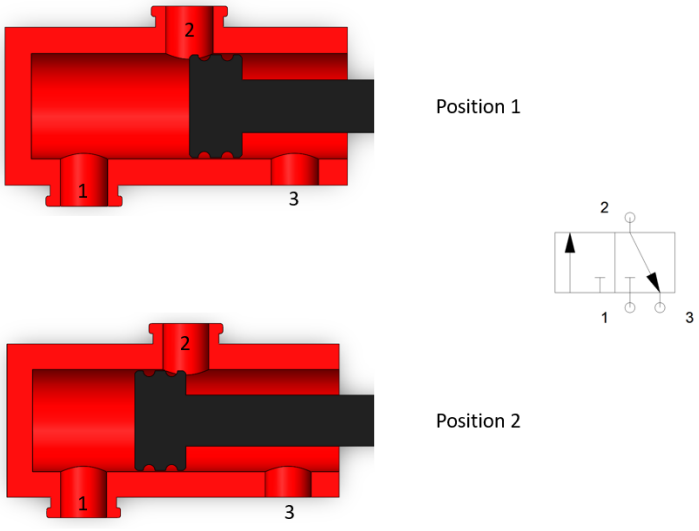

Figure 136- 3-way valve, section view.

The spool has 2 slots for O-rings to prevent the pressurized air from escaping at the contact between the spool and the main body. In position 1, the pressurized air enters hole number 1 and is

directed to hole 2. In position 2, the pressurized air that remains in the cylinder gets out to the environment through holes 2 to 3. The final design can be seen in Figure 137.

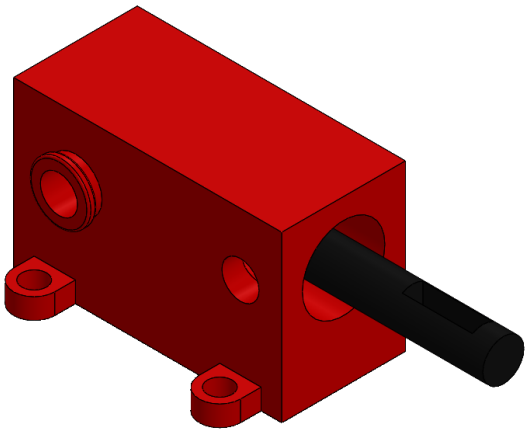

Figure 137- 3-way valve final design.

5.2. Flow Regulator Design

A flow regulator is a device that allows controlling the volume of air that flows out of this device. As a first design, the simplest flow regulator was designed. This one consists of two bodies (green and yellow) that form a channel where air flows. Then there is a needle (red) that is adjusted just like a screw and allows it to close and gradually open the air-out port, Figure 138.

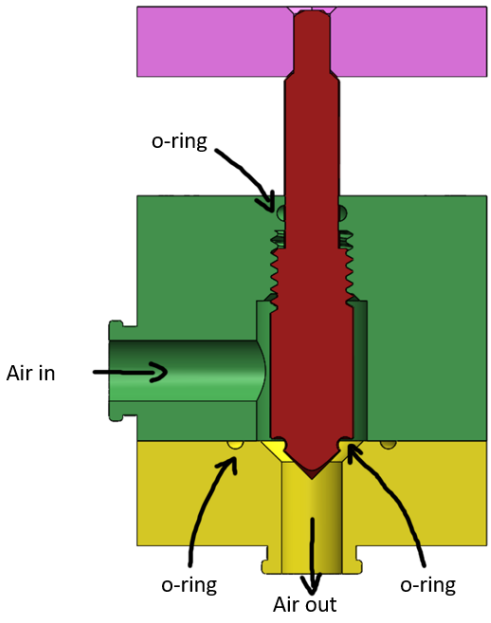

Figure 138- Flow regulator, section view.

Next, an exploded view with the component designation is shown in Figure 139 and Table 8.

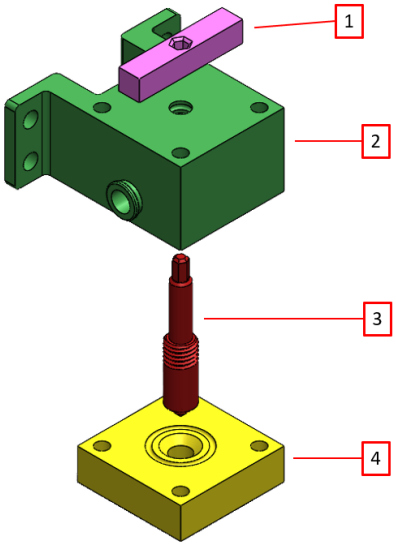

Figure 139- Exploded view of the flow regulator.

Table 8- List of components of the flow regulator.

Nº of the component	Designation
1	Grip
2	In body
3	Needle
4	Out body

This pneumatic system still needs time to be properly developed, as some proper dimensioning and simulation are still needed, and for that reason is future work.

6. FINAL DEVICE

Now that all the simulations, mechanical and motion-related, have been performed and validated, some details will be added to the final design to make it possible to register the angular and linear displacements.

Firstly, a slot was added in the base component so that a graduated ruler sticker could be glued there, Figure 140. This one allows measuring the angular displacement in the eversion/ inversion motion.

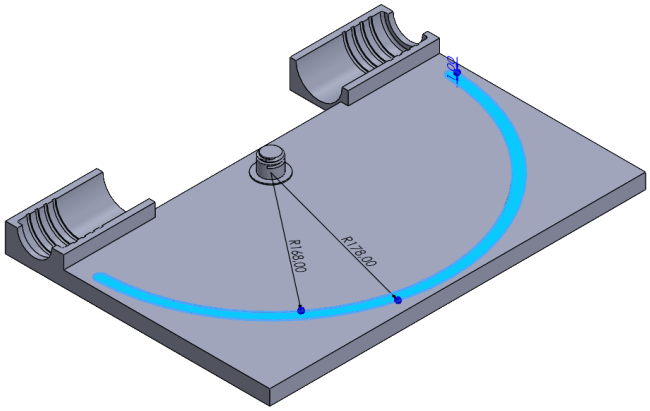

Figure 140- Slot added to measure the eversion angular movement.

Secondly, a slot was added in the rack support component so that a graduated ruler sticker could be glued there, Figure 141. This one allows measuring the angular displacement in the abduction/ adduction motion.

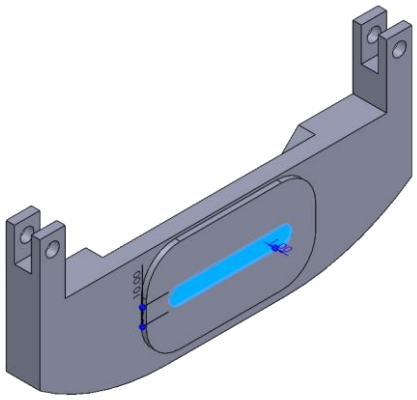

Figure 141- Slot added to measure the angular abduction movement.

Finally, a slot was added in the vertical cylinder shaft component so that a graduated ruler sticker could be glued there, Figure 142. This one allows measuring the linear displacement in the anterior translation motion.

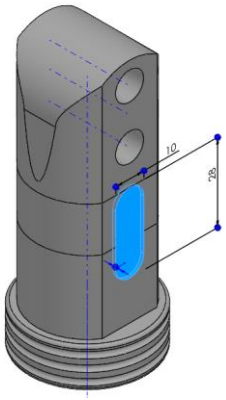

Figure 142- Slot added to measure the anterior translation linear movement.

With these final changes, the final device can be seen in Figure 143, with all the pins and screws that will be used.

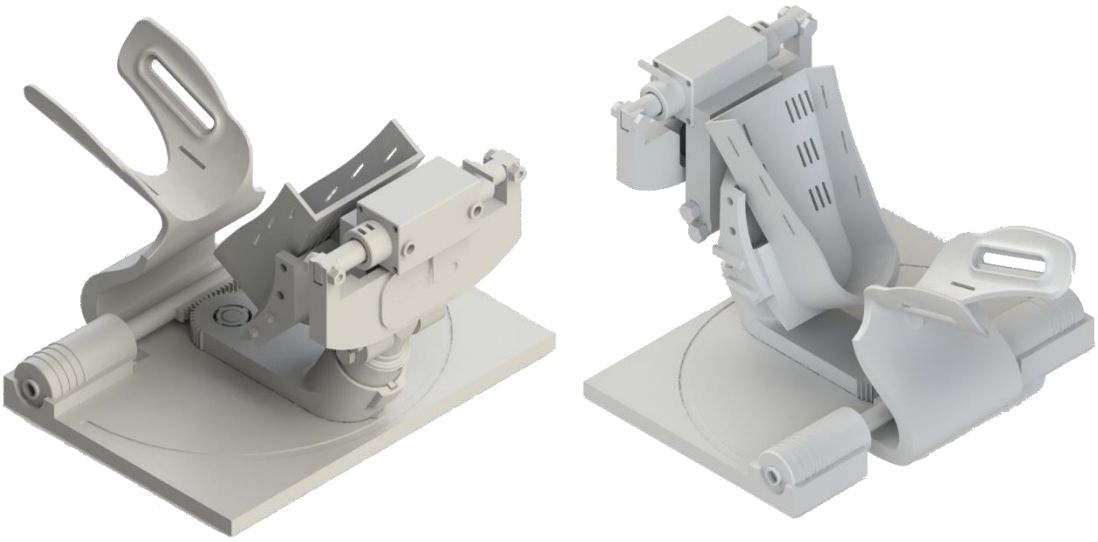

Figure 143- PATD final design.

7. Conclusion and Future Work

As a result of this thesis, the project of a new device that enables the simultaneous execution of two tests to diagnose an ankle joint injury is now almost ready for the first prototype construction. This can be considered a new device because although it started with an old one as its basis, it was so changed that now it is an entirely new product. This new device ensures that all movements required to examine the pathologies in the ankle are possible. All the basic dimensions and geometric requirements connected to the usage of this equipment when conducting an imaging exam were respected and satisfied.

The device's simplicity of use was consistently prioritized in the final product's design. If possible, it was made empirical and intuitive from the perspective of individuals with no prior experience handling machine components. The primary advantage of the current device will be its ability to quantify the maximum angular or linear displacement associated with any movement and pathology in the ankle joint. Such functionality is not yet present in any device on the market since the only existing equipment can only be connected to a low-resolution imaging test such as radiography.

The primary goal of the device used to diagnose pathologies in the ankle joint presented here is to improve the diagnostic process. By doing so, the diagnostic process gains more favourable conditions for both the patient and the healthcare professionals, enabling the realization of a diagnosis based on a more comprehensive and precise data set.

The design process started with the development of various concepts that led to a final one that could comply with all the project requirements and, finally, the preliminary design. This process was made quickly due to the use of CAD tools. After this, the validation phase was also speed-up by the use of CAE tools. In this phase, some geometries were changed so that every part and sub-system could withstand the various loads applied during the exam.

Finally, the actuating system was designed. As the thesis schedule was near the end, this system wasn’t fully completed in terms of verification and validation, so it still needs a decent amount of work to be completed.

In terms of future work:

- Firstly, the actuating system must be fully reviewed and finalized to work smoothly and consistently.
- Secondly, a prototype should be developed as a continuation of the design process since some components may need minor adjustments. This prototype needs to be validated with clinical exams.

APPENDIX A- GEAR DESIGN

First of all, the gear was represented, and the forces that are applied to it were shown,

The torque is applied in the centre of the wheel, which will create a pair of forces in the contact zone, in the scheme is where the load Ft is applied.

The value of torque T is known from the literature, and its maximum value is 4000 Nmm.

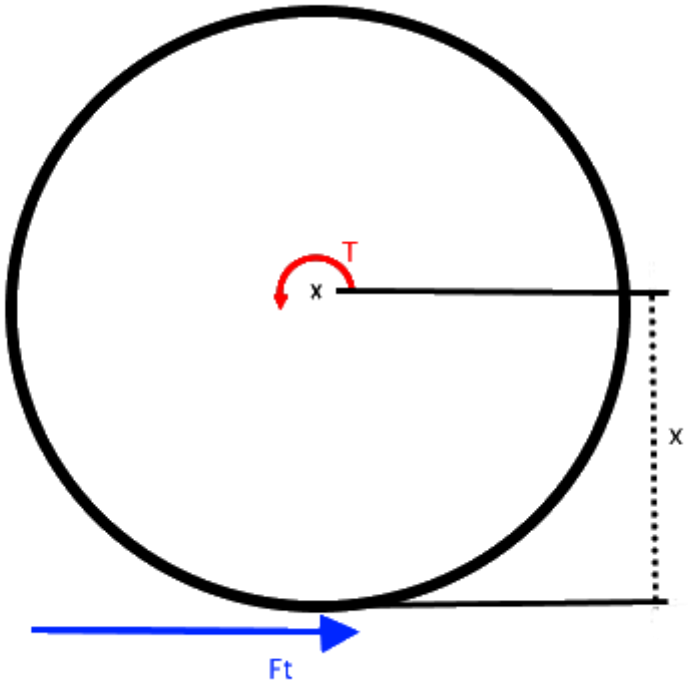

Figure 144- Schematic view of the wheel and rack forces.

Now it is necessary to know the diameter of the wheels, and this was a process of trial and error. In the scope of synthesis, only the final results will be shown.

Considering that the wheel diameter will always be bigger than 40 mm, then x≥20 mm:

$$T = Ft \times x$$

$$Ft = \frac{4000}{20} = 200\ N$$

$$\sigma = \frac{k_v \times W_t}{F \times m_t \times Y}$$

Where:

$$\sigma\ is\ the\ tension$$

$$k_v\ is\ the\ dynamic\ factor$$

$$W_t\ is\ the\ transmitted\ load$$

$$F\ is\ the\ width$$

$$m_t\ is\ the\ metric\ module$$

$$Y\ is\ the\ form\ factor$$

$$v \approx \frac{70}{1} = 70\ mm/s = 0{,}007\ m/s$$

$$k_v = \frac{3{,}56 + \sqrt{0{,}07}}{3{,}56} \approx 1{,}074$$

$$W_t = F_t = 181{,}82$$

$$Y = 0{,}485$$

$$47 \leq \frac{1{,}074 \times 200 \times 1{,}5}{10 \times 10^{-3} \times m_t \times 0{,}485}$$

$$m_t \geq 1{,}41\ mm \sim 1{,}5\ mm$$

APPENDIX B- MATERIALS SHEET

H-5800-0062-01-A
Data sheet: vacuum casting resin 8051

RENISHAW
apply innovation™

Data sheet: vacuum casting resin 8051

Description			**ABS-type**
Features			**High temperature resistance, strong flexing properties**
Suitable for			**Panels, enclosures**
Cured properties			**Test / ISO standard where applicable**
Colour		White	
Transparency		Translucent	
Shore hardness	At 23 °C At 60 °C At 80 °C	84 D 78 D 77 D	868
Flexural strength		85.9 N/mm²	178
Flexural modulus		1965 N/mm²	178
Tensile strength		55.9 N/mm²	R 527
Tensile modulus		2150 N/mm²	R 527
Izod impact		9.8 kJ/m²	180
Yield strength		62 N/mm²	R 527
Elongation yield		5 %	
Elongation at break		8 %	R 527
Tear strength		Not measured	34
Thermal conductivity		0.225 W/mK	BS 874
Heat deflection temperature		92 °C	(test piece 110 mm × 12.7 mm × 6.4 mm)
Glass transition temperature		110 °C	
Processing information			**Notes**
Viscosity	Part A Part B	750 cPs 180 cPs	At 25 °C
Specific gravity	Part A Part B	1.12 1.19	At 25 °C
Mix ratio A:B		100:200	By weight
Mixing time		30 s to 60 s	
Resin temperature		40 °C	Heating chamber
Mould temperature		70 °C	Heating chamber
Curing temperature		70 °C	Heating chamber
Curing time in mould		40 min	
Pot life		300 s	100 g at 25 °C
Post curing process		None	
Typical shrinkage		0.2 % to 0.3 %	

All information is based on results gained from experience and tests and is believed to be accurate but is given without acceptance of liability for loss or damage attributable to reliance thereon. Users should always carry out sufficient tests to establish the suitability of any products for their intended applications.

Renishaw plc
Whitebridge Way
Whitebridge Park, Stone
Staffordshire ST15 8LQ
United Kingdom

T +44 (0) 1785 815651
F +44 (0) 1785 812115
E additive@renishaw.com

www.renishaw.com/additive

RENISHAW
apply innovation™

Handling procedure

Casting procedure

- Shake unopened A and B component cans vigorously for 10 s to 15 s
- Pre-heat mold in oven at 70 °C
- Pre-heat unopened A and B component cans in oven at 70 °C for 2 hours, then place in oven at 40 °C to stabilise prior to use
- Weigh A and B components into separate cups, allowing for cup loss (the amount of resin left in cup A after tipping)
- Add colour pigment to cup A
- Place filled cups in the machine and attach mixing paddle to cup B
- Start vacuum pump
- Switch on mixer motor
- Wait 10 minutes after reaching maximum vacuum level before mixing
- Pour contents of cup A into cup B and mix as fast as possible without splashing
- Pour mixed resin into silicone mould and leak vacuum chamber before the end of the pot life
- Place filled mold in oven to cure resin
- For full instructions on casting procedures refer to *Vacuum Casting Technique: a guide for new users*, available at www.renishaw.com

Special notes

- Exact mould temperature is important
- Exact resin temperature is important
- Use no more than 2 % of total weight colour pigment

Product information

- **Pot life**
  Resin 8051 can be supplied with long pot life A component (10 min, LP/A). Contact Renishaw for details.
- **Mould life**
  Mould life can be increased by using the correct Renishaw release agent and demoulding the casting immediately after curing. Castings over 2 mm thick can be demoulded after 30 min, but need to be cured for a further 60 min at 70 °C.
- **Storage**
  Store unopened cans at > 20 °C
  Protect against frost
  Store opened cans in oven at 40 °C with caps on
  Both components are sensitive to humidity.
- **In case of crystallisation of B-component**
  Place cans in oven at 70 °C for 2 hours to 4 hours and stir resin afterwards.

Please follow the procedure for preparing the vacuum casting system as described in the system operation manual!

Always observe the instructions in the Safety Data Sheets of the product and always work in accordance with the safety instructions of the materials manufacturer! Safety Data Sheets can be found at www.renishaw.com

Wear suitable respiratory protection, safety gloves and safety goggles during the entire filling procedure in accordance with the Safety Data Sheets.

H-5800-0062-01-A
Issued 0612 Part no. H-5800-0062-01-A

COMPARACIÓN DE CARGA* PARA RESINAS DE COLADO BAJO VACÍO

	8051			2160		
CARGA DE FIBRA DE VIDRIO	0	10%	20%	0	10%	20%
RESISTENCIA A LA FLEXIÓN (N/mm2)	85.9	95	117	58	66	89
MODULO DE FLEXIÓN (N/mm2)	1965	2873	4285	1255	2053	3538
RESISTENCIA A LA TENSIÓN (N/mm2)	55.9	62.7	70.1	40.7	48.8	56.7
MODULO DE TENSIÓN (N/mm2)	2150	3614	5696	1270	2874	4346
IMPACTO IZOD (Kj/m2)	9.8			9.1		
ELONGACIÓN A LA RUPTURA %	8			50		
TEMPERATURA DE DEFORMACIÓN (ºC) Pieza de 110mm x 12.7 mm x 6.4 mm	90	# 120	# 140	70		

* Carga: MCP - Fibra de Vidrio 0.2 mm Art. Nº: 036 070

prototyping resin

PR 700

Black polyurethane resin dedicated to the production of prototypes and/or limited series.

Process in vacuum casting machines with silicone moulds.

Its properties allow the realisation of functional pieces.

APPLICATIONS :

Any need for technical parts requiring an outstanding heat resistance and/or mechanical properties, such as:

- Household appliances, electronics, toys
- Automotive industry: lid, heading block, electric wire holder, head light back piece
- Industrial parts with functions of holding, clamping or modelling under variable heat conditions

ADVANTAGES :

- **Mechanical characteristics** such as flexural modulus (2300 Mpa) or thermal resistance (Hdt 130°C) allow, after post curing, the realisation of **resistant parts**, even with **low thickness**
- **Low aggressivity** toward the moulds
- **Low shrinkage** (2mm/m)
- **Easy processing:** the relatively low viscosity of the mix combined with an **adjustable pot life** allow the realisation of thin parts that may require precise details

Synthene

Lieu Dit Ferme de L'Evêché – CS20308
60723 Pont-Sainte-Maxence CEDEX
France
Tél. :03 44 31 72 00 - Tél. international : + 33 3 44 31 72 00
Fax : 01 57 67 44 58 - Fax international : + 33 1 57 67 44 58
E-mail : contact@synthene.com
http://www.synthene.com

PR 700

Mercury free product, RoHS suitable.

References

Polyol : PR 700 P - ST 109 000
Isocyanate : PR 700/ PR 751/ PRA 794 I - ST 000 401

Definition

Polyurethane resin for vacuum casting.
Mercury free product suitable with European directive: 2011/65/EC, 2002/96/EC, 2000/53/EC and 2000/11/EC.
High thermal resistance (HdT : 130°C).
Easy to cast.
Low agressivity on silicon moulds.
Good chemical resistance.

Average physical properties of the components

	PR700 Polyol ST 109000	PR700 Isocyanate ST 000401	PR 700 ST 109401
Aspect – Color	Black liquid	Transparent liquid colorless	Black liquid
Viscosity Brookfield LVT (mPa.s) According to MO-051	**130**	**1200**	**600**
Density at 25°C According to MO-032	**1.13**	**1.15**	**1.14**

Process data

	PR700 Polyol ST 109000	PR700 Isocyanate SH 000401	Mixing ST 109401
Mixing ratio by weight	**80**	**100**	
Mixing ratio by volume	**81,5**	**100**	
Pot life 200g at 25°C (min.) According to MO-062			**6 - 7**
Demoulding time at 70°C (min.) According to MO-116			**Approx. 45**

Average mechanical and thermal properties of the solid piece

		Test methode	
Hardness Shore D1 (1)		ISO 868-2003	**87**
Transition glass (Tg) (1)	(°C)	DSC Perkin Elmer	**> 130**
Heat deflection temperature (HdT) (1)	(°C)	ISO 75 Ae:2001	**130**
Flexural modulus (1)	(MPa)	ISO 178 : 2001	**2300**
Maximal flexural strength (1)	(MPa)	ISO 178 : 2001	**80**
Tensile modulus of elasticity (1)	(MPa)	ISO 527 : 1993	**1800**
Elongation at break (1)	(%)	ISO 527 : 1993	**13**
Tensile strength (1)	(MPa)	ISO 527 : 1993	**60**
Charpy impact (without slight cut) (1)	($KJ.m^{-2}$)	ISO 179/1D : 1994	**60**
Linear shrinkage (3 mm thickness)	(mm/m)	-	**2**

(1)All results are obtained after curing 1 h at 70°C +1 h at 100°C + 2 h at 120°C + 24 h at RT

Lieu Dit Ferme de L'Evêché – CS20308
60723 Pont-Sainte-Maxence CEDEX
France
Tél. :03 44 31 72 00 - Tél. international : + 33 3 44 31 72 00
Fax : 01 57 67 44 58 - Fax international : + 33 1 57 67 44 58
E-mail : contact@synthene.com
http://www.synthene.com

Safety for using

Better wear safety clothes and accessories (gloves and glasses).
For more information, read the medical and safety data sheet of the product.

Process with vacuum casting machine :

Pre-heat polyaddition silicone moulds at 70°C.
Weigh isocyanate part in the upper cup (don't forget the residual product).
Weigh polyol part in the mixing cup (stir well the polyol part before use).
After 10 min of vacuum, pour isocyanate part in polyol part and mix to reach total and perfect homogeneity (approx 50 to 60 sec.)
Pour in the silicone mould.
Put the mould in an oven at 70°C.
Demoulding is possible after 50 mn according to thickness, then post curing is necessary to reach maximal characteristics.

Packaging :

Parcel of 2 kits of (4,0 + 5,0) kg

Storage : 18 months in original and unopened cans stored between15 and 25 °C.

prototyping resin

PR 403–PR 1503

Polyurethane resins dedicated to the production of prototypes and/or limited series.

Process in vacuum casting machines with silicone moulds.

Their properties allow the realisation of functional pieces, mechanical parts similar to polystyrene shock or HDPE thermoplastic types.

APPLICATIONS :

Parts requiring high impact resistance and/or mechanical properties, similar to thermoplastic materials:

- Household appliances, electronics, toys
- Models
- Automotive industry: wire holder, joints...
- Interior covering parts...

ADVANTAGES :

- **Polyol's part dilution** allows gel time adjustment
- **Colouring** possible, according to your needs.
- **Easy processing:** the relatively low viscosity of the mix combined with an **adjustable pot life** facilitate the casting process without increasing the demoulding time

Synthene

Synthene
Nous formulons vos succès !

Lieu Dit Ferme de L'Evêché – CS20308
60723 Pont-Sainte-Maxence CEDEX
France
Tél. :03 44 31 72 00 - Tél. international : + 33 3 44 31 72 00
Fax : 01 57 67 44 58 - Fax international : + 33 1 57 67 44 58
E-mail : contact@synthene.com
http://www.synthene.com

PR 403/PR 1503

References

Polyol : PR 403 P - SH105 000 / PR1503 P - SH115000
Isocyanate : PR 403/1503 I - SH 000170

Definition

Two-components polyurethane resin for vacuum- or hand-casting.
The two products have different reactivity but they both give a polymerised material with the same properties.
The polyols can be associated in order to modify the reactivity of the mixing without moving the other properties.
Polystyrene shock prototype.
For electric or electronic applications, the PR1503 system is suitable with ROHS.

Average physical properties of the components

	PR403P / PR1503P SH105000 / SH115000	PR403/1503 I SH000170	PR403/1503
Aspect – Color	Translucid liquid	Amber Liquid	Milky liquid White solid
Viscosity Brookfield LVT (mPa.s) According to MO-051	320	55	160
Density at 25°C According to MO-032	1.01	1.16	1.10
Mixing ratio by weight	60	100	

Process data

Stir well the two parts before use.

	PR 403 SH 105 170	PR 1503 SH 115 170
Reactivity on 200g at 25°C (min.) According to MO-062	5	15
Demoulding at 25°C 3 mm in thickness According to MO-116	approx. 1 h	approx. 4 h
Demoulding at 70°C 3 mm in thickness According to MO-110	approx. 20 min	approx. 45 min
Complete hardening time at 25°C	approx. 24 h	approx. 4 days

Average mechanical and thermal properties of the solid piece

		Test methode	
Hardness Shore D1 (1)		ISO 868-2003	74
Heat deflection temperature (HdT) (1)	(°C)	ISO 75 Ae:2001	75
Flexural modulus (1)	(MPa)	ISO 178 : 2001	1700
Maximal flexural strength (1)	(MPa)	ISO 178 : 2001	65
Tensile modulus of elasticity (1)	(MPa)	ISO 527 : 1993	1850
Elongation at break (1)	(%)	ISO 527 : 1993	6
Tensile strength (1)	(MPa)	ISO 527 : 1993	47
Charpy impact (without slight cut) (1)	($KJ.m^{-2}$)	ISO 179/1D : 1994	35
Linear shrinkage (3 mm thickness)	(mm/m)	-	2

PR 403-1503 /TDS/UK/ Version 5 – 2012/10/26

BIBLIOGRAPHY

[1] S. N. Khan, G. Erickson, M. J. Sena, and M. C. Gupta, "Use of Flexion and Extension Radiographs of the Cervical Spine to Rule Out Acute Instability in Patients With Negative Computed Tomography Scans." [Online]. Available: www.jorthotrauma.com

[2] R. Andrade *et al.*, "Development of a medical device compatible with MRI/CT to measure ankle joint laxity: the Porto Ankle Testing Device," *Porto Biomed J*, vol. 6, no. 1, p. e122, Jan. 2021, doi: 10.1097/j.pbj.0000000000000122.

[3] F. Guerra-Pinto, R. Andrade, P. Diniz, A. Luisa Neto, J. Espregueira-Mendes, and J. Guimarães Consciência, "Lack of Definition of Chronic Ankle Instability With Arthrometer-Assisted Ankle Joint Stress Testing: A Systematic Review of In Vivo Studies," *Journal of Foot and Ankle Surgery*, vol. 60, no. 6. Academic Press Inc., pp. 1241–1253, Nov. 01, 2021. doi: 10.1053/j.jfas.2020.04.026.

[4] M. Câmara, "Anatomia e Fisiologia Humana," 2014. [Online]. Available: www.ifcursos.com.br

[5] M. da Silva, "Cirurgia para tratamento da Fratura de Tornozelo." https://www.marcosbritto.com/2012/05/fratura-de-tornozelo.html (accessed Mar. 08, 2022).

[6] S. do Mundo, "45 curiosidades incríveis sobre o corpo humano." https://segredosdomundo.r7.com/curiosidades-sobre-o-corpo-humano/ (accessed Mar. 09, 2022).

[7] V. Scanlon and T. Sanders, "Essentials of Anatomy and Physiology," 2007.

[8] toda matéria, "Ossos do pé." https://www.todamateria.com.br/ossos-do-pe/ (accessed Mar. 10, 2022).

[9] Manual MSD, "Entorses do tornozelo." https://www.msdmanuals.com/pt-br/profissional/lesões-intoxicação/entorses-e-outras-lesões-dos-tecidos-moles/entorses-do-tornozelo (accessed Mar. 10, 2022).

[10] S. Roberts, *Kinesiology: Movement in the Context of Activity*, 2nd ed. 2005.

[11] J. Pina, *Anatomia humana da locomoção*, 2nd ed. 1999.

[12] P. Portela, "Cinesiologia," 2016.

[13] M. Caetano, "Funcionalidade Biomecânica." https://www.ctborracha.com/borracha-sintese-historica/aplicacoes/calcado/classificacao-do-calcado/funcionalidade-biomecanica/

[14] R. Ferreira, "Uma nova abordagem na avaliação e monitorização da cinemática da articulação do tornozelo."

https://www.researchgate.net/publication/313902351_UMA_NOVA_ABORDAGEM_NA_AVALIACAO_E_MONITORIZACAO_DA_CINEMATICA_DA_ARTICULACAO_DO_TORNOZELO (accessed Mar. 11, 2022).

[15] R. Frost, *Applied Kinesiology: A Training Manual and Reference Book of Basic Principles and Practices*. 2002.

[16] N. Assefa and Y. Tsige, "LECTURE NOTES Human Anatomy and Physiology."

[17] E. de Pessoa Andrade Filho Francisco Carlos Ferreira Pereira, "Anatomia Geral."

[18] J. Silva, "Ortopedia Pediátrica." http://www.orthopediatrica.com.br/service/entorse-de-tornozelo/ (accessed Mar. 13, 2022).

[19] Wikipedia, "Dorsiflexão." https://pt.wikipedia.org/wiki/Dorsiflexão (accessed Mar. 14, 2022).

[20] F. C. Balduini, J. J. Vegso, J. S. Torg, and E. Torg, "Injury Clinic Management and Rehabilitation of Ligamentous Injuries to the Ankle," 1987.

[21] O. Rasmussen, "Stability of the ankle joint: Analysis of the function and traumatology of the ankle ligaments," *Acta Orthop*, vol. 56, no. S211, pp. 1–75, 1985, doi: 10.3109/17453678509154152.

[22] R. Marder and G. Lian, "Ankle and foot injuries."

[23] K. Phillips, "Foot & Ankle Injuries," 2019. [Online]. Available: http://www.dshs.wa.gov/

[24] W. G. Fernandez, E. E. Yard, and R. D. Comstock, "Epidemiology of Lower Extremity Injuries among U.S. High School Athletes," *Academic Emergency Medicine*, vol. 14, no. 7, pp. 641–645, Jul. 2007, doi: 10.1197/j.aem.2007.03.1354.

[25] E. Giza, C. Fuller, A. Junge, and J. Dvorak, "Mechanisms of Foot and Ankle Injuries in Soccer," 2003.

[26] P. Renstrom *et al.*, "Strain in the lateral ligaments of the ankle," *Foot Ankle*, vol. 9, no. 2, pp. 59–63, 1988, doi: 10.1177/107110078800900201.

[27] N. A. Ferran and N. Maffulli, "Epidemiology of Sprains of the Lateral Ankle Ligament Complex," *Foot and Ankle Clinics*, vol. 11, no. 3. pp. 659–662, Sep. 2006. doi: 10.1016/j.fcl.2006.07.002.

[28] J. G. Garrick, "The frequency of injury, mechanism of injury, and epidemiology of ankle sprains*."

[29] J. v Marymont, M. A. Lynch, and C. E. Henning, "Acute ligamentous diastasis of the ankle without fracture Evaluation by radionuclide imaging."

[30] G. M. Kerkhoffs *et al.*, "Diagnosis, treatment and prevention of ankle sprains: An evidence-based clinical guideline," *Br J Sports Med*, vol. 46, no. 12, pp. 854–860, Sep. 2012, doi: 10.1136/bjsports-2011-090490.

[31] P. M. Boruta, J. O. Bishop, W. G. Braly, and H. S. Tullos, "Acute Lateral Ankle Ligament Injuries: A Literature Review," *Foot & Ankle International*, vol. 11, no. 2. pp. 107–113, 1990. doi: 10.1177/107110079001100210.

[32] D. Fritschy, "An unusual ankle injury in top skiers."

[33] J. Yde, "the lauge hansen classification of malleolar fractures," *Acta Orthop*, vol. 51, no. 1–6, pp. 181–192, 1980, doi: 10.3109/17453678008990784.

[34] Manual MSD, "Entorse de um tornozelo." https://www.msdmanuals.com/pt-pt/casa/lesões-e-envenenamentos/entorses-e-outras-lesões-dos-tecidos-moles/entorses-do-tornozelo (accessed Mar. 15, 2022).

[35] Bauerfeind, "XIII, Entorse de tornozelo?" https://www.bauerfeind.com.br/blogs/news/xiii-entorse-de-tornozelo (accessed Mar. 16, 2022).

[36] M. Chirls, "Inversion injuries of the ankle.," *J Med Soc N J*, vol. 70, no. 10, pp. 751–3, Oct. 1973, [Online]. Available: http://www.ncbi.nlm.nih.gov/pubmed/4201560

[37] P. Sarah Lamb, K. Haywood MCSP, J. Hargreaves MCSP ILTM, and S. Lamb MCSP, "Correspondence Multi-item outcome measures for lateral ligament injury of the ankle: a structured review," 2004.

[38] G. S. Sabino, C. M. Coelho, and R. F. Sampaio, "The use of the International Classification of Functioning, Disability and Health in the physical therapy assessment of individuals with musculoskeletal disorders of the lower limbs and lumbar region," *Acta Fisiátrica*, vol. 15, no. 1, pp. 24–30, Mar. 2008, doi: 10.11606/issn.2317-0190.v15i1a102901.

[39] O. Landeros, H. Frost, and C. Higgins, "Pos-traumatic anterior ankle instability," *Clin Orthop Rel Rev*, 1968.

[40] G. Sabino, C. Coelho, and R. Sampaio, ""Utilização da Classificação Internacional de Funcionalidade, Incapacidade e Saúde na avaliação fisioterapeutica de individuos com problemas musculosqueléticos nos membros inferiores e região lombar," *Acta Fisiatr*, 2008.

[41] J. W. Brantigan, L. R. Pedegana, and F. G. Lippert, "Instability of the subtalar joint. Diagnosis by stress tomography in three cases.," *J Bone Joint Surg Am*, vol. 59, no. 3, pp. 321–4, Apr. 1977, [Online]. Available: http://www.ncbi.nlm.nih.gov/pubmed/849942

[42] J. Karlsson and O. Lansinger, "Chronic Lateral Instability of the Ankle in Athletes," 1993.

[43] A. Pintsaar, J. Brynhildsen, H. Tropp, and H. Tropp, "Postural corrections after standardised perturbations of single limb stance: effect of training and orthotic devices in patients with ankle instability," 1996. [Online]. Available: http://bjsm.bmj.com/

[44] J. Perry, "Anatomy and biomechanics of the hindfoot.," *Clin Orthop Relat Res*, no. 177, pp. 9–15, [Online]. Available: http://www.ncbi.nlm.nih.gov/pubmed/6861413

[45] J. v Marymont, M. A. Lynch, and C. E. Henning, "Acute ligamentous diastasis of the ankle without fracture Evaluation by radionuclide imaging."

[46] F. Halabchi and M. Hassabi, "Acute ankle sprain in athletes: Clinical aspects and algorithmic approach," *World J Orthop*, vol. 11, no. 12, pp. 534–558, Dec. 2020, doi: 10.5312/wjo.v11.i12.534.

[47] J. Silva, L. Schulhan, and B. Moura, "Avaliação etiológica da dor crónica após entorse do tornozelo," *Rev ABTPé*, 2009.

[48] S. C. Brooks, B. T. Potter, and J. B. Rainey, "Inversion injuries of the ankle: clinical assessment and radiographic review.," *BMJ*, vol. 282, no. 6264, pp. 607–608, Feb. 1981, doi: 10.1136/bmj.282.6264.607.

[49] D. Fritschy, "An unusual ankle injury in top skiers."

[50] D. Jackson, R. Ashley, and J. Powell, "Ankle Sprains in Young Athletes," *Clin Orthop*, 1974.

[51] J. Karlsson, G. O. Andreasson, and ; Phd, "The effect of external ankle support in chronic lateral ankle joint instability An electromyographic study."

[52] D. Ivins, "Acute Ankle Sprain: An Update." https://www.aafp.org/pubs/afp/issues/2006/1115/p1714.html (accessed Mar. 17, 2022).

[53] P. F. O'Loughlin, C. W. Hodgkins, and J. G. Kennedy, "Ankle Sprains and Instability in Dancers," *Clinics in Sports Medicine*, vol. 27, no. 2. pp. 247–262, Apr. 2008. doi: 10.1016/j.csm.2007.12.006.

[54] M. J. Breitenseher *et al.*, "MRI versus lateral stress radiography in acute lateral ankle ligament injuries," *J Comput Assist Tomogr*, vol. 21, no. 2, pp. 280–285, 1997, doi: 10.1097/00004728-199703000-00022.

[55] M. Zanetti, C. de Simoni, H. H. Wetz, H. Zollinger, and J. Hodler, "A RT I C L E," 1997.

[56] Telos Medical, "Telos SD 900 Stress Device," Mar. 22, 2022.

[57] Telos, "Diagnostics." https://www.telos-gmbh.com/en/products/diagnostics.html (accessed Mar. 20, 2022).

[58] R. Andrade *et al.*, "Development of a medical device compatible with MRI/CT to measure ankle joint laxity: the Porto Ankle Testing Device," *Porto Biomed J*, vol. 6, no. 1, p. e122, Jan. 2021, doi: 10.1097/j.pbj.0000000000000122.

[59] R. Ferreira, A. Lea, F. Silva, P. Flores, and J. Espregueira-Mendes, "A mechanical device for ankle pathologies diagnosis," in *2015 IFToMM World Congress Proceedings, IFToMM 2015*, 2015. doi: 10.6567/IFToMM.14TH.WC.PS1.005.

[60] F. Guerra-Pinto, R. Andrade, P. Diniz, A. Luisa Neto, J. Espregueira-Mendes, and J. Guimarães Consciência, "Lack of Definition of Chronic Ankle Instability With Arthrometer-Assisted Ankle Joint Stress Testing: A Systematic Review of In Vivo Studies," *Journal of Foot and Ankle Surgery*, vol. 60, no. 6. Academic Press Inc., pp. 1241–1253, Nov. 01, 2021. doi: 10.1053/j.jfas.2020.04.026.

[61] Dassault Systems, "Mesh Quality Checks." https://help.solidworks.com/2021/English/SolidWorks/cworks/c_Mesh_Quality_Checks.htm (accessed May 15, 2022).

[62] Tribology ABC, "Coefficient of friction, Rolling resistance and Aerodynamics." https://www.tribology-abc.com/abc/cof.htm (accessed May 23, 2022).